The Effects of Uncertainties in Fire Emissions Estimates on Predictions of Texas Air Quality

AQRP Project No. 12-018

Elena McDonald-Buller (PI) and Yosuke Kimura
Center for Energy and Environmental Resources
The University of Texas at Austin

Christine Wiedinmyer (Co-PI)
The National Center for Atmospheric Research

Chris Emery (Co-PI) and Ed Tai
ENVIRON International Corporation

Submitted to
Dr. David Sullivan
Center for Energy and Environmental Resources
The University of Texas at Austin

Mr. Clint Harper
Texas Commission on Environmental Quality

November 2013

Table of Contents

1. Background and Study Motivation

1.1 Fires and Air Quality

Wildland fires and open burning can be substantial sources of nitrogen oxides (NO_x), carbon monoxide (CO), and non-methane hydrocarbons (NMHCs), which are precursors to ozone formation, as well as particulate matter (PM), sulfur dioxide (SO_2), and ammonia (NH_3). Achieving attainment with the National Ambient Air Quality Standards (NAAQS) for ozone has been the primary focus of State Implementation Plans (SIPs) for Texas. Accurate characterization of fire events in Texas and other states is necessary for understanding their influence on measured ambient concentrations, for providing a weight of evidence for exceptional event exclusions if necessary, and for conducting air quality modeling for planning and attainment demonstrations. On a national basis, wildfires are among the natural emissions sources that are used in the determination of North American Background (NAB) ozone (formerly Policy Relevant Background or PRB ozone) that is predicted to occur in the U.S. in the absence of anthropogenic emissions in continental North America and has historically informed policy decisions about the National Ambient Air Quality Standard (NAAQS). If more stringent federal standards for ozone are considered in the future, emissions of its precursors from regional and longer-range sources such as fires that can contribute to background concentrations will become increasingly important for understanding the relative effectiveness of local and regional emissions control programs in Texas.

In a critical review of ozone production from wildfires, Jaffe and Wigder (2012) found that NO_x is generally the limiting ozone precursor, but wildfires emit an extensive number of NMHCs and oxygenated volatile organic compounds (OVOCs), many of which remain poorly understood. Ozone production is influenced by complex interactions between many factors, including the nitrogen content of fuels, maximum combustion efficiency (MCE; $CO_2/(CO + CO_2)$ grams of carbon per kilogram of fuel burned) of the biome, meteorological conditions (i.e., ambient temperature, winds, and relative humidity), topography, atmospheric chemical composition and radiative properties, and chemical and photochemical reactions that occur as the fire plume is transported downwind and potentially encounters other emissions sources (Jaff and Wigder, 2012). Jaffe and Wigder (2012) estimated wildfires contribute 174 Tg /year or 3.5% of global in-situ tropospheric ozone production (reference Table 1), with an uncertainty of approximately 50%. Strong regional variations exist, with relatively greater contributions to ozone production in the tropics and southern hemisphere, particularly in El Niño years, than in the temperate northern hemisphere.

Table 1. Global and regional estimates of ozone production from wildfires from Jaffe and Wigder (2012; ref. Table 2 in source).

Fire/time period	CO emissions	O_3 production	Method	Reference
Southern Hemisphere (Africa and South America)/during the dry season	17 Tg month^{-1}	17 Tg month^{-1}	1	Mauzerall et al., 1998
Alaska and Canada/summer 2004	30 Tg	11–15 Tg	2	Pfister et al., 2006
Boreal Northern Hemisphere	38 Tg year^{-1}	13 Tg year^{-1}	3	This work
Temperate Northern Hemisphere	9 Tg year^{-1}	3 Tg year^{-1}	3	This work
Northern Hemisphere Tropical and Equatorial Region (10° S–30° N)	151 Tg year^{-1}	103 Tg year^{-1}	3	This work
Southern Hemisphere south of 10° S	158 Tg year^{-1}	54 Tg year^{-1}	3	This work
Global total	356 Tg year^{-1}	174 Tg year^{-1}	3	This work

1: Total biomass burned (Tg)*CO Tg^{-1} biomass burned*observed $\Delta O_3/\Delta CO$ ratio. Mauzerall et al. (1998) used a relatively low biomass consumption for the southern hemisphere (SH) of 294 Tg month^{-1}, but a relatively high $\Delta O_3/\Delta CO$ of 0.50.

2: Total biomass burned (Tg)*CO Tg^{-1} biomass burned*observed and modeled $\Delta O_3/\Delta CO$ ratio.

3: For our estimates, we used the average CO emissions given by van der Werf et al. (2010) for 1997–2010 and a $\Delta O_3/\Delta CO$ ratio of 0.4 for equatorial and tropical regions and a value of 0.2 for all other regions. We used the van der Werf et al. (2010) classifications as follows: Boreal northern hemisphere (NH) (BONA, BOAS); Temperate NH (TENA, EURO, CEAS); NH Tropical and Equatorial Region (CEAM, NHSA, MIDE, NHAF, SEAS, EQAS) and SH (south of 10S, SHSA, SHAF, AUST).

Fire emissions are often transported over multiple spatial scales and can contribute to exceedances of air quality standards. Jaffe et al. (2004) and Oltmans et al. (2010) demonstrated the impacts of long-range transport of pollution from Siberian boreal fires on air quality in western North America. Within the contiguous United States, California and the western U.S. have had the highest wildfire activity (Pfister et

al., 2007) with measured effects on regional air quality. Mühle et al. (2007) estimated particulate matter concentrations as high as 250 mg/m^3 from thirteen wildfires during Santa Ana winds in southern California in October 2003. Using a combination of surface observations and global model simulations, Pfister et al. (2008) found an average enhancement in surface 8-hour ozone concentrations of 10 ppb during high fire conditions in California in September and October 2007, with effects of as much as 5 ppb in neighboring Nevada. Singh et al. (2012) observed that enhancements in ozone production were greatest when fire influences were associated with urban pollution in the South Coast Air Basin during the June/July 2008 Arctic Research of the Composition of the Troposphere from Aircraft and Satellites - California Air Resources Board (ARCTAS-CARB) campaign. Jaffe et al. (2008a) estimated that for each 1 million acres burned in the western U.S. during summer months (June/July/August) from 1989 - 2004, daytime mean ozone was enhanced across the region by 2.0 ppbv. Average enhancements in summer $PM_{2.5}$ concentrations over the same time period in five western regions, the Northern Rocky Mountains, Central Rocky Mountains, Southwest, California, and Pacific Northwest, were 1.84, 1.09, 0.61, 0.81, and1.21 $\mu g/m^3$, respectively, but could be as much as twice these values during large fire years (Jaffe et al., 2008b).

The influence of fire emissions on ozone and PM concentrations in Texas has been well-documented in previous observational studies (e.g., Junquera er al., 2005; Morris et al., 2006; McMillan et al., 2010; Villanueva-Fierro et al., 2009). Junquera et al. (2005) used fire emissions estimates obtained from observations during the Texas Air Quality Study-2000 (TexAQS-2000) and a photochemical grid model to predict ozone enhancements (of as much as 60 ppb) within 10-100 km of wildfires in the Houston/Galveston-Beaumont-Port Arthur region. Ozone production was enhanced by mixing with urban NO_x emissions. Using chemical markers, Villanueva-Fierro et al. (2009) identified the long-range transport of primary and secondary pollutants from biomass burning in Mexico and Central America and contributions to haze episodes in New Mexico, Texas, Louisiana, and the upper Mississippi River Valley in May 1998. Morris et al. (2009) found evidence of long-range transport of ozone and its precursor species and increases of 50-110% in ozone concentrations between the surface and 5 km altitude in the Houston area associated with Alaskan and western Canadian biomass burning during July 2004. McMillan et al. (2009) used a suite of observations from Atmospheric InfraRed Sounder (AIRS) onboard the Aqua satellite and the Tropospheric Emission Spectrometer (TES) onboard the Aura satellite, as well as surface observations in conjunction with trajectory and chemical transport models, to describe the influence of fires from the Pacific Northwest on Houston's air quality during the Second Texas Air Quality Study in August-September 2006.

1.2 Climate Change and Fires

As Figure 1 indicates, most climate models suggest that droughts will become more severe in the future in Texas as climate changes in response to increased concentrations of greenhouse gases and other radiative forcing species in the atmosphere (U.S. Global Change Research Report, 2009). The increase in drought frequency may have complex effects on the occurrence of fires in the region. The most recent 2010-2012 drought was a severe to extreme drought over the Southern U.S., with Texas experiencing effects that were among the worst. In October 2011, 88% of Texas was under exceptional drought conditions, and only 3% of the state was not classified as extreme or exceptional drought. Drought and the associated heat were associated with 23,835 fires from November 15, 2010 through September 29, 2011 with more than 3.8 million acres burned and 2,763 Texas homes destroyed, making 2011 the worst year for wildfires in Texas history (Texas Forest Service; http://txforestservice.tamu.edu/main/popup.aspx?id=14644). Other states, such as Arizona, New Mexico and Colorado also experienced severe wildfires during the period

Figure 1. Projected future changes in precipitation relative to the recent past as simulated by 15 climate models. Simulations are for late this century, under a higher emissions scenario. Confidence in the projected changes is highest in the hatched areas. Source: U.S. Global Change Research Report, 2009.

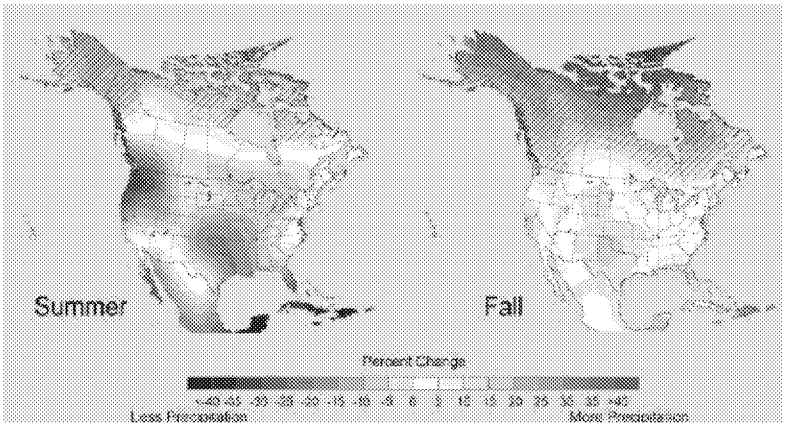

(NOAA/NCDC, 2013). Moritz et al. (2012) developed spatial statistical models of fire probability on a global-scale for two-time periods, 2010-2039 and 2070-2099, using remote-sensed fire activity data and key environmental variables derived from temperature, precipitation, and net primary productivity (2010-2039 only) patterns and driven by multi-model climate datasets (A2 emissions scenario). Figure 2 shows the ensemble mean change and degree of agreement in predicted fire probability among the 16 global climate models (GCMs) for the two time periods relative to baseline probabilities for 1971-2000 from Moritz et al. (2012). The results indicate that although broad agreement in multi-model predictions exists in many regions of the world, uncertainties in vegetation patterns, interannual climate variations, and local human activities warrant further investigation.

Projected changes in climate suggest that fire frequency in the western U.S. may increase (Westerling et al., 2011; Westerling et al., 2006). Westerling and Bryant (2008) use downscaled climate model output to estimate fire probability across the state of California. In all cases, the probability of fire across the state was expected to increase. These changes in climate are estimated to substantially increase emissions of air pollutants (Hurteau et al., 2013), which may in turn have detrimental impacts on air quality.

1.3 Modeling the Impacts of Fire Emissions

To quantify the impacts of open fires on air quality, emissions estimates are used as inputs to chemical transport models. Requirements for the estimation of fire emissions for atmospheric modeling are highly variable with the application; global-scale studies may require estimates at spatial scales of 100 km and monthly time periods (Urbanski et al., 2011; Al-Saadi et al., 2008). In contrast, regional-scale modeling applications frequently require spatial scales of less than 10 km and daily time periods (Urbanski et al., 2011). Understanding these needs is critical to the selection of the fire emissions estimation approach. Wiedinmyer et al (2011) identified recent studies that serve as representative examples of differences in approaches for estimating emissions across spatial scales: (1) *fire-specific estimates* from the Oregon Biscuit fire (Campbell et al., 2007) and Australian Black Saturday fires (Paton-Walsh et al., 2012); (2) *regional efforts* in Asia Africa, and North and South Americas (Reid et al. 2008), in the Himalayas (Vandrevu et al. 2011), in the Western U.S. (Urbanski et al. 2011), in North America (Wiedinmyer et al. 2006), in Asia (Song et al. 2010), and in Western Africa (Liousse et al. 2010); and (3) *global inventories*, such as the Global Fire Emissions Database (GFED; van der Werf et al. 2010) and the Fire INventory from NCAR version 1 (FINNv1; Wiedinmyer et al. 2011).

Figure 2. From Mortiz et al. (2012): Ensemble mean change (A, C) and degree of model agreement (B, D) in predicted fire probability among 16 climate models for 2010–2039 and 2070–2099 time periods (change assessed from baseline probabilities 1971–2000). Predictions for 2010–2039 are based on "Climate+Baseline NPP" models, and 2070–2099 are based on ''Climate only'' models. Pie charts indicate global proportions in each agreement class: "likely decrease", "likely increase", and "low agreement" correspond to 8.1%, 37.8%, and 54.1% for the 2010–2039 period, and to 20.2%, 61.9%, and 17.9% for the 2070–2099 period.

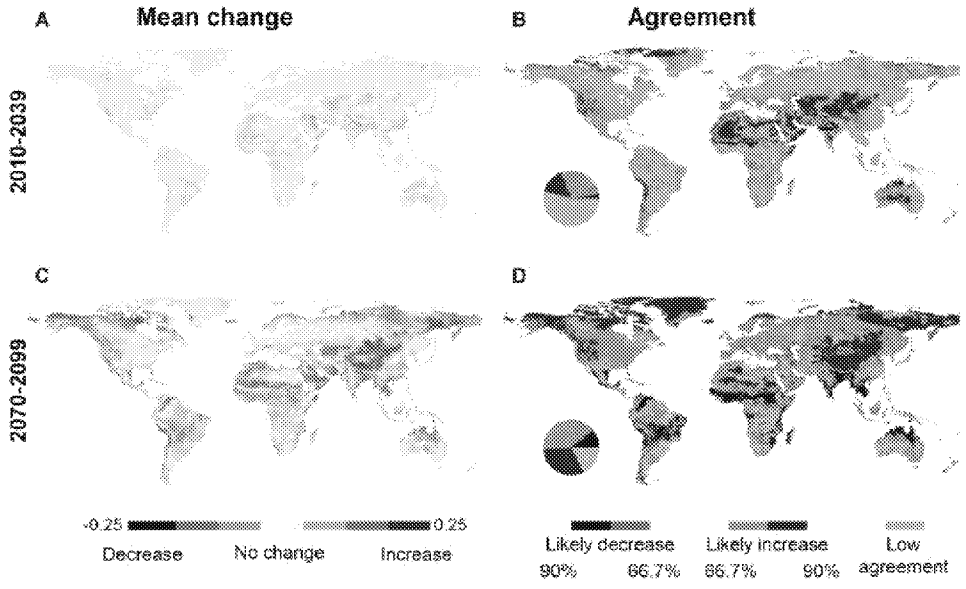

More than thirty years ago, Seiler and Crutzen (1980) proposed a method for estimating total carbon emissions from fires based on area burned, biomass (i.e., fuel) loading, biomass carbon fraction, and fuel consumption (i.e., fraction of biomass burned; combustion factor). Emissions of trace gases and particulate matter have commonly been estimated by incorporating emission factors (e.g., mass of gas or particulate matter emitted per mass of fuel or carbon burned) into this basic framework (French et al., 2011). Despite the importance of wildland fires and open burning on atmospheric trace gas and particulate matter concentrations (e.g., Akagi et al., 2011) and the increasingly frequent applications of satellite remote sensing observations and *in situ* observations (e.g., Wiedinmyer et al., 2006, 2011; Roy et al., 2007) for model input parameters, estimating emissions from these sources is a highly uncertain process.

In some cases, agreement between fire emission models has been quite reasonable. For example, Wiedinmyer et al. (2011; ref Table 9) found that global annual emissions of CO and several other trace gases estimated by the Fire Inventory from NCAR (FINN) version 1 and Global Fire Emissions Database version 3.1 (GFEDv.3.1) to be within approximately 5-35%, with much larger regional variations. However, many studies have indicated much greater variability between emissions models. Al-Saadi et al. (2008) compared the area burned and CO emissions in North America from four different fire emissions models over seven months during 2006. Monthly estimates varied between the models by as much as a factor of ten. Substantial differences between the models were associated with the detection of small, short-duration fires and estimation of their area burned, and with net CO emission rates per unit area within particular ecosystems and vegetation classes across the Continental United States (CONUS). French et al. (2011) compared total carbon emissions for five locations in the western United States and Canada using as many as six models with spatial scales ranging from local to global; these included the First Order Fire Effects Model (FOFEM) 5.7, CONSUME 3.0, Wildland Fire Emissions Information

System (WFEIS), the Canadian Forest Service's CanFIRE 2.0 model, GFED3, and the Canadian Forest Fire Behavior Prediction (FBP) System. Overall uncertainty in the estimates from the ensemble of models was 25%, but French et al. (2011) noted large variability between models for specific locations. Quantification of burn area, characterization of fuel amount, composition, and vertical structure, representation of canopy consumption (crown versus surface fire), and characterization of fuel moisture conditions were identified as major drivers of model variability within and between sites. Paton-Walsh et al. (2012) compared a "bottom-up" approach using area burned and biomass loadings from the Moderate Resolution Imaging Spectroradiometer aboard NASA's Terra and Aqua satellites with FINN, a "top-down" approach using the Fire Emissions Estimate Via Aerosol Optical Depth (FEEV-AOD) method, and the GFEDv3.1 model for estimating emissions of trace gases from Australia's "Black Saturday" fires. Estimates of emissions of CO and other gas-phase species from the "top-down" FEEV-AOD approach were 50% higher than GFEDV3.1 estimates, while the "bottom-up" method produced estimates that were consistently lower by approximately a factor of three. Differences were associated with fire detections and area burned as well as underestimation of fuel loading and fuel consumption resulting from the preceding extreme drought and heat.

Urbanski et al. (2011) used the Wildland Fire Emission Inventory (WFEI) model to estimate the magnitude and intra- and inter-annual variability of CO and $PM_{2.5}$ emissions across spatio-temporal scales from non-agricultural burning in the Western United States during 2003-2008. The study highlighted the needs for quantification of uncertainty in model components and emissions estimates and for assessments of the sensitivity of emissions estimates to model components. A figure of merit identified as the half mass uncertainty was utilized for evaluating inventory uncertainty (i.e., $\tilde{u}_{ECO}$ or $\tilde{u}_{EPM2.5}$) across spatio-temporal scales. At spatial scales relevant to regional models (Δx = 10 km, Δt =1 day), Urbanski et al. (2011) found that WFEI estimated 50% of total CO emissions with an uncertainty of <133% and 50% of total $PM_{2.5}$ emissions with an uncertainty of <146%; uncertainty in burned area dominated uncertainties in emissions at regional spatial scales. In contrast, at spatial scales representative of global models (Δx = 100 km, Δt =30 days), 50% of total CO emissions were estimated by WFEI with an uncertainty of <50% and half of $PM_{2.5}$ emissions were estimated with an uncertainty <64%; uncertainty in CO emissions at global spatial scales was primarily associated with fuel loading consumed while uncertainty in $PM_{2.5}$ emissions was dominated by uncertainty in the emission factor. WFEI was designed to estimate emissions for NO_x, non-methane organic compounds (NMOCs), and other pollutants associated with wildland fires. In contrast to the uncertainty associated with CO emissions, the authors speculated that it is likely that uncertainty in emission factors for NMOCs are likely to have more significant contributions to their estimated emissions. Emission intensities of NMOCs are a strong function of MCE, a metric of flaming versus smoldering combustion, and emission factors associated with combustion phase remain poorly characterized for many vegetation types (Urbanski et al., 2011).

The Western Regional Air Partnership (WRAP; http://www.wrapair2.org/default.aspx) recently completed the "Deterministic and Empirical Assessment of Smoke's Contribution to Ozone" (DEASCO3) Project (http://deasco3.wraptools.org/) sponsored by the Joint Fire Sciences Program (JFSP), a partnership among federal land management agencies. DEASCO3 has produced an updated 2008 fire emissions inventory for the U.S., which was used to support annual modeling of the western U.S. under the West-Wide Jump Start Air Quality Modeling Study (WestJump). DEASCO3 employed the WRAP Fire Emissions Tracking System (FETS; http://wrapfets.org/methods.cfm), a web-enabled database tool for planned and unplanned fire events, which is intended for daily smoke management coordination and retrospective analyses such as emission inventories and regional haze air quality planning tasks. FETS obtains daily fire location/size data from such sources as the EPA's Bluesky system and calculates emissions using CONSUME 3.0. Fuels information is based on the Fuel Characteristic Classification System (FCCS) v.1.1 and corresponding fuel loadings provided by the Pacific Northwest Research Station, as well as GIS-processed fuel moisture maps. Although the results of DEASCO3 were not yet

available at the time of this study, it is a promising resource for future model intercomparison studies focused on the western U.S.

In Texas, uncertainties in fire emissions estimates and the impacts on air quality have yet to be evaluated, although the regional and local influences of fire emissions on air quality have been well-documented. This project examines the effects of uncertainties in fire emissions estimates on modeled ozone and particulate matter concentrations in Texas using FINN version 1 and the Comprehensive Air Quality Model with extensions (CAMx). FINN has been used as input to global and regional chemical transport models (e.g., Hodnebrog et al., 2012; de Foy et al., 2011; Emmons et al., 2010; Fast et al., 2009; Hodzic et al., 2007; Pfister et al., 2011). FINN updates are on-going in response to insights gained from model evaluations. For example, Pfister et al. (2011) showed that CO concentrations simulated by WRF-Chem with FINN emissions were underestimated relative to airborne observations during ARCTAS. A cause of the bias was the misclassification of forested areas as shrub lands in California by the MODIS Land Cover Type product that led to lowered modeled fuel loading. Hodnebrog et al. (2012) identified a similar bias in CO emissions, but not for other components in the FINN inventory used in WRF-Chem, relative to observations from the Ozone Monitoring Instrument (OMI) during the heat waves and wildfires in the Eastern Mediterranean in the summer of 2007. The results of the study of Pfister et al. (2011) and others are in part leading to improvements in the FINN model. Concurrently, addressing areas of uncertainty related to the representation of fires in chemical transport models including grid resolution, chemical reaction mechanism, and plume dynamics will also be critical (Jaffe and Wigder, 2012).

2. Objectives

It is essential that studies with FINN and other fire emission models focus on the accuracy and uncertainties associated with model input parameters. This project evaluates the sensitivity of emissions estimates from FINN to variability in input parameters and the effects on modeled ozone and particulate matter concentrations using CAMx. The specific objectives of this collaborative effort, between the University of Texas at Austin, the National Center for Atmospheric Research, and ENVIRON International Corporation, are to:

1. Generate fire emissions estimates for April - October 2008 for a regional domain encompassing Texas using the default configuration of FINN (Wiedinmyer et al., 2011).
2. Perform sensitivity analyses of FINN emissions estimates to key model uncertainties, such as land use/land cover data, fuel loading estimates, and emission factors.
3. Process the FINN emissions inventories from (1) - (3) for input to CAMx, to evaluate the effects on predicted ozone and particulate matter concentrations in Texas.
4. Compare fire emissions estimates and modeled ozone concentrations obtained from FINN with those obtained from BlueSky/EPA SmartFire 2, which was the approach used to generate fire inputs for the April - October 2008 CAMx modeling database to be used in this work.

The project is expected to result in fire emissions estimates for air quality modeling in Texas that reflect the state of the science and in guidance for achieving future improvements.

3. Fire INventory from NCAR (FINN): Default Configuration

FINN (Wiedinmyer et al., 2011) is a global fire emissions model that estimates daily emissions of trace gases and particles from open burning of biomass, which includes wildfires, agricultural fires, and prescribed burning (but not biofuel use or trash burning), for input to air quality models at a resolution of approximately 1 km^2. FINN is especially applicable for use in global and regional chemical transport models because of its high spatial and temporal resolution necessary for capturing daily and diurnal variations in emissions and chemistry, consistency across geopolitical boundaries, and chemical speciation profiles for volatile organic compound (VOC) emissions associated with fires. FINN and its framework are described in detail by Wiedinmyer et al. (2011) and are summarized here.

Estimates of emissions from a fire in the FINN framework depend on several factors, including the timing and location of the fire, area of the fire, amount of fuel burned within that area, and assumed emissions factors. Emissions are estimated using:

$$E_i = A\,(x,t) * B(x) * FB * ef_i \qquad (1)$$

where the mass emission of species i (E_i) is equal to the area burned at time t and location x [$A(x,t)$] multiplied by the biomass loading at location x [$B(x)$], the fraction of that biomass that is burned in the fire (FB), and the emission factor of species i (ef_i, mass of i emitted per mass of biomass burned). All biomass terms are on a dry weight basis. In the next sections, the default configuration of the FINN methodology is described. It should be noted, however, that the FINN methodology has been developed such that the inputs and parameterizations are flexible and can be readily changed.

3.1 Fire Detection

The default FINN methodology employs global observations from the Moderate Resolution Imaging Spectroradiometer (MODIS) instrument on-board NASA's Terra and Aqua satellites. Processed fire detections from the MODIS Rapid Response (MRR) identify burn time and location and are obtained directly from the University of Maryland (2002; Davies et al., 2009). More information can be found in the MODIS Fire Users Guide (http://maps.geog.umd.edu/ products/MODIS Fire Users Guide 2.4.pdf and http://maps.geog.umd.edu/firms/faq.htm). The MRR can be readily downloaded from several locations. For global output, the MODIS hot spot observations can be requested from the NASA Near Real-Time data site Archive Download Tool (https://earthdata.nasa.gov/data/near-real-time-data/firms/active-fire-data#tab-content-6). The U.S. Forest Service Remote Sensing Application Center (RSAC) also provides these data processed for North America at http://activefiremaps.fs.fed.us/gisdata.php. Data used for this work were obtained from the NASA portal.

The MODIS fire detection data provide daily fire detections with a nominal horizontal resolution of ~1 km^2 and include the location, overpass time (UTC), and confidence of the detection. Among the uncertainties with daily fire detections, "double counting" of fires within a day is possible because observations from both the Terra and Aqua satellites are applied. Wiedinmyer et al. (2011) addressed this issue for their global assessment by identifying multiple detections of the same fire pixel for each day of interest and removing fire detections for a single day that fall within a 1-km^2 radius of another fire detection, according to the approach of Al-Saadi et al. (2008). Consequently, for each 1- km^2 hot spot, there is a constraint of one fire per day, but fires that occur the following day at the same location are counted again. It should be noted that the MODIS satellite observations do not provide daily global coverage at latitudes between approximately 30° N and 30°S, due to the observational swath path; this area includes portions of southern Texas. The FINN model does account for this in the processing of fires 30° and -30°, the details of which are described by Wiedinmyer et al. (2011).

3.2 Land Use/Land Cover Classification

The type of vegetation burned at each fire pixel is determined by the MODIS Land Cover Type (LCT) product, which has a spatial resolution of 1 km^2. Each fire pixel defined by the MRR is assigned to one of MODIS LCT 17 land cover/land use (LULC) classifications defined by the International Geosphere Biosphere Programme (IGBP). This classification scheme includes 11 natural vegetation classes, 3 developed and mosiacked land classes, and three non-vegetated land classes. The MODIS Vegetation Continuous Fields (VCF) product is used to identify the density of the vegetation at each active fire location. The VCF product has a spatial resolution of 500m and provides information about the percent tree, herbaceous, and bare ground cover (Hansen et al., 2003, 2005; Carroll et al., 2011). VCF data are scaled to 1 km spatial resolution to match the fire detection and LCT datasets.

In their global assessment of FINN emission estimates, Wiedinmyer et al. (2011) addressed several inconsistencies between the datasets during the processing. Fire detections were removed in areas with LCT classifications for water, snow, or ice. The total cover from the VCF product was scaled to 100% when it fully encompassed each pixel after the scaling of the product from 500 m to 1 km. In addition, fire detections that were within areas assigned as 100% bare cover or unclassified according to the VCF product, were reassigned vegetation coverage based on the LCT classification: for fires located in LCT forest classifications, the percent coverage was reassigned to 60% tree cover and 40% herbaceous cover; for fires in LCT shrubland classifications, the percent cover was reassigned to 50% tree cover and 50 % herbaceous cover; for fires in LCT grassland classifications that did not have associated VCF cover information, the percent vegetative cover was reassigned to 20% tree cover and 80% herbaceous cover. Fire points assigned by the LCT product as "urban" or "bare/sparsely vegetated" were reassigned a land cover type based on the total tree and non-tree vegetation cover as determined by the VCF product. For fire points with less than 40% tree cover, urban or sparsely vegetated land cover was reassigned to grasslands; for areas with 40-60 % tree cover, the point was reassigned as shrublands; and for areas with tree cover greater than 60 %, the point was reassigned as a forest.

The global land use/land cover classifications of the MODIS LCT map are lumped into six generic categories that are linked with associated fuel loadings and emissions factors: savanna and grasslands (SG), woody savannas and shrublands (WS), tropical forest (TROP), temperate forest (TEMP), boreal forest (BOR), and cropland (CROP). Evergreen, deciduous, and mixed forest land covers of the LCT are assigned based on the latitude of the point; points at latitude greater than 50°N are identified as boreal; otherwise these forest land covers are identified as temperate.

3.3 Area Burned

FINN currently assumes an upper limit of 1 km^2 for area burned in its default configuration, except for fires located in grasslands and savannas which are assigned a burned area of 0.75 km^2 (Wiedinmyer et al., 2006; Al-Saadi et al., 2008). This burned area is then scaled by the percent bare cover in the VCF product. For example, in a forested area with 10% bare cover, the area burned is assumed to be 0.9 km^2.

3.4 Biomass Loadings

The amount of biomass that can be burned in each fire for five of the six land use/land cover classification are assigned to world regions based on Table 2. Fuel loadings in (g/m^2) by world region and FINN land cover classification from Wiedinmyer et al. (2011) are based on the work of Hoelzemann et al. (2004). Croplands are assigned the same fuel loading as the grasslands of each world region. For North America, this value is 976 g/m^2.

Table 2. Biomass loadings (g/m2) assigned in the FINN framework (Wiedinmyer et al., 2011).

Global Region	Tropical Forest	Temperate Forest	Boreal Forest	Woody Savanna/ Shrublands	Savanna and Grasslands
North America	28,076[b]	10,492	25,000[a]	5,705	976
Central America	20,260	11,000[a]		2,224	418
South America	25,659	7,400[a]		3,077	552
Northern Africa	25,366	3,497		2,501	318
Southern Africa	25,295	6,100		2,483	360
Western Europe	28,076[b]	7,120	6,228	4,523	1,321
Eastern Europe	28,076[b]	11,386	8,146	7,752	1,612
North Central Asia	6,181[c]	20,807	25,000[a]	11,009	2,170
Near East	6,181[c]	10,316		2,946	655
East Asia	6,181[c]	7,865		4,292	722
Southern Asia	27,969	14,629		5,028	1,445
Oceania	16,376	11,696[d]		1,271	245
Based on Akagi et al. [2010] and references therein, updated these values					
Taken as the average of Tropical and Temperate forest for Oceania (to account for Eucalyptus forest in Australia					
Added tropical forest to Western and Eastern Forest (equal to the value for North America)					

[a] Akagi et al. [2010] and references therein

[b] Added a tropical forest class to North America and Europe (in LCT)

[c] All Asia assigned equal tropical forest values

[d] Taken as the average of Tropical and Temperate forest for Oceania

3.5 Fraction of Biomass Burned

Wiedinmyer et al. (2011) assign the fraction of the biomass assumed to burn at each fire point as a function of tree cover in the default FINN configurations. This method is described by Wiedinmyer et al. (2006) and based on the approach of Ito and Penner (2004). For areas defined as 60% or more tree cover by the VCF product, FB is 0.3 for the woody fuel and 0.9 for the herbaceous cover. For areas with less than 40 % tree cover, no woody fuel is assumed to burn and the FB is 0.98 for the herbaceous cover. For fires in areas with 40% - 60% tree cover, the FB is 0.3 for woody fuels and calculated as the following for herbaceous fuels: $e^{-0.13 \times \text{fraction of tree cover}}$. The fraction of tree cover and fuel loading by land cover type and global region are used to determine the amount of woody fuel available; the herbaceous fuel loading is assigned the grassland fuel loading by global region.

3.6 Emissions Factors

Emission factors, specific for the generic land cover classifications assigned to each fire, are obtained from the literature (Table 3). Emission factors for NO and NO_2 were used instead of NO_x for this work.

3.7 Chemical Speciation Profiles

Most regional and global-scale air quality models require the use of simplified chemical mechanisms for non-methane hydrocarbons. Based on previous studies of species-specific emissions factors, Wiedinmyer

et al. (2011) recommend chemical speciation factors for the conversion of total emissions of non-methane organic compounds (NMOCs) to moles of emitted of individual organic compounds or lumped species for the GEOS-Chem (Bey et al., 2001; http://www.geos-chem.org/), MOZART-4 (Emmons et al., 2010a), and SAPRC99 (Carter et al., 2000) chemical mechanisms. The chemical speciation profile for MOZART-4 is shown in Table 4 and is used in this work with a processing algorithm developed by ENVIRON to obtain a profile for the Carbon Bond 05 (CB05) mechanism used in CAMx.

Table 3. Emission factors* (g kg Biomass Burned^{-1}) by land cover type (generic and MODIS) used in the default configuration of FINN (Wiedinmyer et al., 2011).

LCT	GenVegDescript	CO_2	CO	CH_4	NMOC	H_2	NO_XasNO	SO_2	$PM_{2.5}$	TPM	TPC	OC	BC	NH_3	NO	NO_2	PM_{10}
1	Boreal	1514	118	6	28	2.3	1.8	1	13	18	8.3	7.8	0.2	3.5	1.5	3	14.0
2	Tropical Forest	1643	92	5.1	24	3.2	2.6	0.45	9.7	13	5.2	4.7	0.52	0.76	0.91	3.6	12.3
3	Boreal	1514	118	6	28	2.3	3	1	13	18	8.3	7.8	0.2	3.5	1.5	3	14.
4	Temperate Forest	1630	102	5	11	1.8	1.3	1	13	18	9.7	9.2	0.56	1.5	0.34	2.7	17.0
5	Temperate Forest	1630	102	5	11	1.8	1.3	1	13	18	9.7	9.2	0.56	1.5	0.34	2.7	17.0
6	Woody Savannah	1716	68	2.6	4.8	0.97	3.9	0.68	9.3	15.4	7.1	6.6	0.5	1.2	1.4	1.4	11.4
7	Woody Savannah	1716	68	2.6	4.8	0.97	3.9	0.68	9.3	15.4	7.1	6.6	0.5	1.2	1.4	1.4	11.4
8	Woody Savannah	1716	68	2.6	4.8	0.97	3.9	0.68	9.3	15.4	7.1	6.6	0.5	1.2	1.4	1.4	11.4
9	Savanna and Grasslands	1692	59	1.5	9.3	0.97	2.8	0.48	5.4	8.3	3	2.6	0.37	0.49	0.74	3.2	7.13
10	Savanna and Grasslands	1692	59	1.5	9.3	0.97	2.8	0.48	5.4	8.3	3	2.6	0.37	0.49	0.74	3.2	7.13
11	Savanna and Grasslands	1692	59	1.5	9.3	0.97	2.8	0.48	5.4	8.3	3	2.6	0.37	0.49	0.74	3.2	7.13
12	Crops	1537	111	6	57	2.4	3.5	0.4	5.8	13	4	3.3	0.69	2.3	1.7	3.9	7.02
14	Savanna and Grasslands	1692	59	1.5	9.3	0.97	2.8	0.48	5.4	8.3	3	2.6	0.37	0.49	0.74	3.2	7.13
16	Savanna and Grasslands	1692	59	1.5	9.3	0.97	2.8	0.48	5.4	8.3	3	2.6	0.37	0.49	0.74	3.2	7.13

* TPM: Total particulate matter
TPC: Total particulate carbon
OC: Particulate organic carbon
BC: Particulate black carbon

Table 4. From Wiedinmyer et al. (2011). Chemical speciation factors for the conversion of NMOC emissions (kg day^{-1}) to MOZART-4 chemical species (moles-species day^{-1}) for each generic land cover class in the default configuration of FINN. Reference Emmons et al. (2010a) for description of lumped species.

	Generic Land Cover Type					
MOZART 4 Species	Savanna/ Grasslands	Tropical Forest	Temperate Forest	Agriculture	Boreal Forest	Shrublands
BIGALD	0.02	0.01	0.01	0.01	0.01	0.02
BIGALK	0.20	0.13	0.11	0.09	0.16	0.42
BIGENE	0.45	0.52	0.22	0.37	0.35	0.63
$C_{10}H_{16}$	0.01	0.04	0.03	0.00	0.04	0.01
C_2H_4	2.27	1.38	1.11	1.08	1.62	2.30
C_2H_5OH	0.02	0.01	0.01	0.01	0.01	0.02
C_2H_6	0.82	0.82	0.29	0.43	1.63	1.01
C_3H_6	0.43	0.56	0.26	0.38	0.76	0.77
C_3H_8	0.18	0.10	0.10	0.08	0.13	0.37
CH_2O	2.12	2.08	1.33	1.84	1.46	2.23
CH_3CHO	1.03	1.27	0.38	3.05	0.67	0.96
CH_3CN	0.21	0.36	0.12	0.55	0.13	0.41
CH_3COCH_3	0.22	0.39	0.20	0.83	0.20	0.71
CH_3COCHO	0.81	0.37	0.17	0.19	0.28	0.86
CH_3COOH	2.08	1.87	0.53	2.19	1.80	1.24
CH_3OH	1.92	2.60	1.51	2.11	2.50	2.49
CRESOL	0.44	0.17	0.07	0.60	0.85	0.00
GLYALD	0.50	0.79	0.28	1.68	0.25	1.39
HCN	1.01	0.56	0.51	0.33	2.49	1.29
HYAC	1.01	0.55	8.03	0.00	0.77	0.00
ISOP	0.05	0.07	0.03	0.60	0.14	0.03
MACR	0.00	0.08	0.00	0.00	0.00	0.00
MEK	1.31	0.85	0.41	0.79	1.64	1.16
MVK	0.00	0.20	0.00	0.00	0.00	0.00
NO	0.38	0.74	0.26	0.09	0.70	0.74
TOLUENE	1.16	2.06	0.61	1.07	1.30	1.32
HCOOH	0.65	0.44	0.26	0.90	0.57	0.16
C_2H_2	0.72	0.36	0.14	0.21	0.20	0.55

4. CAMx Base Case

4.1 Configuration

A 2008 CAMx dataset developed by Alpine Geophysics for the Eight Hour Coalition (a cooperative of Houston petrochemical and refining companies) was selected for this work. The episode spans April 1 – October 18, 2008. The model configuration and default input data are summarized in Table 5. The dataset included ozone and particulate matter precursor emissions from the Texas Commission on Environmental Quality (TCEQ) and the U.S. Environmental Protection Agency (EPA), a 36-km grid over the continental U.S., and a 12 km grid over Texas and many surrounding states (Figure 3). A 4-km grid was also developed for southeastern Texas. Simulations were performed inclusive of the nested grid, although the analyses were based on aggregated output from the coarser resolution domain. Biogenic emissions are available from both MEGAN and GloBEIS; GloBEIS was selected for this work because it has been used by the TCEQ in support of the development of State Implementation Plans (SIP) for Texas and its use also provides consistency with another Texas Air Quality Research Program (AQRP) project (AQRP Project No. 12-011: *Analysis of Global Models as a Source of Regional Background Ozone in Texas*) for which its use is cost-shared. All emissions are speciated for the CB05 chemistry mechanism.

Table 5. Model configuration and default input data for the 2008 CAMx model.

Model Component	**Description**
Modeling Period	April 1 - October 18, 2008
Modeling Domain	36/12/4 km
Vertical Structure	30 Vertical Layers
Meteorological Model	WRF
Chemical Mechanism	CB05
Boundary Conditions	MOZART4
Deposition	Zhang
Emissions	
• Biogenics	MEGAN or GloBEIS
• On Road Mobile	MOVES
• Off Road Mobile	EPA NEI
• Shipping	EPA NEI
• Area Source	EPA NEI
• Point Source	TCEQ
• Wildfire	BlueSky/EPA SmartFire 2

Figure 3. CAMx modeling grids: Outer 36 km grid, 12 km nest (red), 4 km nest (green). Note the 4-km grid will not be used for this work.

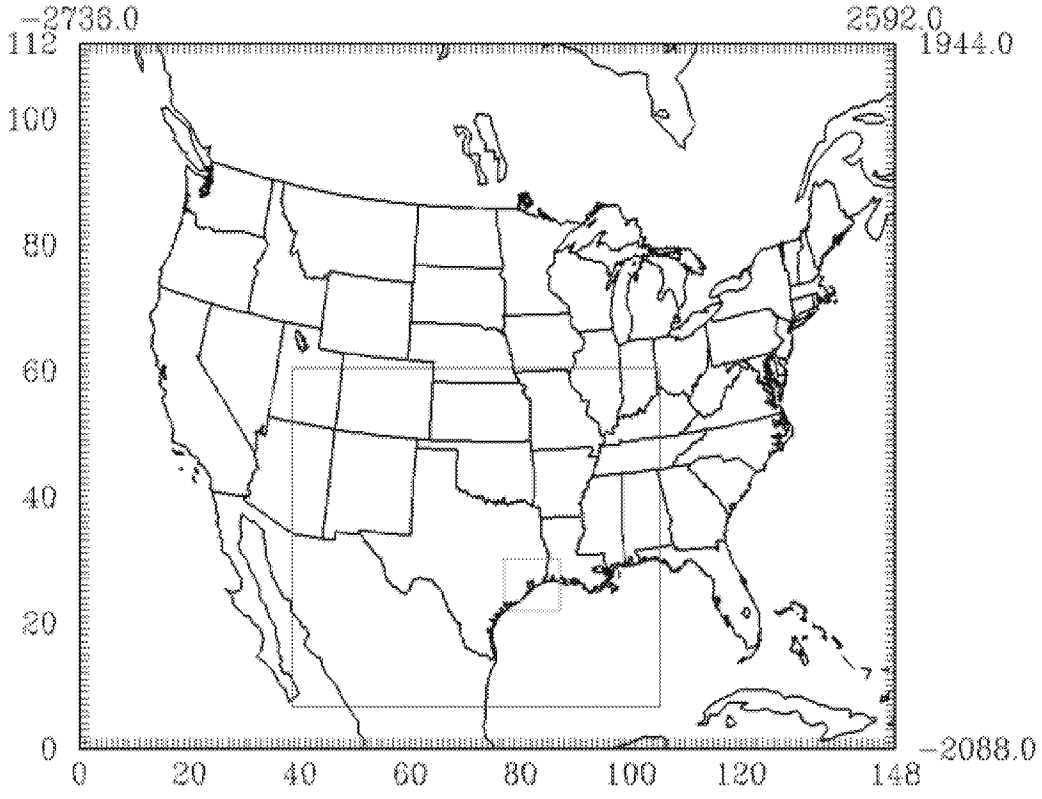

4.2 BlueSky/SmartFire 2 Emissions Inventory

Wildfire emissions for this CAMx dataset were originally developed from products generated by the BlueSky system and the EPA Satellite Mapping Automatic Reanalysis Tools for Fire Incident Reconciliation (SmartFire), version 2. As described by Larkin and Raffuse (2012) and Chinkin et al. (2009), BlueSky and SmartFire are not models, but rather form a framework for fire emissions modeling. As shown in Figure 4 from Larkin and Raffuse (2012), the BlueSky/SmartFire frameworks incorporate multiple model and data source component options for fire detection, area burned, fuel loading and characteristics, total fuel consumption, time rate of consumption, and emissions factors. The BlueSky framework was developed for estimating smoke emissions, while SmartFire was a later addition designed for the reconciliation and unification of disparate sources (e.g. satellite, ground-based, expert) of fire information (Raffuse et al., 2009; Larkin and Raffuse, 2012; Chinkin et al., 2009).

Figure 4. From Larkin and Raffuse (2012). BlueSky and SmartFire framework and options for model components.

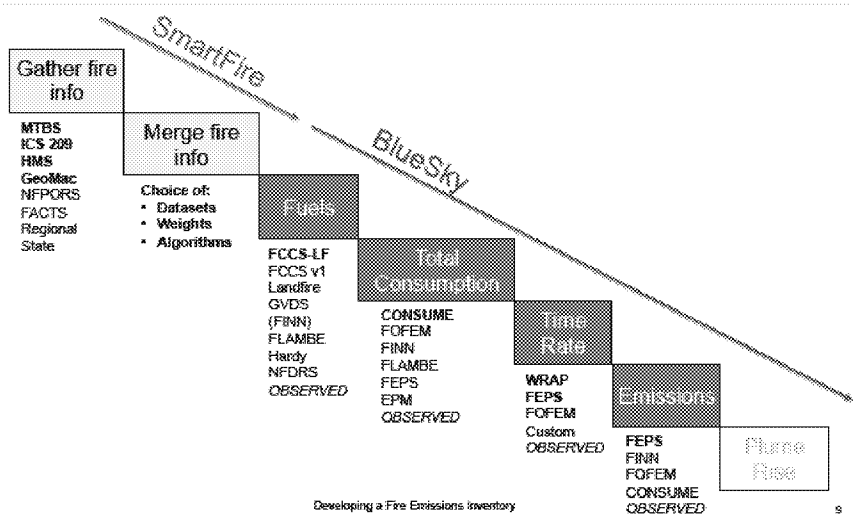

The development of 2008 BlueSky/SmartFire fire emissions estimates was conducted by Sonoma Technology, Inc. (STI) and is described by Pollard et al. (2011). This particular database was developed to support the EPA's National Emissions Inventory (NEI) program for the years 2006 through 2009; fire inventories were generated in EPA's Emissions Inventory System (EIS) "Events" format (Pollard et al., 2011). Pollard et al. (2011) later documented revisions to the 2008 inventory, which were used by Alpine Geophysics in developing the CAMx modeling database to be used in this project. A summary is presented here.

STI used BlueSky to prepare daily emission estimates for wildland fires, wildland fire use, and prescribed burns for the lower 48 states. Within BlueSky, the most recent versions of FCCS, CONSUME 3.0, and the Fire Emission Production Simulator (FEPS) models were used to model vegetation distribution, fuel consumption, and emission rates, respectively. SmartFire was used to reconcile ICS-209 ground reports with information from the National Oceanic and Atmospheric Administration (NOAA) Hazard Mapping System (HMS). HMS data consist of fire information obtained from satellite borne sensors (i.e., Moderate Resolution Imaging Spectroradiometer (MODIS), Advanced Very High Resolution Radiometer (AVHRR), and Geostationary Earth Observing Satellite (GOES) Instruments) and "enhanced by human quality control" (Pollard et al, 2011). STI conducted manual inspections of the fire reporting data aimed at improving the fire information. STI used the FCCS module within BlueSky for fire typing to distinguish wildland and agricultural fires, shown in Figure 5.

Figure 5. Distribution of wildland and agricultural fires in the 2008 STI inventory (Pollard et al., 2011).

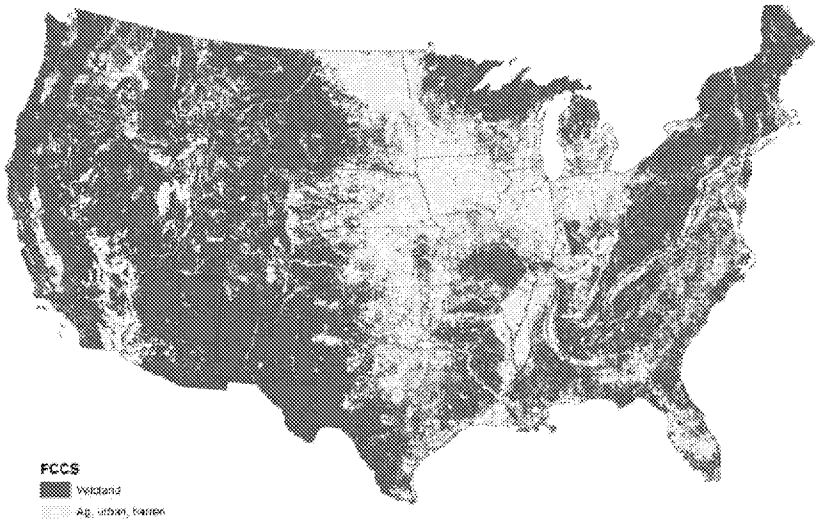

Alpine Geophysics used the Sparse Matrix Operator Kernel Emissions (SMOKE) model, version 2.7, to process the Bluesky/SmartFire fire inventory database into model-ready formats. Fire estimates included wild and prescribed/agricultural fires. SMOKE allocated discrete fire location data to the 36 and 12 km grid systems, determined hourly plume rise and depth according to the size of area burned and fuel loading (UNC, 2010), and speciated criteria pollutants (NOx, VOC, CO, PM) into modeled compounds specific for the CB05 chemistry mechanism. Model-ready emission files were output from SMOKE in CMAQ formats, and were then converted to CAMx formats using separate software. SMOKE placed emissions directly into the three-dimensional grid system, so individual fire locations were aggregated to single injection points at the midpoints of each grid cell horizontally and vertically.

The SMOKE spatial allocation process differs from the approach to be used in this project, for which FINN emission estimates are processed by the Emissions Processing System, version 3 (EPS3) as individual point sources with little loss of spatial information. Additionally, the fire plume rise calculations in EPS3 are based on techniques developed for regional modeling by the Western Regional Air Partnership (WRAP; Morris et al., 2012). EPS3 generates fire point source data directly into CAMx-ready formats. The EPS3 processing methodology used for to obtain CAMx-ready input from FINN emissions estimates work is described in Section 4.3.

4.3 EPS3 Processing of FINN Emissions

Seven fire emission inventories, described in Section 7, were developed with FINN framework and processed for use with CAMx using EPS3. One of the six inventories utilized SmartFire for the identification of fire locations and estimated area burned; this inventory required a different processing methodology. The six FINN datasets consisted of daily emissions at each fire point, which typically represented the center of a 1-km^2 area that coincided with a satellite pixel. The SmartFire inventory listed the actual fire size for each location. Emission species included NO, NO_2, CO, SO_2, NH_3, various PM components, and NMOC's chemically speciated to MOZART-4 species (reference Table 4) for six fire types – tropical, temperate, and boreal forests, cropland, shrublands, and grasslands. Emissions were processed into CAMx binary point source files using an updated version of EPS3 v3.20 and two preprocessors – firespec and grouppts. Firespec filtered and removed the fires outside of the CAMx 36 km domain and remapped the MOZART-4 species to CAMx CB05 species listed in Table 6. Grouppts

Table 6. Mapping of MOZART-4 species to CAMx CB05 species. Note that FPRM, PSO4, and PNO3 were allocated using default WRAP profiles for agricultural burning (applied to shrubs, grasslands, and agricultural burning) and for wildfires (applied to all forest fires).

CAMx	MOZART-4
NO	NO
NO2	NO2
CO	CO
FORM	CH2O
ALD2	CH3CHO
ALDX	GLYALD
ETOH	C2H5OH
MEOH	CH3OH
ETHA	C2H6
AACD	CH3COOH
FACD	HCOOH
PAR	C3H6 + 1.7*BIGENE + 5.0*BIGALK + 1.5*C3H8 +3.0*CH3COCH3 + 4.0*MEK + 1.0*C2H2 + 3.0*HYAC
ETH	C2H4
OLE	C3H6 + BIGENE
ISOP	ISOP
ISPD	MACR + MVK
TERP	C10H16
TOL	0.3*TOLUENE
XYL	0.1*TOLUENE
CRES	CRESOL
OPEN	BIGALD
MGLY	CH3COCHO
SO2	SO2
NH3	NH3
BENZ	0.6*TOLUENE
TOLA	0.3*TOLUENE
XYLA	0.1*TOLUENE
ISP	ISOP
TRP	C10H16
NR	C2H2 + 1.5*C3H8 + 0.5*TOLUENE + 0.3*BIGENE
CH3CN	2.0*CH3CN
HCN	HCN
CH4	CH4
POA	1.7*OC
PEC	BC
CPRM	PM10 – PM25
FPRM + PSO4 + PNO3[a]	Max(0.0, PM25 – 1.7*OC – 1.0*BC)

identified fire points that were within 5 km of one another and assigned each of these fire points properties of a larger fire; the program also formatted the data to make it ready for EPS3 processing.

EPS3 incorporated the WRAP methodology[1] to temporally and vertically allocate the fire emissions. One of the inputs needed for this computation was the virtual area for each fire, which was a function of the fire size and fuel loading. The virtual area was used to classify each fire into one of five fire size bins, which determined the values used to calculate the fraction of emissions allocated to the first vertical layer in CAMx and the heights of the plume bottom and top for each hour of the day. Larger virtual areas resulted in taller plumes, as illustrated Figure 6.

Since the FINN fire inventories consisted of fires that were always less than or equal to 1 km^2 in size, fire points that were within 5 km of one another were assumed to be part of the same fire; the virtual areas of each of these points were summed together in the grouppts preprocessor so they would have characteristics of a larger fire. Fuel loading data were not available in the FINN fire inventory, so the virtual areas were estimated from a regression line using an existing 2005 MODIS fire inventory of the same 36 km domain in which a strong linear relationship was found between the virtual area and daily NO_x emissions (Figure 7).

Figure 6. Diurnal profile of the vertical distribution of the fire plumes (red) and the fraction of hourly emissions allocated to CAMx vertical layer 1 (green) in each of the five fire classes.

Class 1: Virtual area < 10 acres	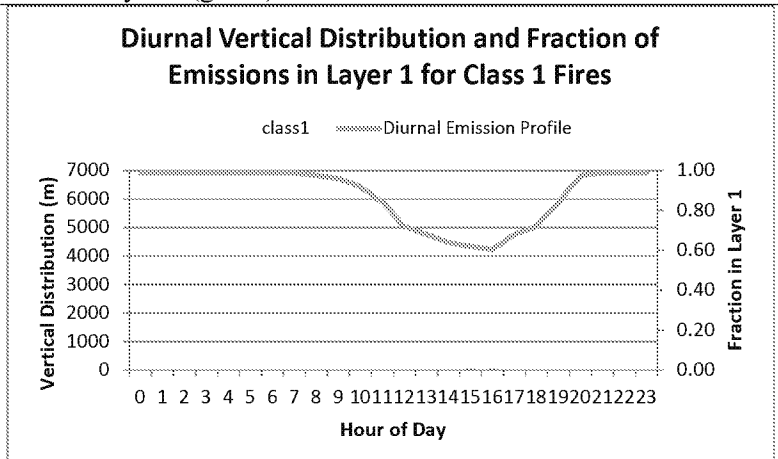
Class 2: Virtual area 10-100 acres	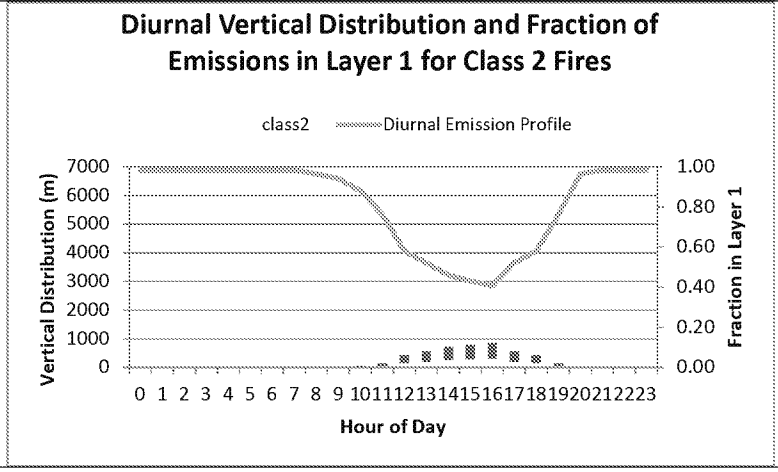

[1] http://www.wrapair.org/forums/fejf/documents/WRAP_2002_PhII_EI_Report_20050722.pdf

Class 3: Virtual area 100 – 1000 acres	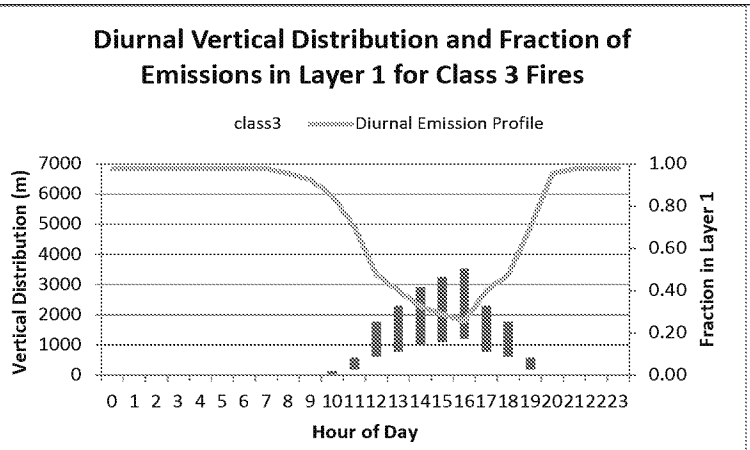	
Class 4: Virtual area = 1000 – 5000 acres	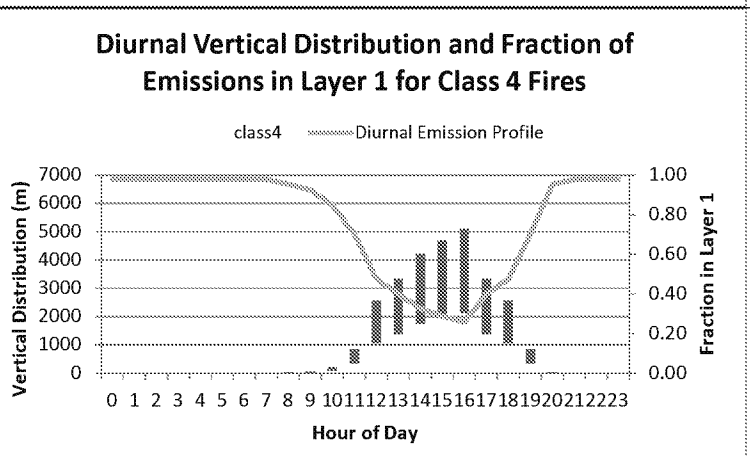	
Class 5: Virtual area > 5000 acres	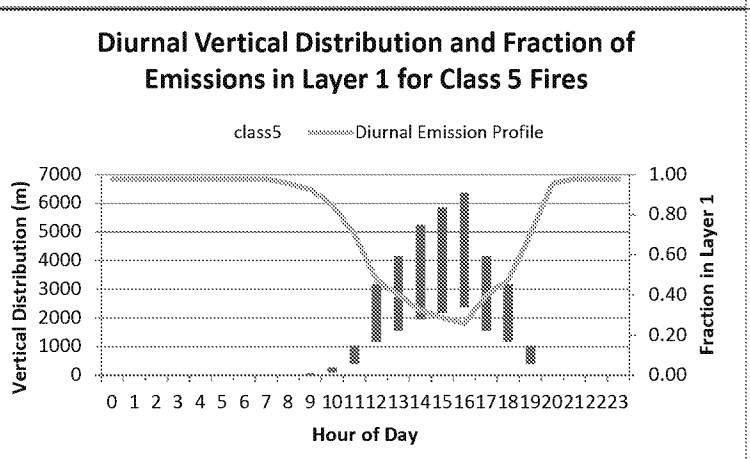	

Figure 7. Scatterplot showing the relationship between NO_x fire emissions and the virtual area.

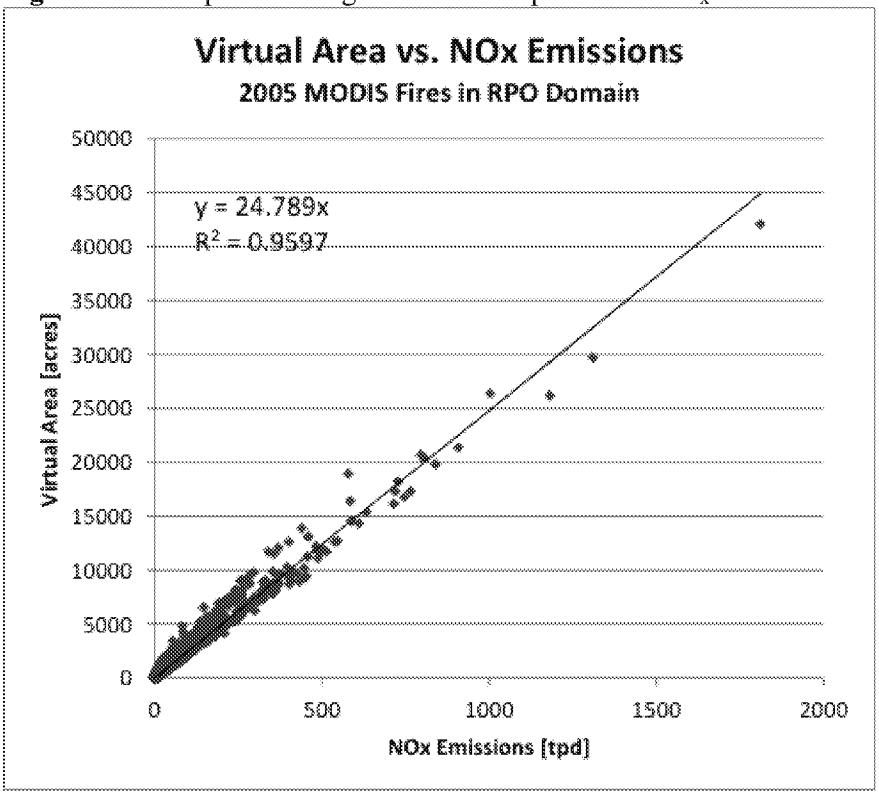

EPS3 was run using the following modules:

- PREFIR – reads in fire data
- CHMSPL – speciates the emissions (already performed in the firespec preprocessor)
- TMPRL – allocates emissions temporally
- PSTFIR – allocates emissions vertically and outputs results in ascii files
- PIGEMS – converts the PSTFIR outputs to CAMx binary point source files

Temporally, the same diurnal profile in local time was applied to all fires such that emissions were highest in the early afternoon and lowest at night, as shown in Figure 8. The time zone of each fire was approximated based on its longitude and time zones assigned to each 15 degree longitudinal section. For example, all fires located between 97.5W and 82.5W assumed GMT-6 (i.e. CST), and fires between 82.5W and 67.5W assumed GMT-5 (EST). Any emissions allocated to the next date due to a time zone shift were assigned to the same hour of the current date to maintain all daily total emissions in one daily emissions file. Vertically, a fraction of each hour's emissions was assigned to the lowest layer; the rest was distributed into multiple point sources with one point assigned to each CAMx layer between the plume bottom and plume top, weighted by the thickness of each layer. All fire points were flagged to avoid additional plume rise computation within the CAMx model. The emissions were then time-shifted to GMT to coincide with the other CAMx inputs.

All FINN datasets were processed in the same manner, except the virtual area of each fire point was modified to have the same virtual area as the co-located fire in the FINN default case. This allowed differences in CAMx to be a result of changes in the emission rates and not to changes in the plume distribution. Fires in the sensitivity study inventories that were not within 5 km of a fire in the default case retained the virtual area based on the NO_x emissions regression line.

Figure 8. Diurnal distribution of fire emissions.

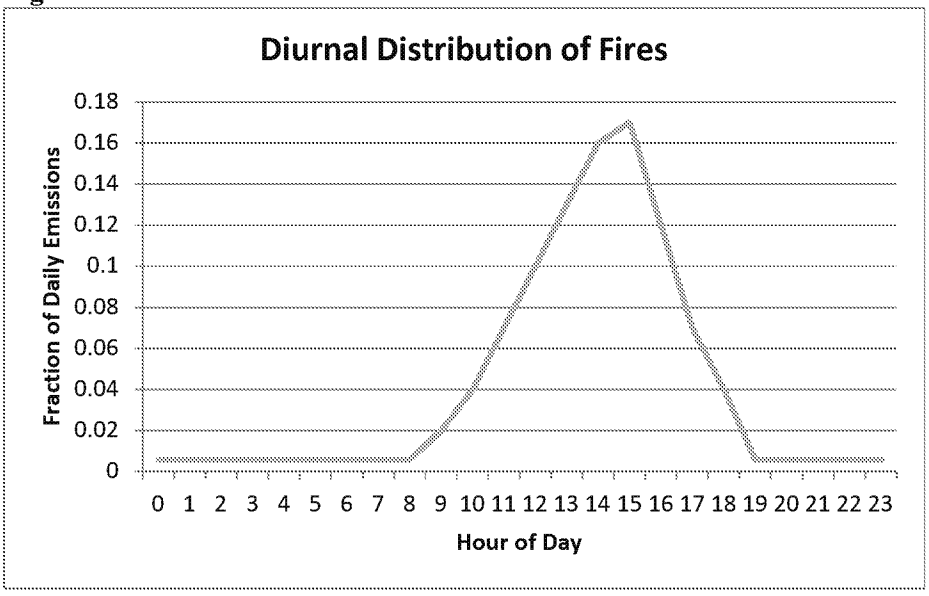

The emissions inventory that utilized SmartFire for the identification of fire locations and estimated area burned included two additional variables – fire type (wildfire, wild land fire use, or prescribed) and fuel loading. In addition, the fire size that was provided actually represented the true size, unlike the FINN default, which divided large fires into multiple 1-km^2 fires. Sufficient data were available in the SmartFire inventory to compute the virtual area using the WRAP method with no need to group nearby fires together. The non-U.S. FINN default fires were added to the SmartFire inventory, which only included data within the U.S. The non-U.S. FINN default fires were also added to the U.S.-only FINN FCCS fuel sensitivity.

5. Climatology of Fires

Figure 9 indicates that estimated monthly average CO emissions from fires during 2008 from the FINN default configuration were close to the 11-year average for 2002-2012 in the 12-km domain.

Figure 9. Comparison of predicted monthly CO emissions (kg/month) between 2008 and the 11-year average for 2002-2012 for the 12-km domain for the FINN default configuration.

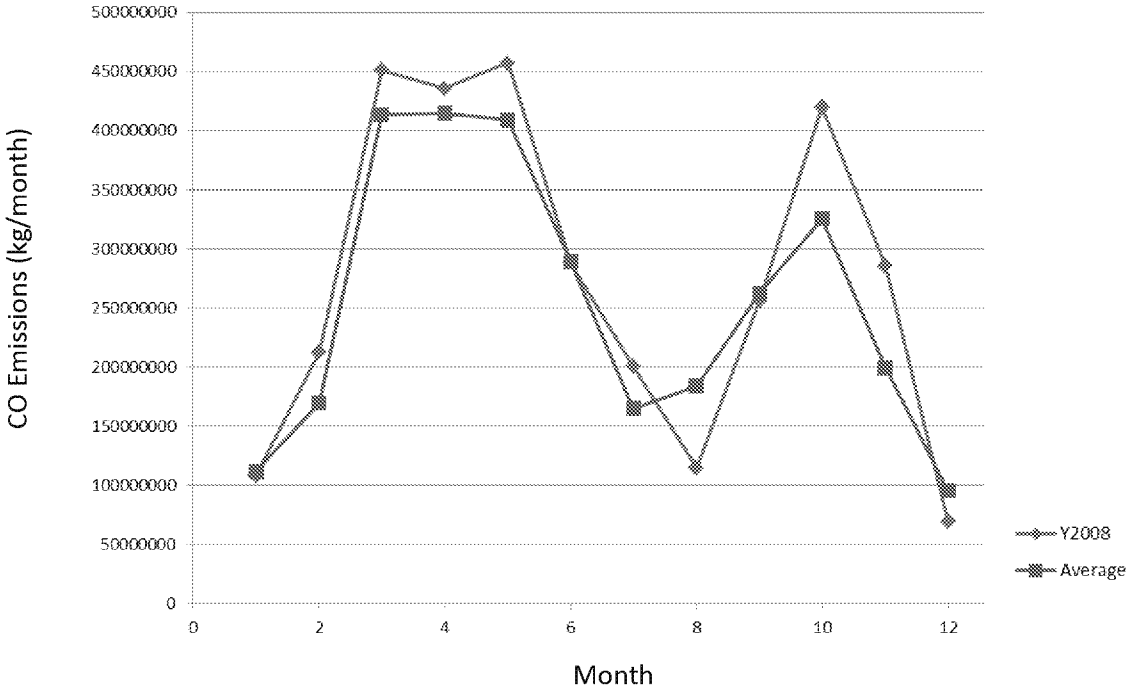

The variability in the monthly and interannual fire climatologies was explored using predicted emissions of CO (kg/month) in Texas, Louisiana, five central states (Arkansas, Kansas, Missouri, Mississippi, Oklahoma), 11 western states (New Mexico, Colorado, Wyoming, Montana, Idaho Washington, Oregon, California, Arizona, and Utah), Mexico, Central America (Guatemala, Belize Nicaragua, Costa Rica), and Western Canada. Figure 10 shows 11-year (2002-2012) monthly average CO emissions estimates from the FINN default configuration for these regions. Maps of monthly total CO fire emissions in the FINN default scenario during April through October 18th of 2008 are shown in Figure 11. Table 8 presents the interannual variability in estimated CO emissions by month and region.

Figure 10. The 11-year (2002-2012) monthly average CO emissions estimates from the FINN default configuration for (a) Texas, (b) Louisiana, (c) 5 central states (Arkansas, Kansas, Missouri, Mississippi, Oklahoma), (d) 11 western states (New Mexico, Colorado, Wyoming, Montana, Idaho Washington, Oregon, California, Arizona, Nevada and Utah), (e) Mexico, (f) Central America (Guatemala, Belize Nicaragua, Costa Rica), and (g) Western Canada.

(a)

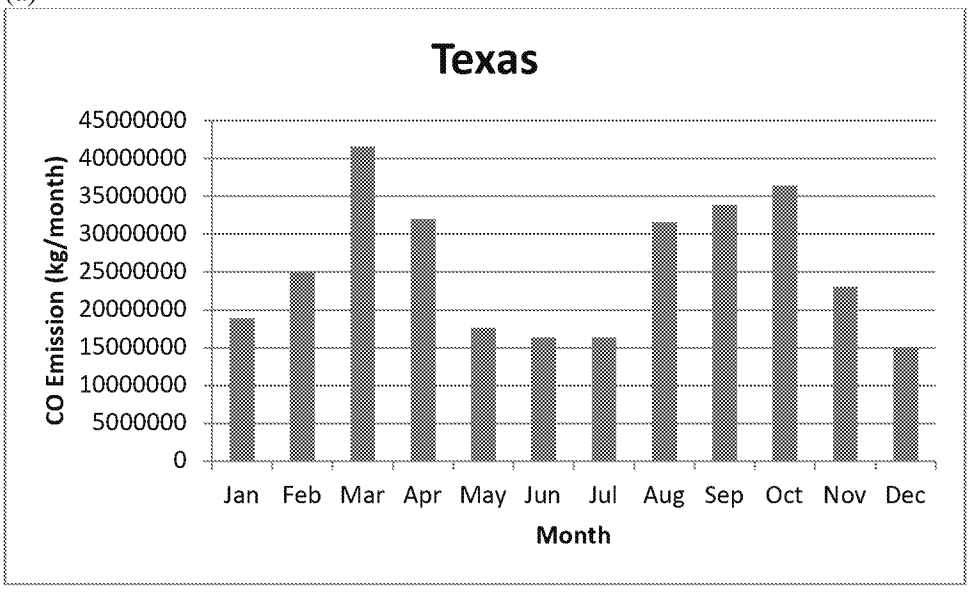

(b)

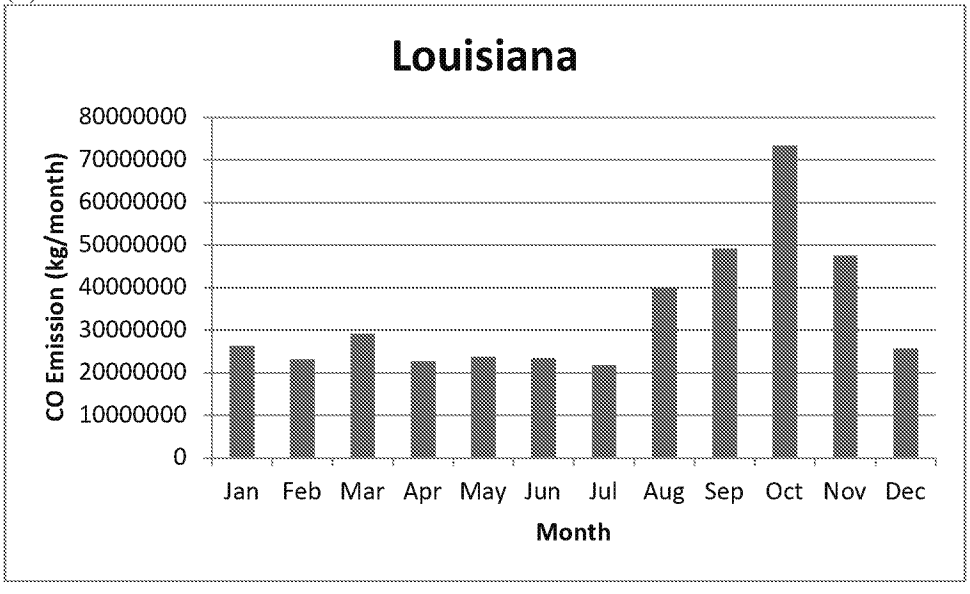

(c)

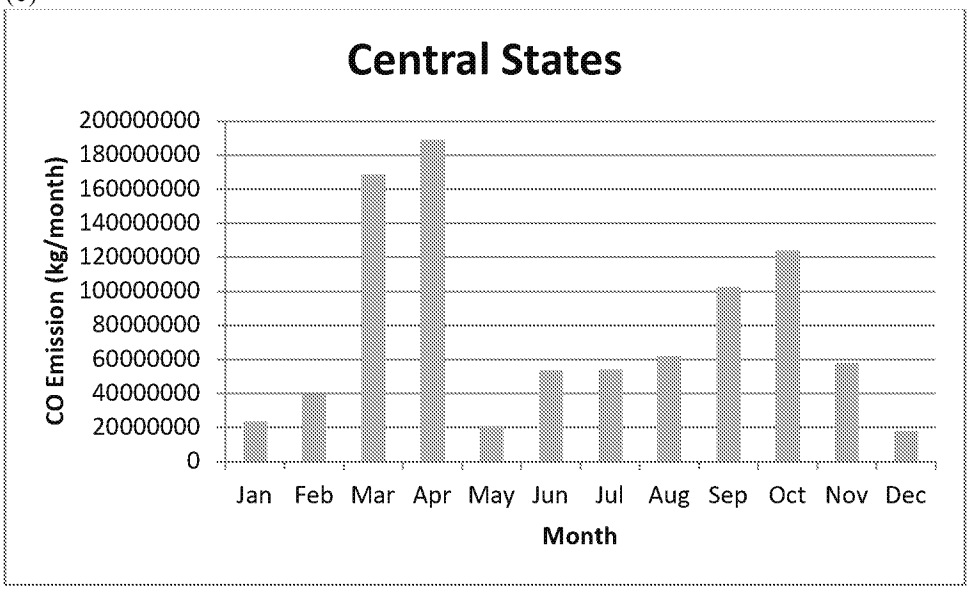
Central States
CO Emission (kg/month)
200000000
180000000
160000000
140000000
120000000
100000000
80000000
60000000
40000000
20000000
0
Jan Feb Mar Apr May Jun Jul Aug Sep Oct Nov Dec
Month

(d)

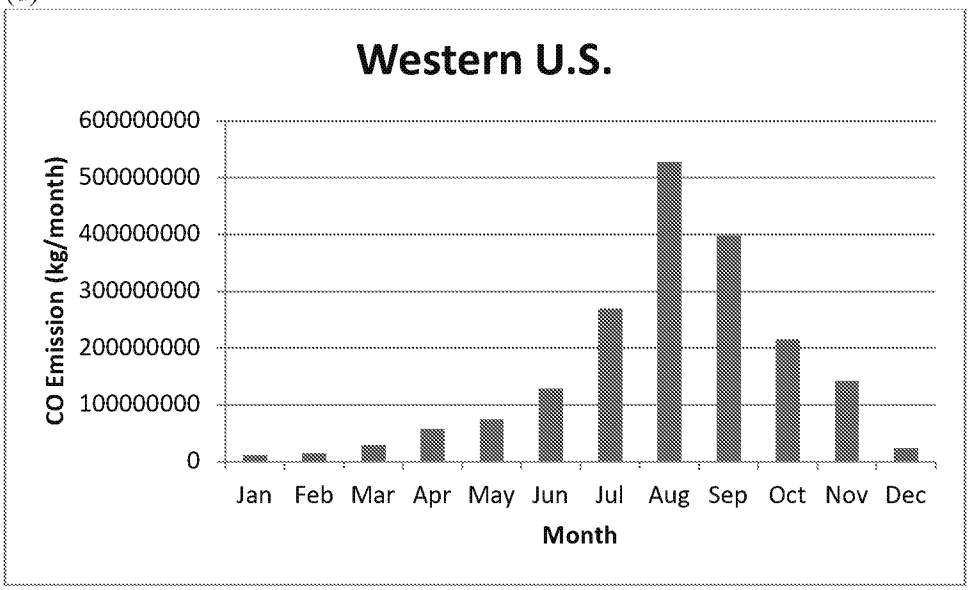
Western U.S.
CO Emission (kg/month)
600000000
500000000
400000000
300000000
200000000
100000000
0
Jan Feb Mar Apr May Jun Jul Aug Sep Oct Nov Dec
Month

(e)

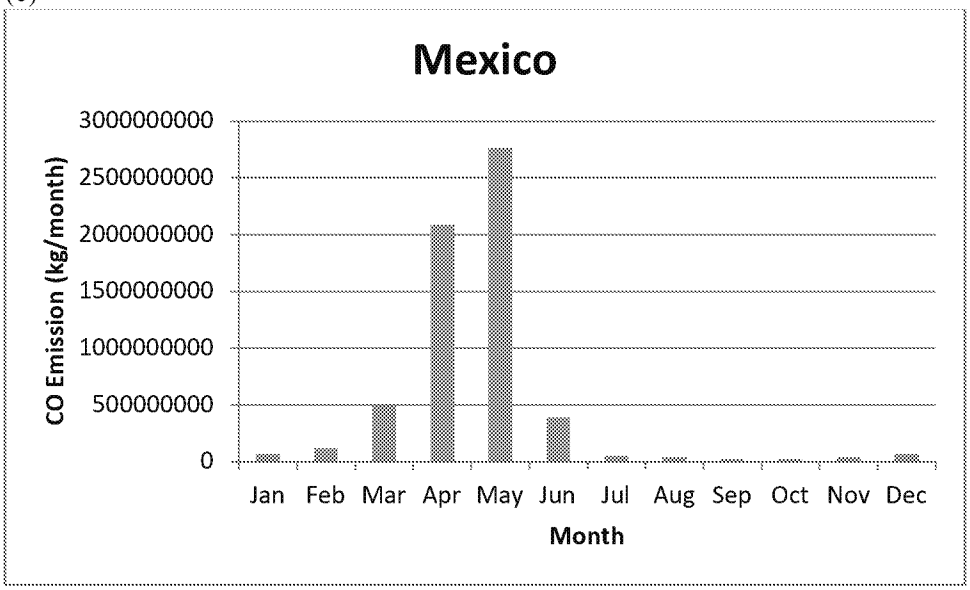
Mexico
CO Emission (kg/month)
3000000000
2500000000
2000000000
1500000000
1000000000
500000000
0
Jan Feb Mar Apr May Jun Jul Aug Sep Oct Nov Dec
Month

(f)

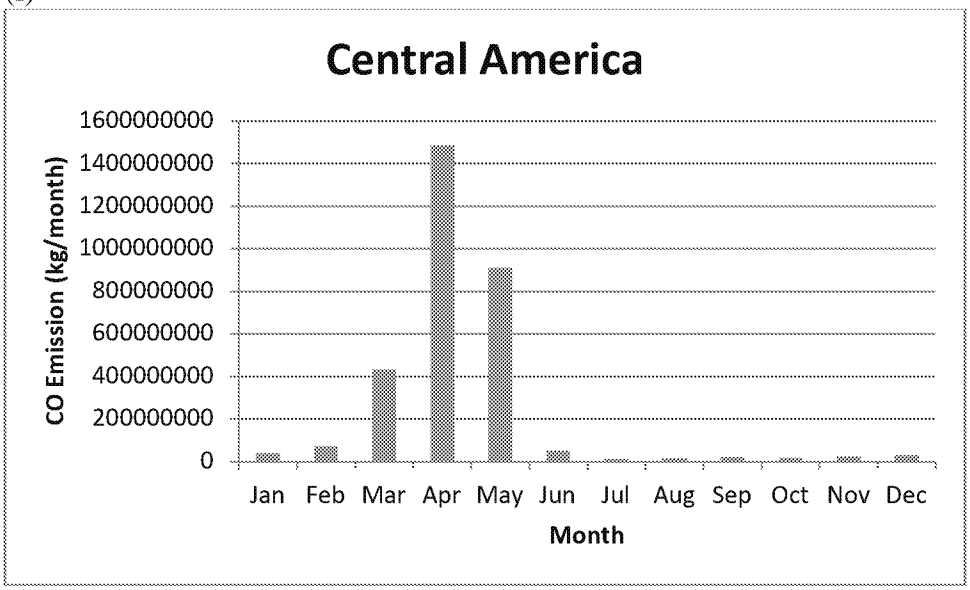
Central America
CO Emission (kg/month)
1600000000
1400000000
1200000000
1000000000
800000000
600000000
400000000
200000000
0
Jan Feb Mar Apr May Jun Jul Aug Sep Oct Nov Dec
Month

(g)

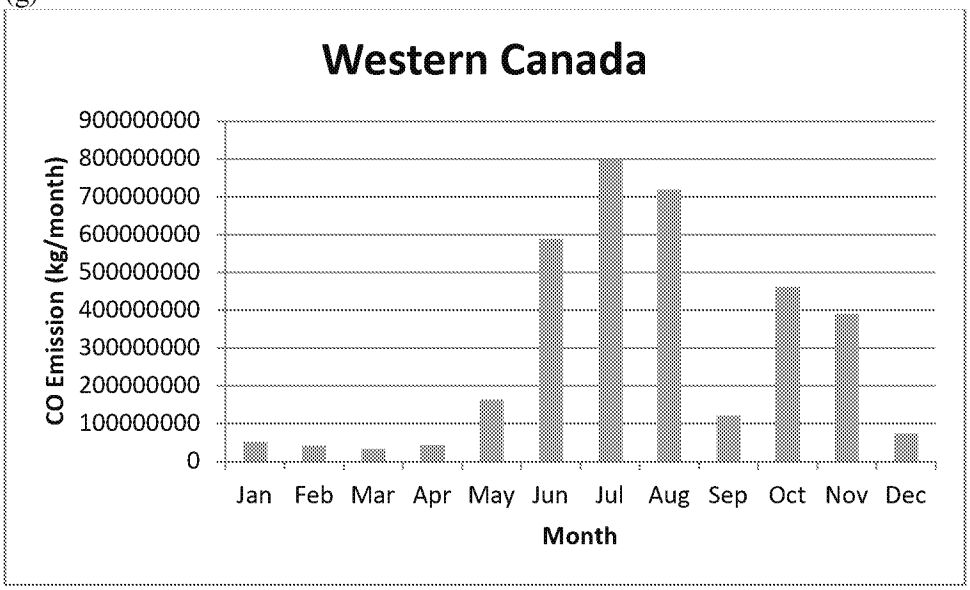
Western Canada
CO Emission (kg/month)
900000000
800000000
700000000
600000000
500000000
400000000
300000000
200000000
100000000
0
Jan
Feb
Mar
Apr
May
Jun
Jul
Aug
Sep
Oct
Nov
Dec
Month

Figure 11. Maps of monthly total CO fire emissions [tons/month] from the FINN default configuration during April through October 18th of 2008.

(a) April 2008

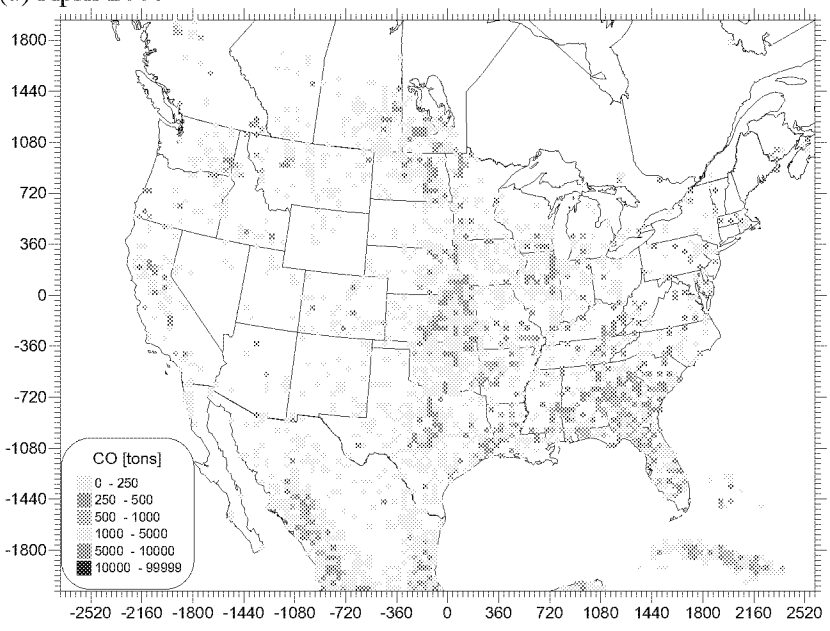

(b) May 2008

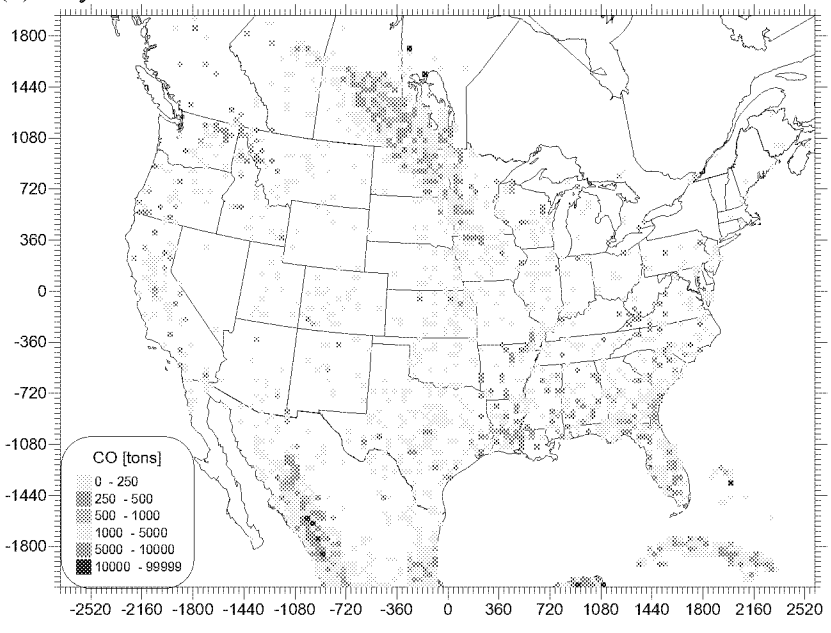

(c) June 2008

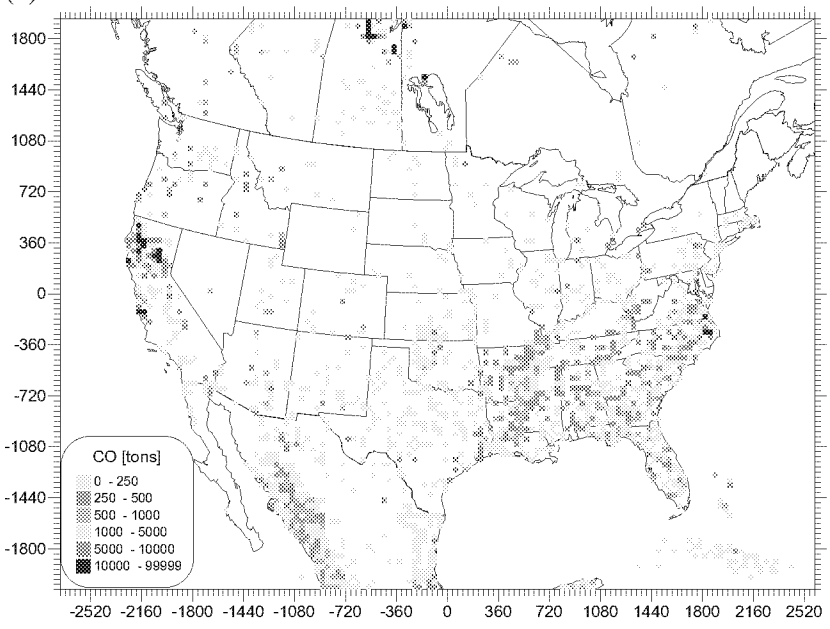

(d) July 2008

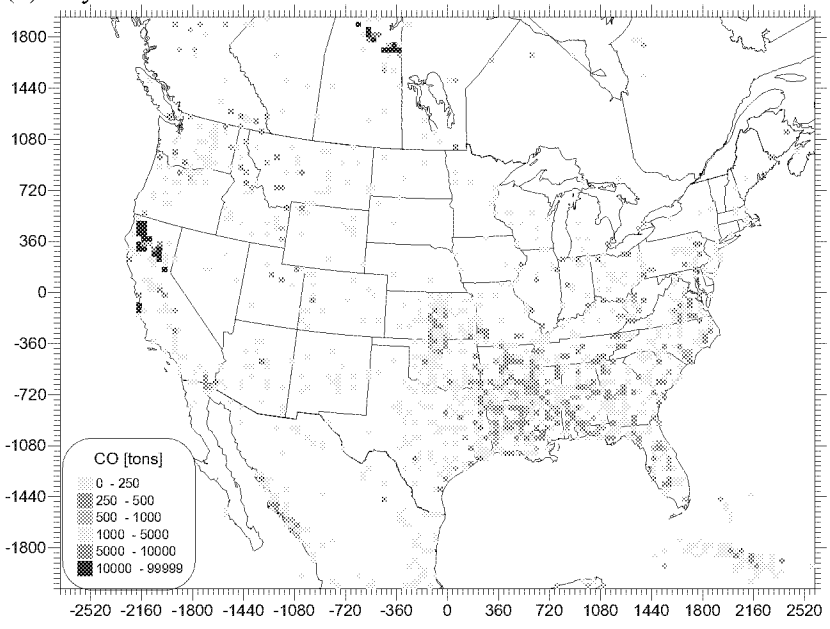

(e) August 2008

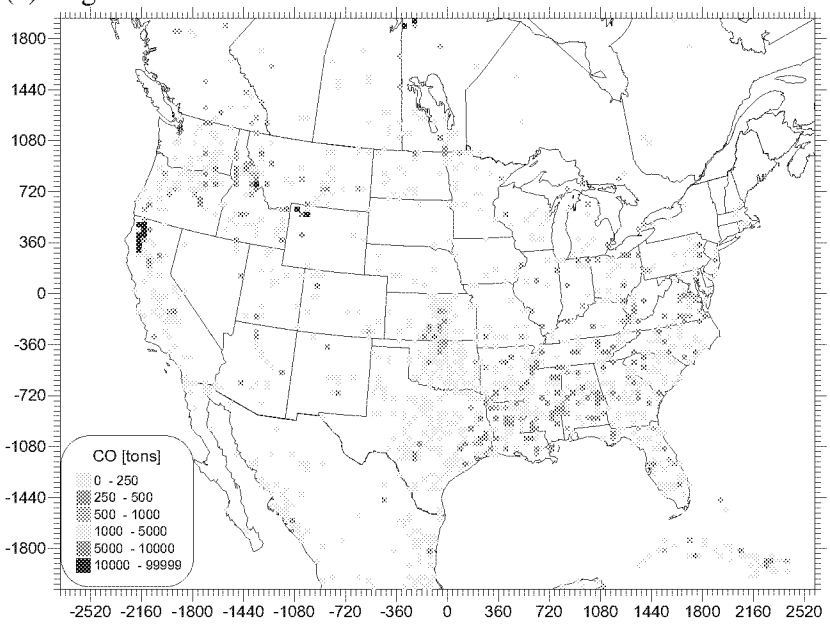

(f) September 2008

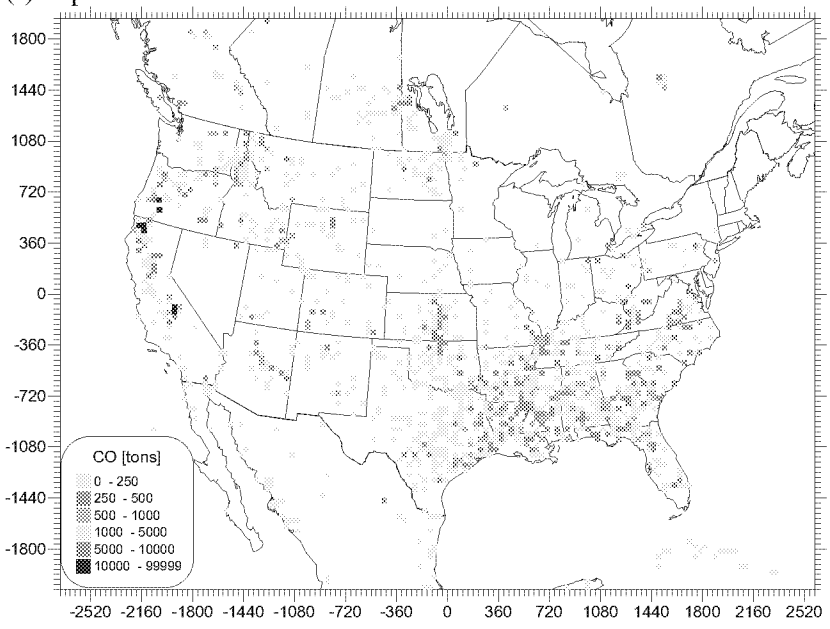

(g) October 1-18, 2008

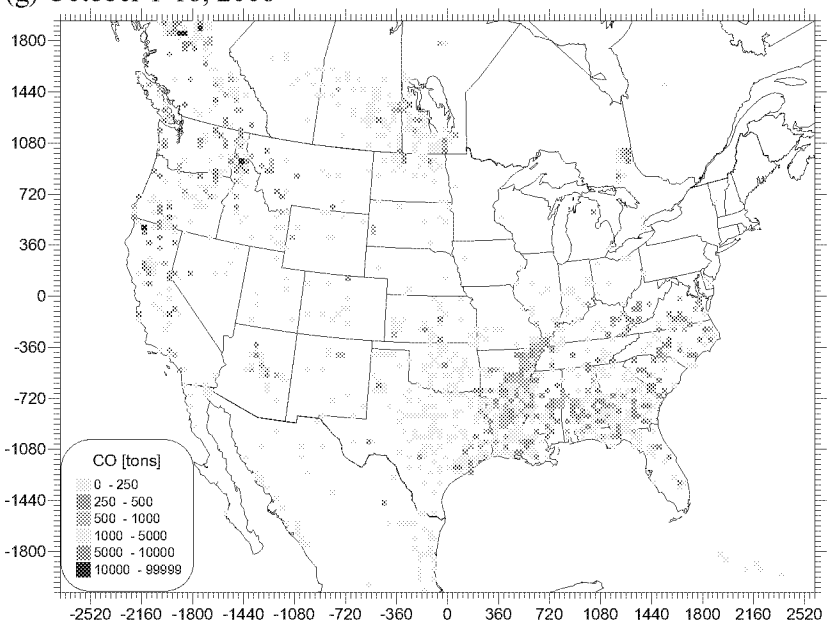

Interannual variations in CO emissions are evident in each state/region and may exceed a factor of two. Seasonal signals are pronounced. In Mexico and Central America, emissions peak in the spring associated with agricultural burning and land clearing. CO emissions across the western states peak in the mid- to late-summer and are primarily driven by wildfires. In Texas, emissions exhibit a bimodal distribution with most activity during March-April and August-October. This temporal profile reflects the combination of prescribed burning, burning in agricultural areas, and wildfires. Emissions during August-October in Louisiana are associated with burning in agricultural areas. .

Table 8. Average interannual variability* of CO emissions from fires from the FINN default configuration by region and month during 2002- 2012.

	Jan	Feb	Mar	Apr	May	Jun	Jul	Aug	Sep	Oct	Nov	Dec
Texas	46%	44%	34%	45%	40%	38%	27%	23%	21%	35%	26%	45%
Louisiana	50%	57%	40%	35%	23%	37%	27%	32%	23%	38%	22%	36%
Central States	55%	44%	11%	27%	38%	18%	22%	24%	29%	41%	30%	51%
Western U.S.	45%	38%	54%	32%	21%	56%	74%	65%	46%	24%	21%	33%
Mexico	45%	39%	55%	33%	30%	44%	39%	38%	36%	34%	33%	25%
Central America	31%	38%	76%	51%	47%	57%	59%	43%	45%	35%	29%	23%
Western Canada	64%	47%	39%	38%	91%	62%	77%	107%	83%	41%	29%	44%

* Interannual variability was determined as the average absolute percent departure from the 2002 through 2011 mean according to the approach of Tawfik et al. (2012):

$$IAV_m = \frac{1}{n}\sum_{y=2002}^{2011}\left|\frac{E_{y,m} - \overline{E_m}}{\overline{E_m}}\right| \times 100$$

where $E_{y,m}$ is monthly CO emission for year y, month m, $\overline{E_m}$ is the average monthly emission across all years (2002 - 2011), n is number of years (n=10)

6. Emissions Estimates from the FINN Default Configuration and BlueSky/SmartFire Inventories

Estimates of episode (April 1- October 18, 2008) total emissions of CO, NO_x, VOC, and $PM_{2.5}$ from the FINN default configuration and BlueSky/SmartFire inventory are shown in Figure 12 for Texas, Louisiana, five central states (Arkansas, Kansas, Missouri, Mississippi, Oklahoma), and 11 western states (New Mexico, Colorado, Wyoming, Montana, Idaho Washington, Oregon, California, Arizona, Nevada and Utah). Time series of emissions in Texas during the episode period are shown in Figure 13. The spatial distributions of emissions from the two modeling configuration within the 12-km domain are shown in Figure 14.

Emission estimates between the FINN and BlueSky/SmartFire frameworks varied by as much as a factor of seven; with the exception of NO_x, emissions from BlueSky/SmartFire were generally larger than those from FINN. One reason underlying the differences was associated with estimates of burned area using SmartFire. The SmartFire model uses a combination of reported area burn information in conjunction with multiple satellite detections of fire activity to determine daily fire location and size. This often (although not always) results in a considerably larger estimate of burned acreage than the default FINN method, which relies on a single product derived from MODIS observations. For example, in Texas for the months of April through September 2008, the SmartFire estimate of area burned was $3.6e^5$ ha, 85% more than the $2.0e^5$ ha estimated by FINN. The increase in acreage burned leads to higher emission estimates, when all else is relatively equal. This is clearly not the case for NO_x emissions. Despite larger estimates of area burned by SmartFire, FINN emission estimates are much greater for NO_x. This is most pronounced in areas with significant crop and agricultural burning (ref. Figures 12 and 13). Emission factors applied by FINN in croplands are 1.7 g NO/kg burned and 3.9 g NO_2/kg burned, following values from Akagi et al. (2011). A hypothesis is that higher emission factors compensate for the lower estimates of acreage burned in the central US.

Figure 12. Episode (April 1- October 18, 2008) total emissions (short tons) for (a) CO, (b) NOx, (c) VOC, and (d) $PM_{2.5}$ from the FINN default configuration and BlueSky/SmartFire inventory for (a) Texas, (b) Louisiana, (c) 5 central states (Arkansas, Kansas, Missouri, Mississippi, Oklahoma), (d) 11 western states (New Mexico, Colorado, Wyoming, Montana, Idaho Washington, Oregon, California, Arizona, Nevada and Utah). Note differences between scales for emissions estimates for the western U.S. and other areas.

(a)

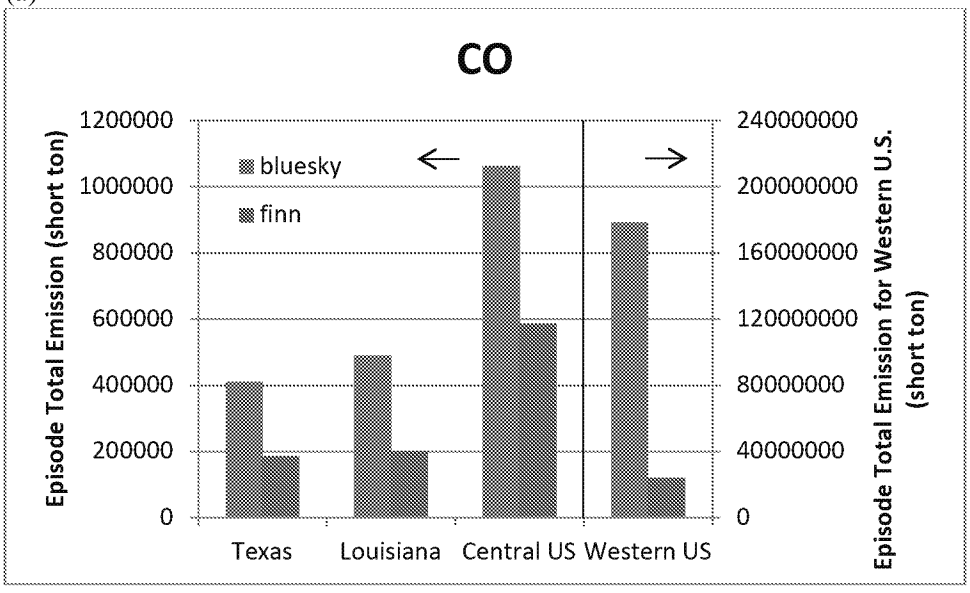

(b)

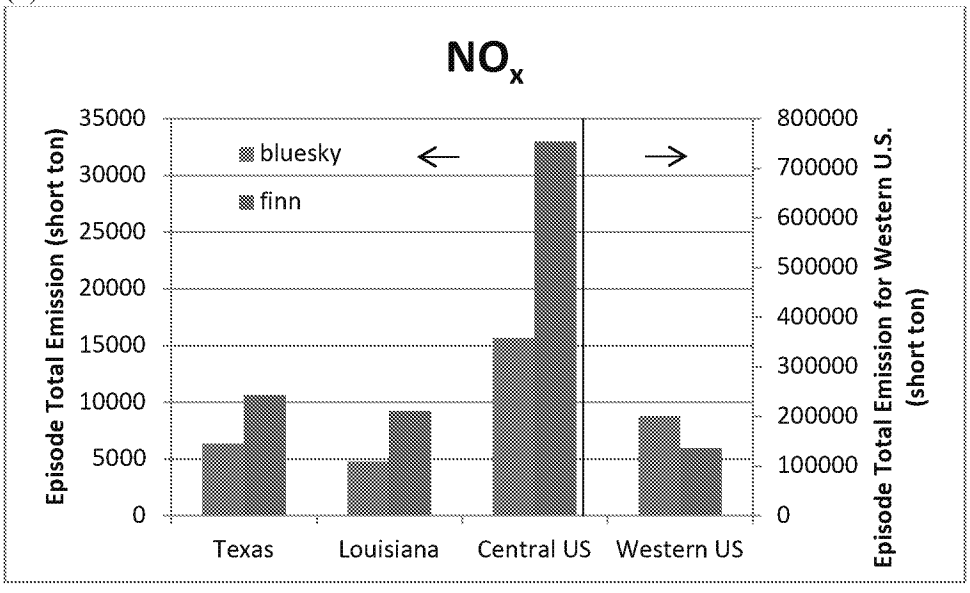

(c)

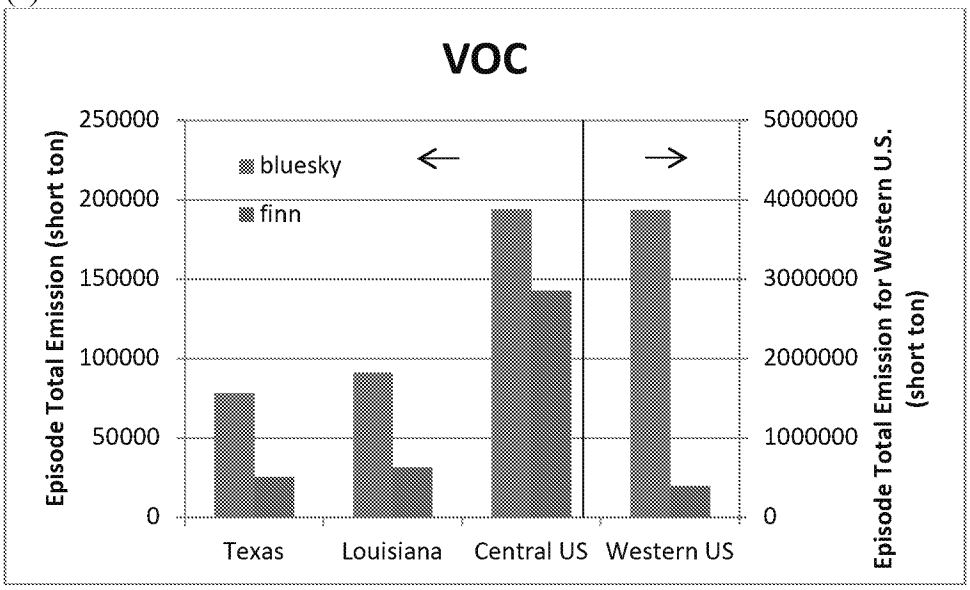
VOC
Episode Total Emission (short ton)
250000
200000
150000
100000
50000
0
bluesky
finn
5000000
4000000
3000000
2000000
1000000
0
Episode Total Emission for Western U.S. (short ton)
Texas
Louisiana
Central US
Western US

(e)

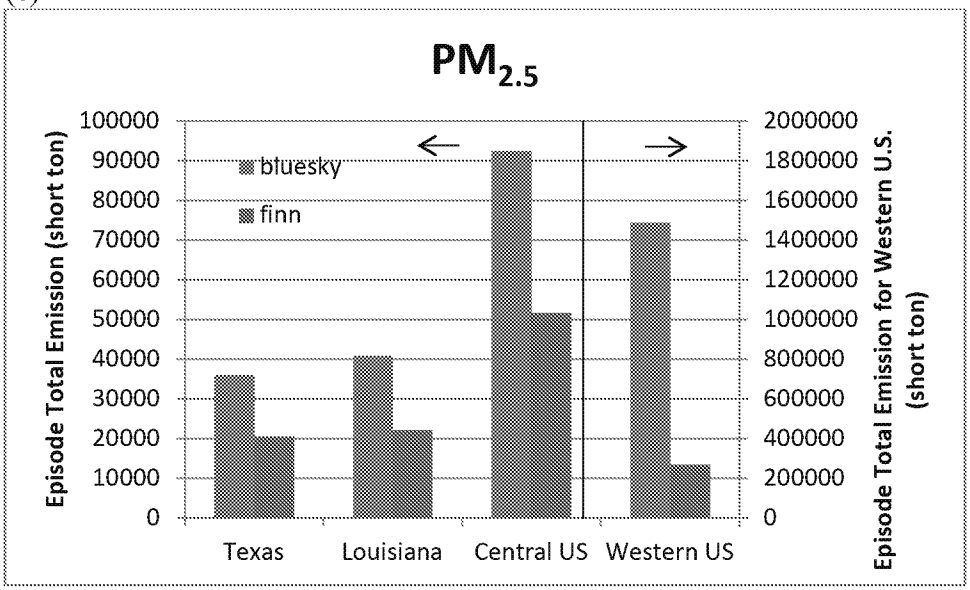
PM2.5
Episode Total Emission (short ton)
100000
90000
80000
70000
60000
50000
40000
30000
20000
10000
0
bluesky
finn
2000000
1800000
1600000
1400000
1200000
1000000
800000
600000
400000
200000
0
Episode Total Emission for Western U.S. (short ton)
Texas
Louisiana
Central US
Western US

Figure 13. Time series of emissions (short tons) of (a) CO, (b) NOx, (c) VOC, and (d) $PM_{2.5}$ in Texas from the FINN default configuration and BlueSky/SmartFire inventory during April 1- October 18, 2008.

(a)

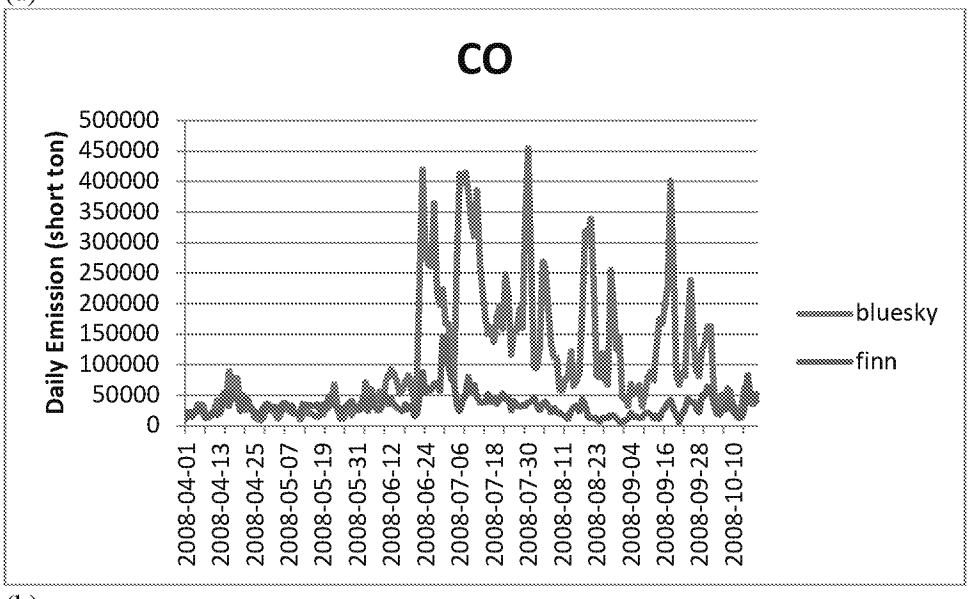

(b)

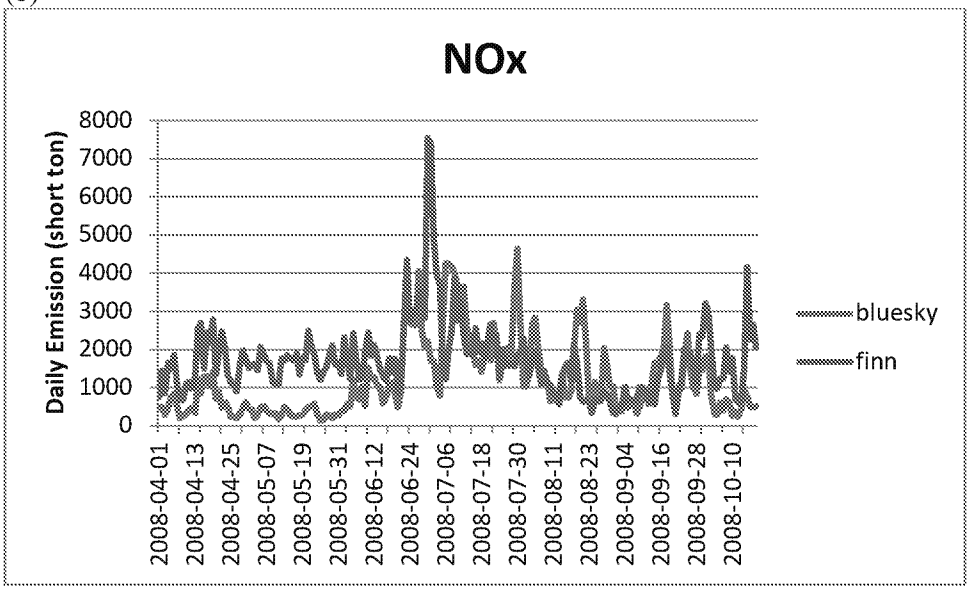

(c)

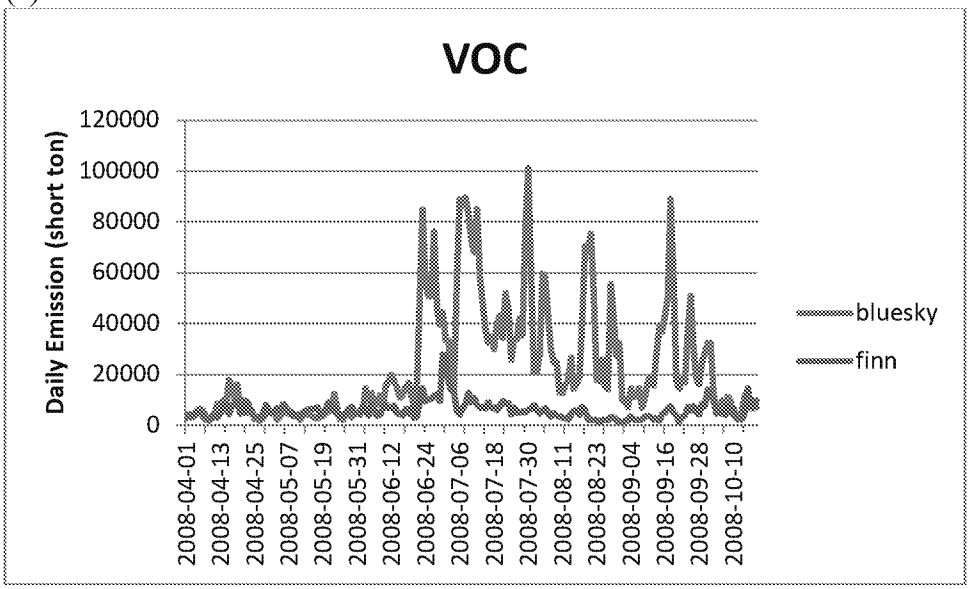
VOC
Daily Emission (short ton)
120000
100000
80000
60000
40000
20000
0
2008-04-01
2008-04-13
2008-04-25
2008-05-07
2008-05-19
2008-05-31
2008-06-12
2008-06-24
2008-07-06
2008-07-18
2008-07-30
2008-08-11
2008-08-23
2008-09-04
2008-09-16
2008-09-28
2008-10-10
bluesky
finn

(d)

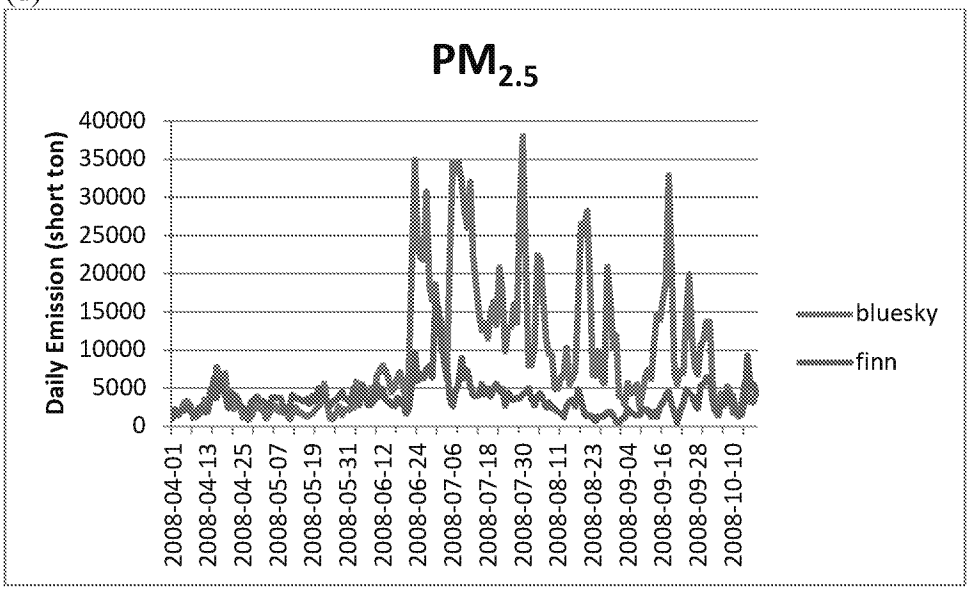
PM2.5
Daily Emission (short ton)
40000
35000
30000
25000
20000
15000
10000
5000
0
2008-04-01
2008-04-13
2008-04-25
2008-05-07
2008-05-19
2008-05-31
2008-06-12
2008-06-24
2008-07-06
2008-07-18
2008-07-30
2008-08-11
2008-08-23
2008-09-04
2008-09-16
2008-09-28
2008-10-10
bluesky
finn

Figure 14. Episode (April 1 – October 18, 2008) total emissions (short tons) of (a) CO, (b) NO_x, (c) VOC and (d) $PM_{2.5}$ from the BlueSky/SmartFire inventory (left) and FINN default configuration (right) for states within the 12-km CAMx domain. Note that BlueSky/SmartFire does not include estimates for emissions outside of the continental United States.

(a)

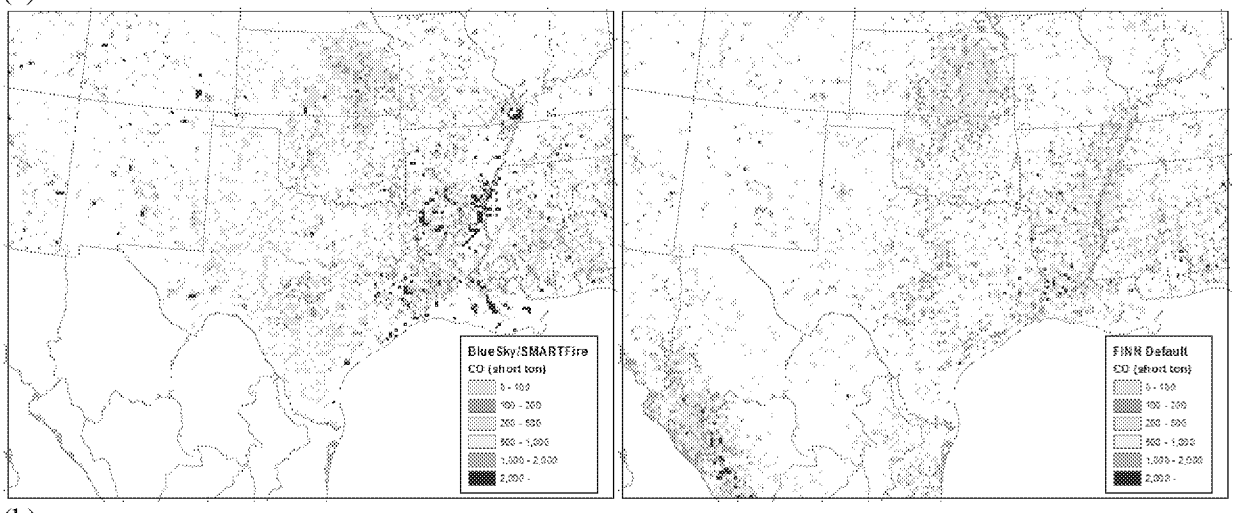

(b)

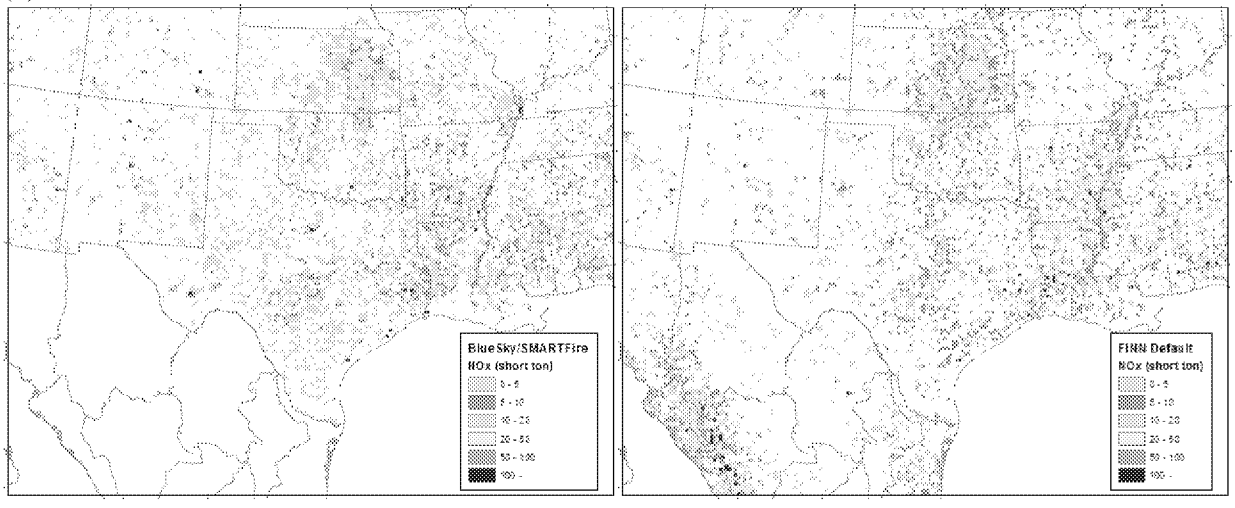

(c)

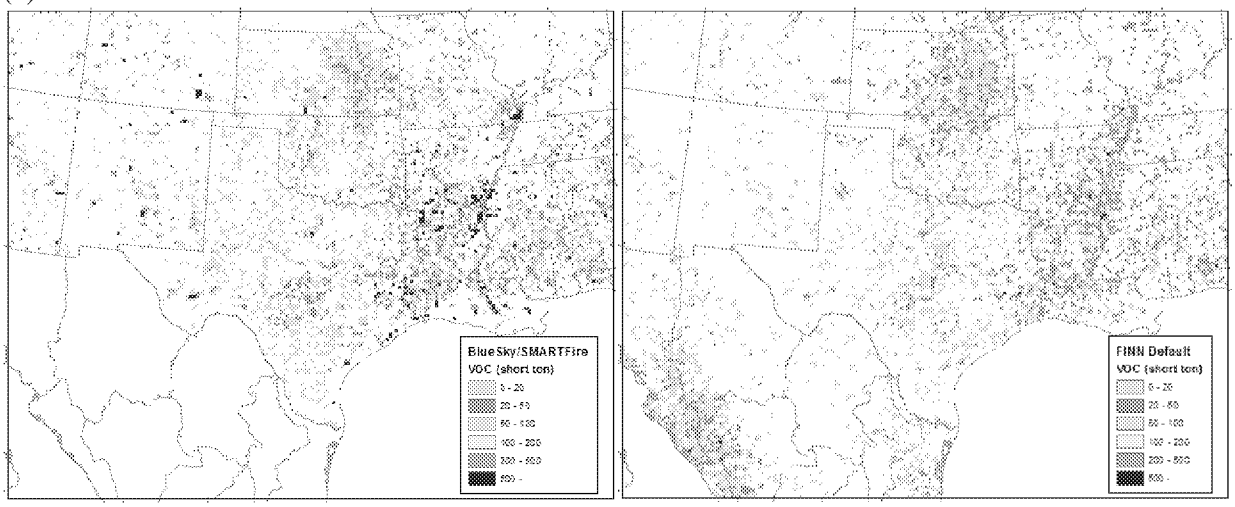

(d)

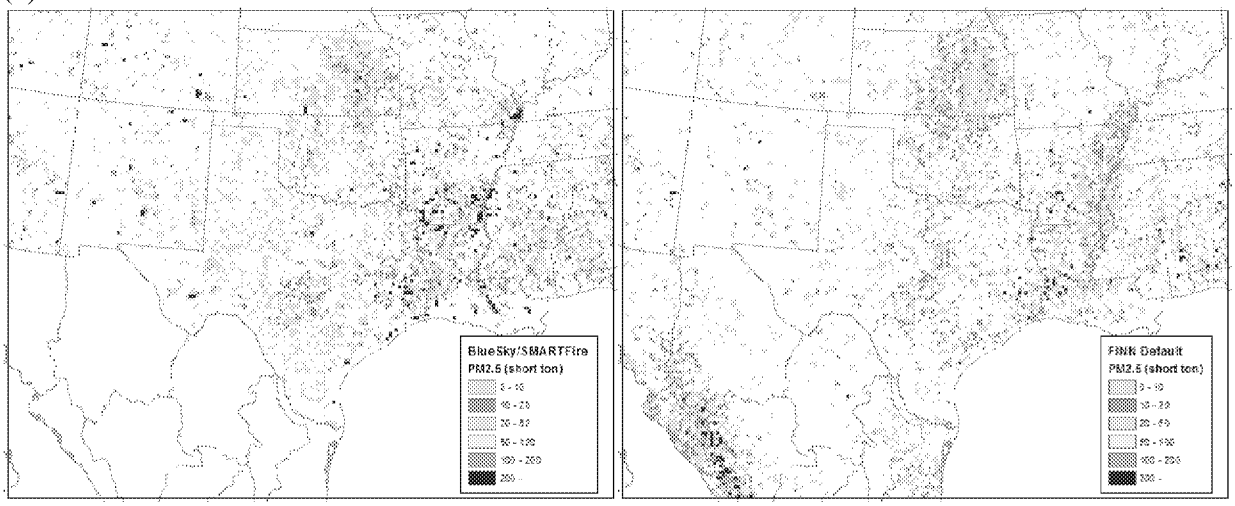

7. FINN Sensitivity Studies

Sensitivity studies were conducted with the FINN framework to examine uncertainties in the modeling process, including those associated with land use/land cover characterization, fuel loading, fire detection/burned area, and emissions factors. Scenarios varied only the input parameter under investigation; the simulations otherwise remained the same as the FINN default model configuration. The simulations are summarized in Table 9.

Table 9. Sensitivity studies performed with FINN*

RUN NAME	LAND COVER	FUEL LOADING	EMISSION FACTOR	FIRE DETECTION/ BURN AREA
DEFAULT	default	default	default	default
GlobCover	GlobCover	default	default	default
NEWEMIS	default	default	NEW	default
HIGHEMIS	default	default	HIGH**	default
LOWEMIS	default	default	LOW**	default
NEWEMIS_TEMPFOR	default	TEMPFOR+	NEW^	default
SmartFire	default	default	default	SmartFire
FCCS	FCCS	FCCS	default	default

*Default refers to inputs/parameters included in Wiedinmyer et al. (2011) for FINN version 1 and described in Section 3 of this report.
**Note that LOWEMIS and HIGHEMIS represented modifications to the NEWEMIS scenario (not the FINN default scenario).
^ This simulation was a version of the NEWEMIS that include additional changes in vegetation assignment (described below).
+ Evergreen forests were assigned corresponding fuel loadings of temperate forest rather than boreal forest as assumed in the default configuration.

7.1 Emissions Factors

Emission factors in FINN were updated from the original values used in the default model (Table 3). These new emission factors (New) were based on updates to the results of Akagi et al. (2011), reported by Akagi et al (2013) and are available at http://bai.acd.ucar.edu/Data/fire/ (ref. version 3 emission factor tables). Akagi et al. (2011; 2013) included estimates of uncertainty with the reported emission factors. Upper (High) and lower (Low) limits of the new emission factors by adding and subtracting the uncertainty to its respective emission factors. Table 10 includes the new emission factors applied and the associated uncertainties. In the default version of FINN, all evergreen and deciduous needleleaf forests were assigned emission factors for boreal forests, which was assumed to be most appropriate at the time of development. In the most current release of emission factors from S. Akagi and R. Yokelson (Yokelson et al, 2013; Akagi et al. 2013), additional data were included for temperate evergreen forests (ref. version 3, obtained from http://bai.acd.ucar.edu/Data/fire/). Consequently, in the NEWEMIS scenarios considered here, needleleaf forests were assigned emissions factors based on latitude: those forests located at latitudes greater than 50°N were assigned emissions factors for boreal forests. In contrast, those at latitudes less than 50°N were assigned emission factors for temperate evergreen forests. Table 11 shows the differences in these emission factors. Another significant change in the model was also undertaken for the NEWEMIS_TEMPFOR scenario. Not only were evergreen forests assigned new emission factors based on their latitude, they were also assigned the corresponding fuel loading of forests in that region. Therefore, temperate evergreen forests were assigned the fuel loading of temperate forest rather than boreal forest (10.5 kg/m^2 versus 25 kg/m^2). Very few emission uncertainty values have been reported for

NO and NO_2 emission factors. In order to include the uncertainty in these emissions, the uncertainty of the NO_x emission factors was applied to the NO and NO_2 emission factors in the sensitivity study.

Table 10. Emission factors (g species/kg fuel burned) for CO_2, CO, CH_4, NMOC, NO, NO2, NO_x as NO, SO_2, $PM_{2.5}$, NH3, and PM10 for the NEWEMIS scenario (Source: Akagi et al., 2011; 2013). Estimates of uncertainty in reported emissions factors from Akagi et al. (2011; 2013) are in parentheses. Upper (HIGHEMIS) and lower (LOWEMIS) limits of the new emission factors were obtained by adding and subtracting the uncertainty from its respective emission factor. The colors reflect the sources of the new numbers, which are listed below the table.

LCT	LCT Description	General Vegetation Type	General Vegetation Description	CO2	CO	CH4	NMOC	NOXasNO	NO	NO2	SO2	PM2.5	NH3	PM10
1	Evergreen Needleleaf Forest	5	Boreal	1489 (121)	127 (45)	5.96 (3.14)	29.3 (10.1)	0.9 (0.69)	1.5 (1.2)	3 (2.3)	1	15.3 (5.9)	2.72 (2.32)	18
2	Evergreen Broadleaf Forest	3	Tropical Forest	1643 (58)	93 (27)	5.07 (1.98)	26 (8.8)	2.55 (1.4)	0.91 (0.5)	3.6 (2.0)	0.4 (0.4)	9.1 (3.5)	1.33 (1.21)	18.5 (4.1)
3	Deciduous Needleleaf Forest	5	Boreal	1489 (121)	127 (45)	5.96 (3.14)	29.3 (10.1)	0.9 (0.69)	1.5 (1.2)	3 (2.3)	1	15.3 (5.9)	2.72 (2.32)	18
4	Deciduous Broadleaf Forest	4	Temperate Forest	1637 (71)	89 (32)	3.92 (2.39)	11.9 (7.6)	2.51 (1.02)	[illegible]	[illegible]	[illegible]	12.7 (7.5)	0.78 (0.82)	16.97
5	Mixed Forests	4	Temperate Forest	1604 (54)	99 (26)	4.6 (1.7)	22.7 (8.2)	1.97 (0.82)	1.1 (0.45)	2.8 (1.2)	0.9 (0.25)	12.5 (6.6)	1.4 (0.6)	16.97
6	Closed Shrublands	2	Woody Savannah	1703 (38)	71 (13)	2.74 (0.74)	6.6 (2.3)	3.29 (1.02)	1.4 (0.43)	1.4 (0.43)	0.68 (0.13)	12.2 (5.7)	1.26 (0.62)	15.4
7	Open Shrublands	2	Woody Savannah	1703 (38)	71 (13)	2.74 (0.74)	6.6 (2.3)	3.29 (1.02)	1.4 (0.43)	1.4 (0.43)	0.68 (0.13)	12.2 (5.7)	1.26 (0.62)	15.4
8	Woody Savannas	2	Woody Savannah	1703 (38)	71 (13)	2.74 (0.74)	6.6 (2.3)	3.29 (1.02)	1.4 (0.43)	1.4 (0.43)	0.68 (0.13)	12.2 (5.7)	1.26 (0.62)	15.4
9	Savannas	1	Savanna and Grasslands	1686 (38)	63 (17)	1.94 (0.85)	12.4 (6.2)	3.9 (0.8)	0.74 (0.15)	3.2 (0.66)	0.48 (0.27)	7.17 (3.42)	0.52 (0.35)	8.3
10	Grasslands	1	Savanna and Grasslands	1686 (38)	63 (17)	1.94 (0.85)	12.4 (6.2)	3.9 (0.8)	0.74 (0.15)	3.2 (0.66)	0.48 (0.27)	7.17 (3.42)	0.52 (0.35)	8.3
11	Permanent Wetlands	1	Savanna and Grasslands	1686 (38)	63 (17)	1.94 (0.85)	12.4 (6.2)	3.9 (0.8)	0.74 (0.15)	3.2 (0.66)	0.48 (0.27)	7.17 (3.42)	0.52 (0.35)	8.3
12	Croplands	9	Crops	1585 (100)	102 (33)	3.82 (3.56)	23.7 (9.8)	3.11 (1.57)	1.7 (0.86)	3.9 (2.0)	0.4 (0.4)	6.26 (2.36)	2.17 (1.27)	13
14	Cropland/Natural Vegetation Mosaic	1	Savanna and Grasslands	1686 (38)	63 (17)	1.94 (0.85)	12.4 (6.2)	3.9 (0.8)	0.74 (0.15)	3.2 (0.66)	0.48 (0.27)	7.17 (3.42)	0.52 (0.35)	13
16	Barren or Sparsely Vegetated	1	Savanna and Grasslands	1686 (38)	63 (17)	1.94 (0.85)	12.4 (6.2)	3.9 (0.8)	0.74 (0.15)	3.2 (0.66)	0.48 (0.27)	7.17 (3.42)	0.52 (0.35)	8.3

Akagi Boreal Forest EFs (Version 3)
Akagi Tropical Forest EF (Version 2)
Akagi Temperate Forest (Version 2)
Average of Temperate forest and evergreen Needleaf forest from Akagi (version 3)
Akagi Chaparell EFs (Version 3)
Akagi Savanna Efs (Version 2)
Akagi Crop Residue EFs (Version 2)
Akagi Temparate Evergreen Forest (Version 3)
[illegible]
Akagi Extratropical Forest EFs (Version 2)
PM10 set to reported TPM

Table 11. Emission factors applied to evergreen forests in the FINN default and new emissions (NEWEMIS) simulations.

	GenVegDescript	CO2	CO	CH4	NMOC	H2	NOXasNO	SO2	PM25	TPM	TPC	OC	BC	NH3	NO	NO2	NMHC	PM10
FINN DEFAULT	Boreal	1514	118	6	28	2.3	1.8	1	13	18	8.3	7.8	0.2	3.5	1.5	3	5.7	14
NEWemis	Boreal	1489	127	6.0	29	2.3	0.9	1	15	18	8.3	7.8	0.2	2.7	1.5	3	5.7	18
	% difference between default and new boreal	-1.7	7.1	-0.7	4.4		-100		15					-29				22
NEWemis	Temperate Evergreen Forest	1647	88	3.4	24	2.03	1.9	1.1	13	18	8.3	9.2	0.6	0.8	1.0	2.3	5.7	14
	% difference between default and new temperate evergreen	8.8	-25	-44	-16	-12	6.7	10	-0.8			17	180	-76	-37	-22		

7.2 Land Use/Land Cover Characterization

Estimation of land cover and land use from satellite observations can be highly uncertain. Differences in classification systems and pixel identification exist between data products. For example, the MODIS LCT product may classify a pixel as a mixed forest and another product could classify the same pixel as wood savanna. This can have drastic differences in the estimated emissions from a fire at that pixel. The fuel loadings of forests in FINN are much different than the fuel loadings for shrub lands and savannas (ref. Table 2). Variability in emission factors applied to these differing land covers also exists (ref. Tables 3 and 10). Therefore, the classification of land cover at the surface, and the potential variability associated with the classification, can lead to potential uncertainties in fire emission estimates.

In order to test the sensitivity of FINN emission estimates to the land cover/land use data used as input, the default MODIS LCT data were replaced by the project data. GlobCover is a land cover data product derived from observations by the MERIS sensor aboard the ENVISAT satellite mission. The data used for the sensitivity study here is version 2.2 for the years 2005-2006 and can be downloaded from http://due.esrin.esa.int/GlobCover/. The GlobCover data have a resolution of ~ 500m; these data were scaled to 1km^2. Figure 15 shows the GlobCover and the MODIS LCT data for the central U.S. As the legends indicate, classifications between the two land cover datasets are not equivalent. Therefore, for the purposes of this sensitivity analysis, GlobCover classes were mapped to the LCT classes and the generic vegetation classifications that are used in the FINN model (croplands, grasslands/savannas, shrublands/woody savannas, tropical forests, temperate forests, and boreal forests). Figure 16 shows the MODIS LCT and the GlobCover data mapped to the generic vegetation codes used by FINN. As can be seen from the two maps in Figure 16, there are significant differences between the generic land cover mapping for the MODIS LCT and the GlobCover datasets. The MODIS LCT has much more area assigned as shrublands or grasslands in the central and western U.S. The GlobCover dataset has much more area assigned as forest and shrublands. The fuel loadings and emission factors assigned to these land cover classes are quite different and will therefore result in variability in the emission estimates. The emission for both cases are scaled to the density of the vegetation, as assigned by the MODIS VCF product. This is not accounted for in the comparison presented here.

Figure 15. Maps of the (a) the MODIS LCT (b) original GlobCover land cover.

(a)

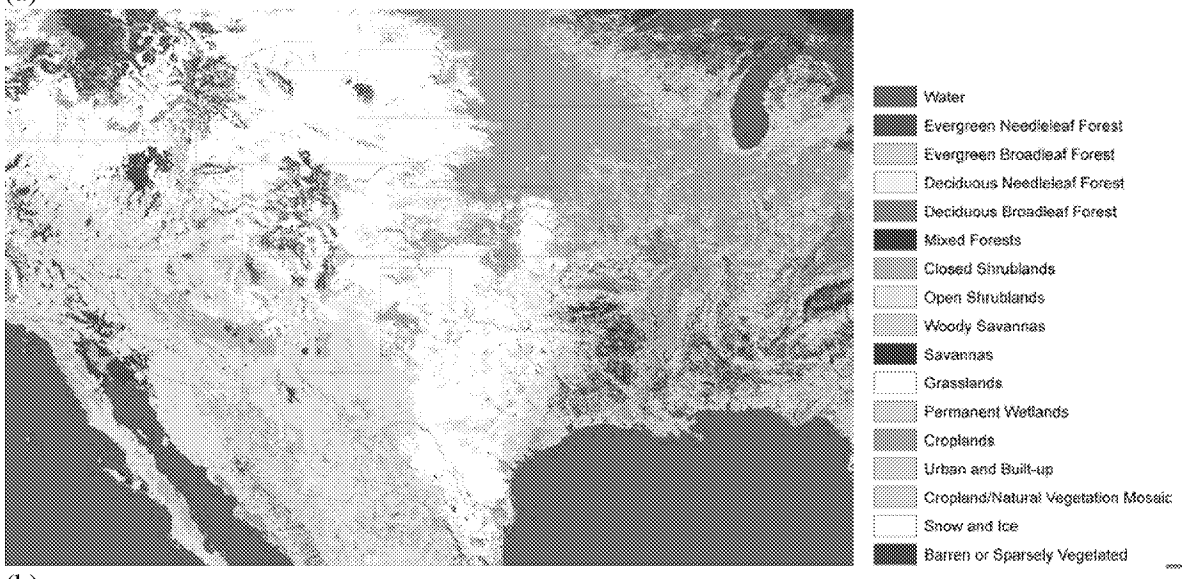

(b)

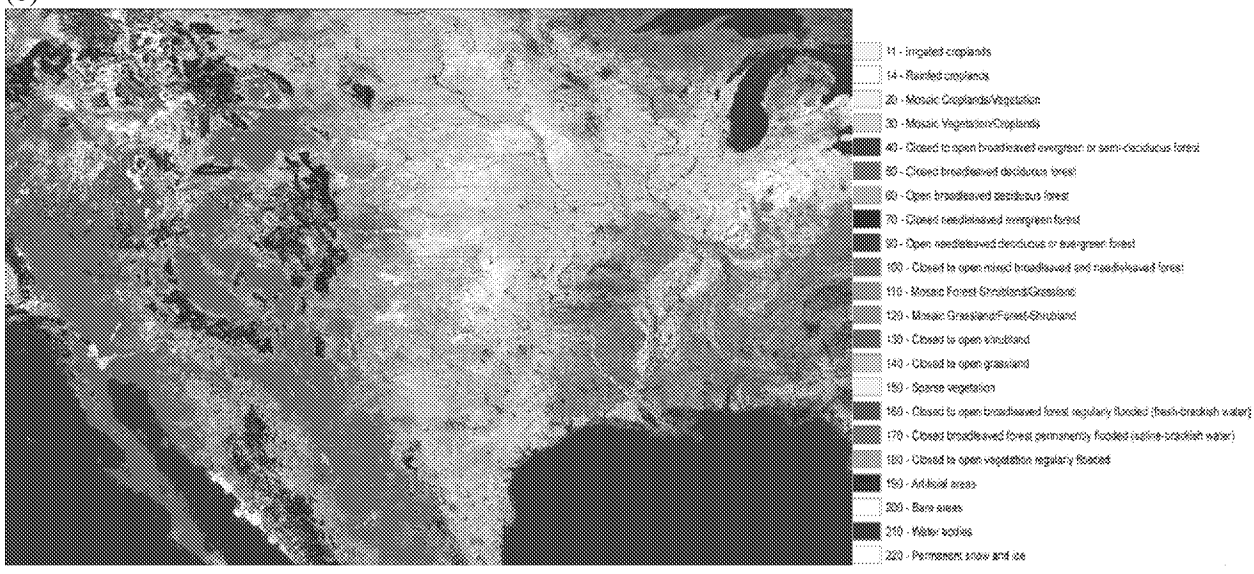

Figure 16. (a) MODIS LCT (A) and (b) GlobCover data mapped to the generic vegetation codes used in FINN. For the purposes of this illustration, urban and developed areas in both mappings are assigned the shrublands generic vegetation code.

(a)

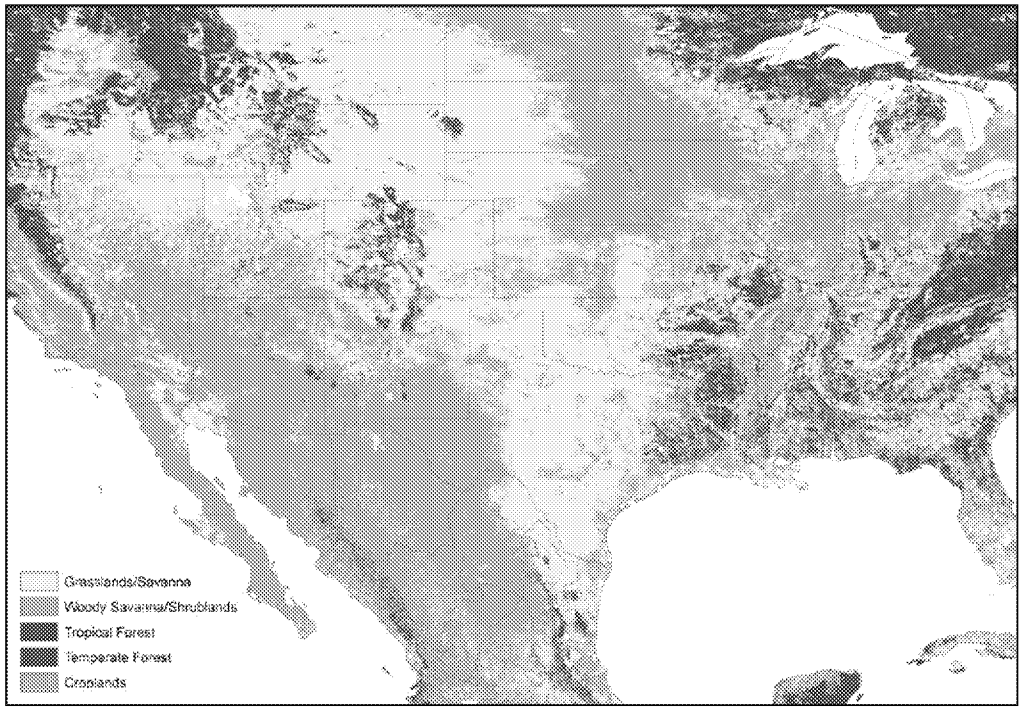

(b)

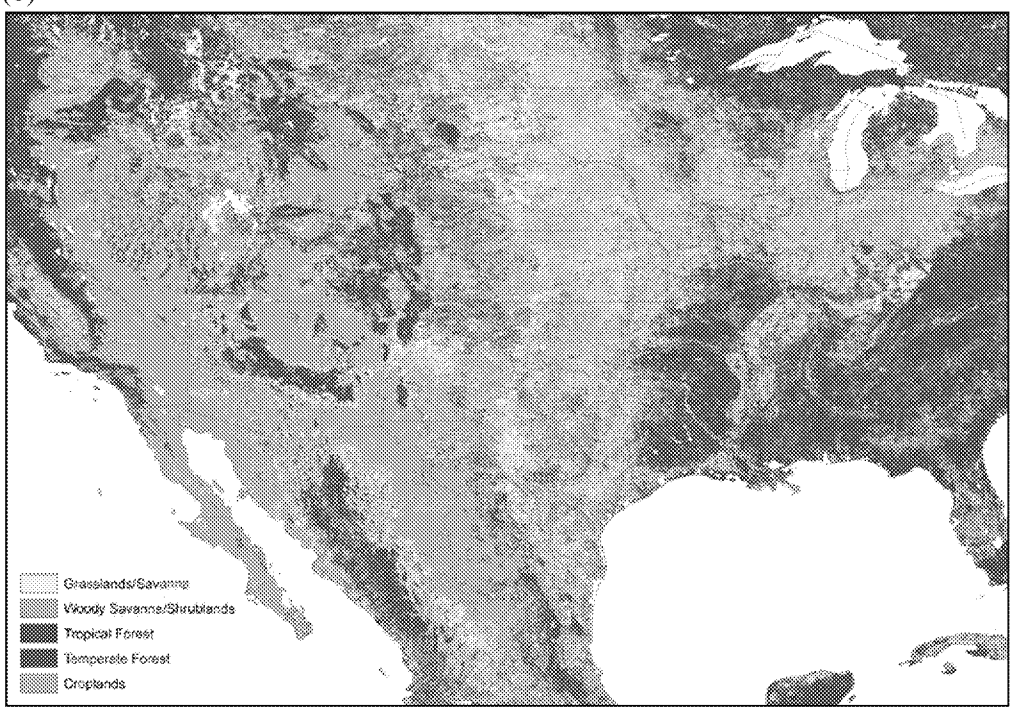

7.3 Fuel Loading

Despite the potentially high variability in fuel loadings over regions, fuel loading estimates used in the default FINN configuration are static for each vegetation class and global region (Table 2). In order to examine the sensitivity of FINN estimates to input fuel loading, the Fuel Characteristic Classification System (FCCS, http://www.fs.fed.us/pnw/fera/fccs/) data were used in place of the default values. The GIS layers of the FCCS fuelbeds for the contiguous U.S. aggregated to 1 km were downloaded and used for this application (http://www.fs.fed.us/pnw/fera/fccs/maps.shtml). The FCCS provides detailed fuels information for ecosystems of the United States. The FCCS includes a map of 250 different vegetation types for which associated fuels information is provided. These fuels data include fuel loadings specific to different fuel types (e.g., non-woody dead, 1-hour, 10-hour and 100-hour fuels) for each vegetation class. To enable these data to work within the FINN framework, the total fuel load and the fraction of woody and non-woody fuels for each vegetation type in the FCCS were calculated. Additionally, each specific vegetation type of the FCCS was assigned an equivalent LCT classification. Each fire detection was assigned the FCCS type to which it was overlaid, and the corresponding fuel loading and LCT equivalent was applied in place of the default LCT classifications and fuel loading. Further, the fraction of woody and herbaceous fuels calculated for the FCCS class was used in place of the MODIS VCF information. As Table 9 indicates, these collective modifications resulted in changes to both the land cover and fuel loading for this scenario; the intent was to maintain internal consistency within the data source.

The FCCS assigns barren, agriculture, and urban areas to one land cover type. For this model simulation, all areas assigned with this code were assumed to be agricultural, with 100% herbaceous cover. Since the FCCS does not assign a fuel loading to this code, the FINN default fuel loading (0.98 kg/m^2) was used.

Differences between the FCCS fuel loadings and the FINN default fuel loadings varied depending on location within the U.S. Total fuel loadings calculated from the FCCS vegetation types range from 0.02 to 20.7 kg/m^2. FINN default values (Table 2, North America) range from 0.98 kg/m^2 for grasslands/savannas to 28 kg/m^2 in forests. These values, however, are scaled to the percent cover within the model framework. In the default version, this is defined by the MODIS VCF product. For the FCCS simulation, the woody and herbaceous cover is defined by the information in the FCCS. It is therefore difficult to directly compare the inputs between the two fuel loading scenarios.

7.4 Fire Location and Burned Area: SmartFire

As described in Section 4, the FINN default configuration assumes that each detection represents a fire with a default area of either 1 km^2 or 0.75 km^2 (grasslands). This burned area estimate is then scaled to the amount of bare ground in each pixel as observed by the MODIS VCF product. An inherent assumption is that the uncertainty in burned area is high, since the true burned area of a "hot spot" detected from space- based observations can be variable. Wiedinmyer et al. (2011) assumed that the estimate of area burned was an upper limit for each hot spot applied in the model.

The application of the MODIS rapid response (MRR) fire detections in this process has several uncertainties. The two MODIS instruments are aboard the polar orbiting NASA Aqua and Terra satellites, and, thus, have one daytime and one nighttime observation per day. If a fire occurs at a time after an overpass, it will not be detected. Additionally, smoke and clouds can obscure the view and prevent detections from occurring. The opportunity for missed fire detections can be high, particularly with small fires, understory fires, and in areas of high cloud cover.

In order to test the sensitivity of the input fire detections and assumed area burned to the choice of inputs in FINN, the MRR fire detections were replaced by the fire location and area burned produced by SmartFire for the same time period. These inputs provide area burned, the type of fire, and the point

location (latitude/longitude) of the fire. The FINN inputs and code were modified to use these inputs to calculate fire emissions for this sensitivity scenario. As described above, SmartFire uses a combination of fire information from incident reports and remotely-sensed fire detections. Because SmartFire includes MODIS fire detections within this particular case along with the other fire data, it is not surprising that the number of SmartFire points and, at times, area burned is greater than that calculated with the default FINN estimates. The two methods also have differing procedures for evaluating the applicability of the fire inputs; therefore, the satellite detections used by both can vary. Figure 17 shows the fire points from the MRR and from SmartFire for 01 April through 31 July 2008. SmartFire points are scaled to the area assigned to each point.

Figure 17. MODIS MRR and SmartFire fires for April 1st through July 31st, 2008. Note that SmartFire has fire points only within the U.S.

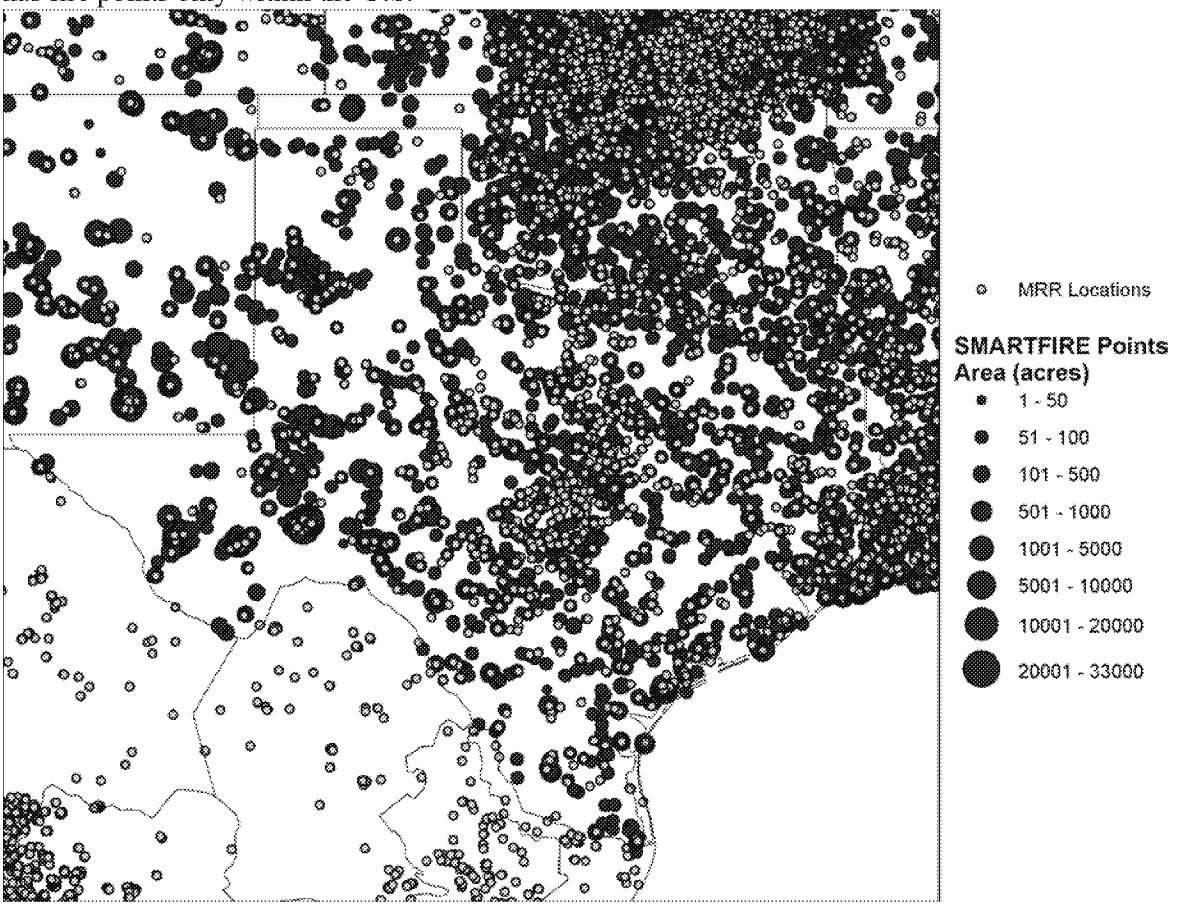

7.5 Emissions Estimates

Episode total emissions of NO_x, VOC, $PM_{2.5}$, and CO for the FINN default configuration and sensitivity studies are shown by region in Figure 18.

Figure 18. Episode total emissions of NO_x, VOC, $PM_{2.5}$, and for the FINN default configuration and sensitivity studies for (a) Texas, (b) Louisiana, (c) 5 central states (Arkansas, Kansas, Missouri, Mississippi, Oklahoma), (d) 11 western states (New Mexico, Colorado, Wyoming, Montana, Idaho Washington, Oregon, California, Arizona, Nevada and Utah), (e) Mexico, and (f) Western Canada. Note difference in scale for CO emissions estimates.

(a)

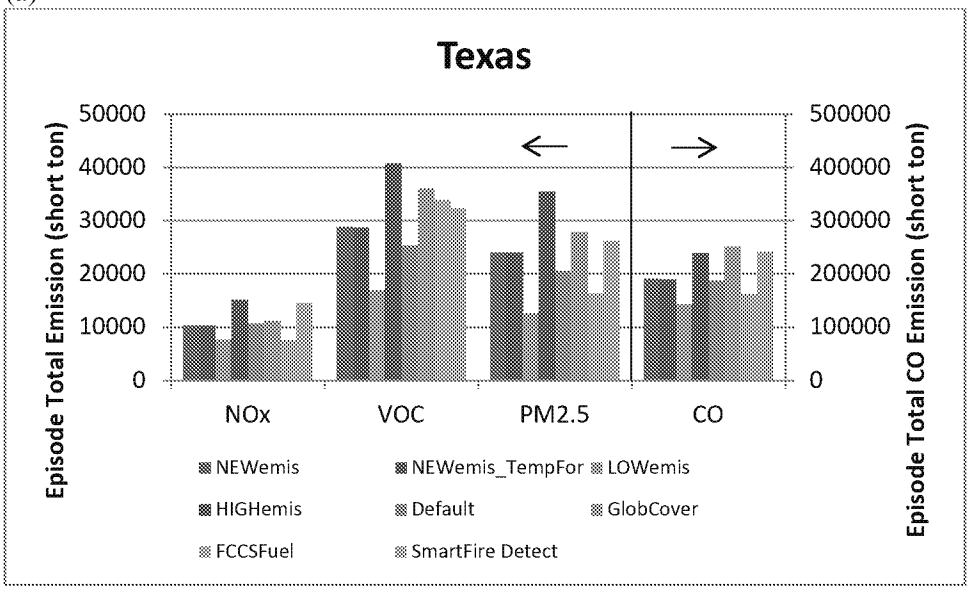

(b)

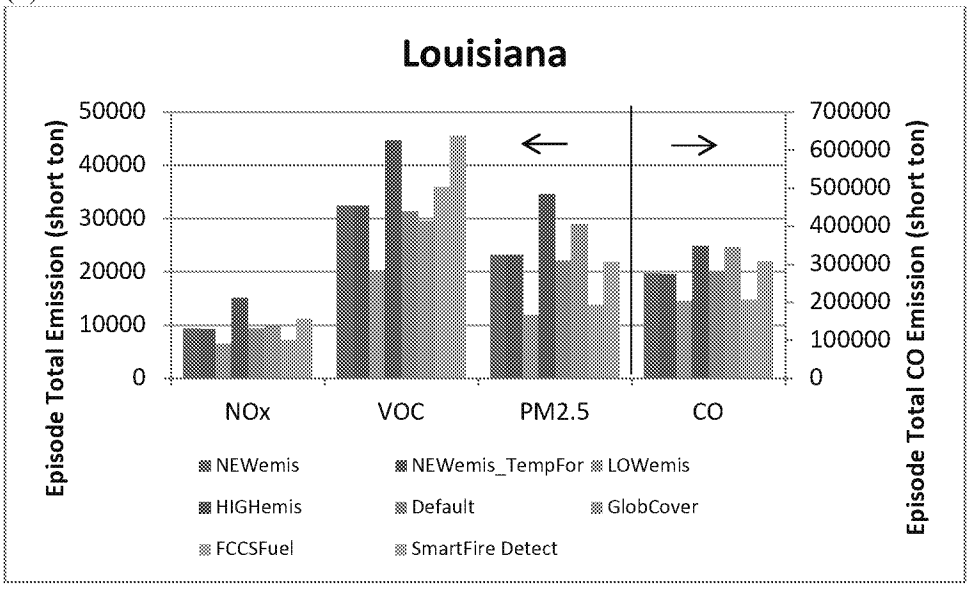

(c)

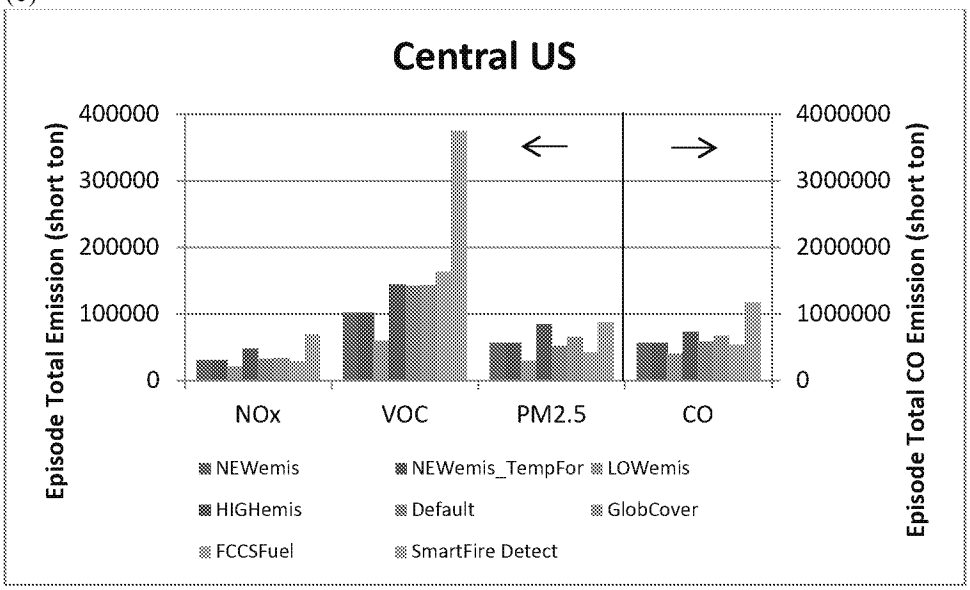
Central US
Episode Total Emission (short ton)
400000
300000
200000
100000
0
4000000
3000000
2000000
1000000
0
Episode Total CO Emission (short ton)
NOx
VOC
PM2.5
CO
NEWemis
NEWemis_TempFor
LOWemis
HIGHemis
Default
GlobCover
FCCSFuel
SmartFire Detect

(d)

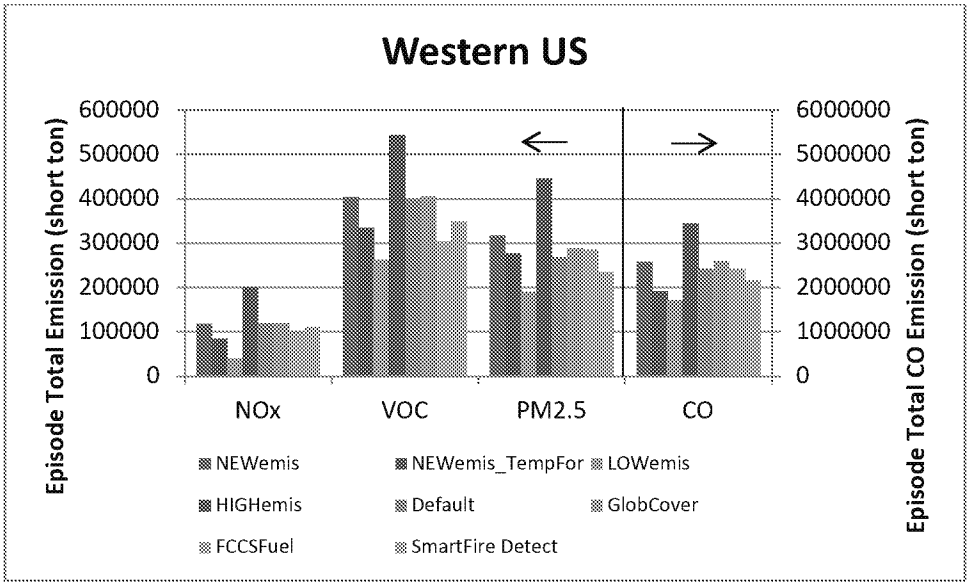
Western US
Episode Total Emission (short ton)
600000
500000
400000
300000
200000
100000
0
6000000
5000000
4000000
3000000
2000000
1000000
0
Episode Total CO Emission (short ton)
NOx
VOC
PM2.5
CO
NEWemis
NEWemis_TempFor
LOWemis
HIGHemis
Default
GlobCover
FCCSFuel
SmartFire Detect

(e)

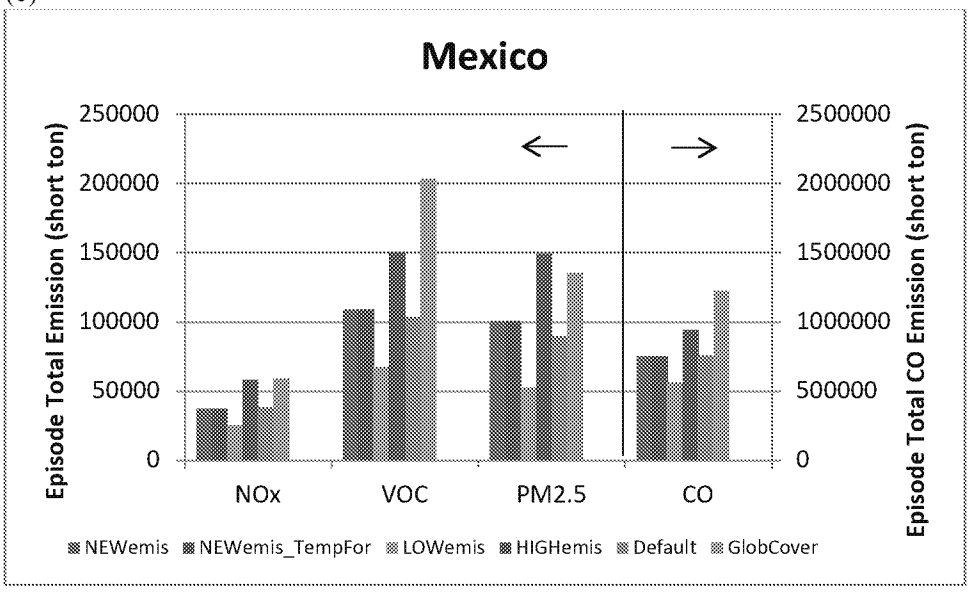
Mexico
Episode Total Emission (short ton)
250000
200000
150000
100000
50000
0
2500000
2000000
1500000
1000000
500000
0
Episode Total CO Emission (short ton)
NOx
VOC
PM2.5
CO
NEWemis
NEWemis_TempFor
LOWemis
HIGHemis
Default
GlobCover

(f)

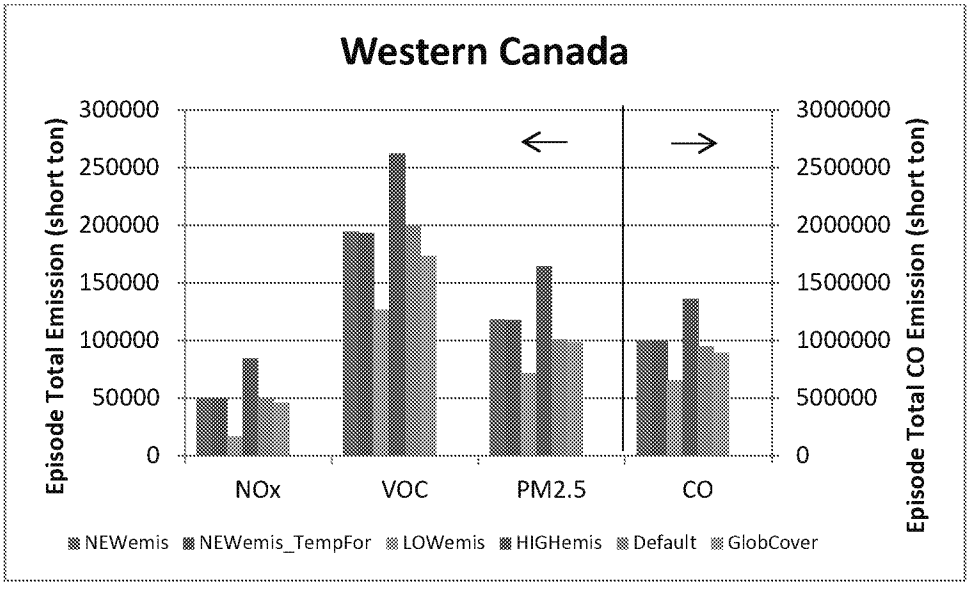
Western Canada
Episode Total Emission (short ton)
300000
250000
200000
150000
100000
50000
0
3000000
2500000
2000000
1500000
1000000
500000
0
Episode Total CO Emission (short ton)
NOx
VOC
PM2.5
CO
NEWemis
NEWemis_TempFor
LOWemis
HIGHemis
Default
GlobCover

Figure 18 indicates that the variability in emissions associated with uncertainties in emissions factors between scenarios can exceed a factor of two. Emissions estimates for the HIGHEMIS and LOWEMIS scenarios bound estimates from the NEWEMIS scenario. Comparisons between the LOWEMIS and HIGHEMIS results show the range of emissions estimates expected as a result of the uncertainty in emission factors, which is dependent on the region and the land cover type burned. Figures 19 through 22 show total CO, NO_x, VOC, and $PM_{2.5}$ emissions between September 1st – October 17th, 2008 from the FINN default configuration, as well as difference in emissions between the NEWEMIS and FINN default scenarios and differences in CO emissions between the LOWEMIS and HIGHEMIS and the NEWEMIS_TEMPFOR scenarios. Analogous results are shown for the April 15th – May 30th, 2008 in Figures S1 through S4 in the Supplemental Information. Differences in the geographical responses to modifications from the FINN default scenario reflect the climatology of fires described above. For example, responses to the uncertainty in emissions factors are evident in Mexico, Saskatchewan, Canada, and the southern and southeastern United States in the spring and California, the southern United States, and British Columbia, Canada in the late summer/early fall. The combination of changes in both emission factors and fuel loadings for evergreen temperate forests are the primary reason for dramatically reduced emissions in the western U.S. in the NEWEMIS_TEMPFOR scenario relative to the FINN default configuration. The substantial variability in estimates of VOC emissions suggested the need for targeted improvements in measurement techniques and validation of model estimates.

The FCCS typically applied much lower fuel loadings than the default FINN inputs, which would lead to lower emission estimates, particularly in areas with forests (e.g., Western US). However, because the FCCS assigns 100% herbaceous cover to areas designated as croplands, the maximum area burned is 0.75 km^2 and will often result in larger emission estimates than the DEFAULT version that uses the MODIS VCF product to define the vegetation coverage. Consequently, direct comparisons between the two fuel loading scenarios are difficult. Modification of the FINN default configuration to use FCCS data for input fuel loadings affected only the continental United States. Figure 23 shows differences in emissions of CO, NO_x, VOC, and $PM_{2.5}$ during September 1st – October 17th, 2008 between the FCCS scenario and the FINN default scenario. Analogous results are shown for April 15th – May 30th, 2008 in Figure S5 of the Supplemental Information. Overall, the FCCS fuel loadings are lower than the FINN default configuration, as described in Section 7.3. However, it is possible for individual fires to have higher fuel loadings in the FCCS scenario than FINN default scenario. It is also possible for the land cover type assigned to an FCCS class to differ from the land cover type class overlaid with the FINN default fire point. In cases such as this, it is conceivable for the FCCS scenario to classify an area as forest, whereas the FINN default land cover type map assigns the area as shrubland or grassland, thus, resulting in different emission factors.

The effects of applying SmartFire for fire detection and estimation of area burned varied across regions. In some cases, the number of fires detected and the area burned using SmartFire was significantly larger than the FINN default scenario. However, because the locations of the SmartFire and FINN default points differed, points identified by SmartFire could be assigned to a land cover type class that differed from that assigned in the FINN default scenario for the same fire. This could result in wide variations in emissions estimates due to differences in fuel loading and emission factors.

SmartFire uses a combination of incident reports and remotely sensed fire detections from several satellite-borne sensors, including MODIS, for fire detection. In contrast, the FINN default configuration relies on only the MRR and MODIS VCF products to determine a fire location and assumed area burned. Figure 24 shows differences in emissions of CO, NO_x, VOC, and $PM_{2.5}$ between September 1st – October 17th, 2008 between the SmartFireDetect scenario and the FINN default scenario. Analogous results are shown for April 15th – May 30th, 2008 in Figure S6 of the Supplemental Information. These differences have a particularly large influence in the Arkansas-Louisiana area during September and October and to a lesser extent in this region and the central states in the spring and the western states in the fall.

It is interesting to note that the FINN default configuration results in greater estimates of emissions than SmartFire near the Texas-Louisiana border, but markedly lower emissions in Arkansas-Louisiana during the fall. To explain the differences in the FINN default and the SmartFire emission estimates in the fall in Texas, Louisiana, and Arkansas, we examined differences in the inputs for a time period between September 16th through 30th, 2008. Figure 25 shows fires from both input files in this region during this period. In Arkansas, the SmartFire inputs included a total of 517 fires with 74,015 acres burned. Eighty-three percent of the fires in the SmartFire input were assigned as croplands. The DEFAULT input had 261 fires, 54% of which were croplands, and 41% were forests. Assuming the maximum area burned, the DEFAULT simulation should have had approximately 53,000 acres burned. The acreage burned is approximated 40% larger in the SmartFire file than what was calculated with the FINN default simulation. Furthermore, 78% of the SmartFire fires were assigned as croplands, whereas only 54% in the FINN default simulation were assigned as croplands. For VOCs, the emission factor for croplands is double that for forests. Therefore, it is not unexpected that the SmartFire emission estimates are much larger than the FINN default estimates in Arkansas during the fall.

During September 16th through 30th, 2008 in Texas (west to -101° longitude), SmartFire detected 277 fires with a total of 38,100 acres burned. The FINN default input file had 302 fires. Assuming the maximum acreage was burned for these fires, the upper estimate of total acreage burned for this scenario was 64,000 acres, almost double that of SmartFire. Therefore, for this area and time period, emissions from the DEFAULT scenario were larger than for the SmartFire scenario.

Marked differences between the DEFAULT and GlobCover scenarios were also evident (Figure 26). Differences in vegetation types between the land cover maps for the two datasets shown in Figures 15 and 16, suggested that emissions from the GlobCover scenario would be much larger than the FINN default scenario because the GlobCover data contains more forests and shrublands that have higher fuel loadings and, potentially, more biomass burned at each fire detected. However, the emissions factors applied may compensate for the potentially higher fuel loadings and biomass burned. For example, if an area of woody savanna/shrublands is classified instead as forest, the fuel loading increases and the VOC emission factor increases by approximately a factor of five (reference Tables 2 and 3). However, if cropland is classified instead as forest, the fuel loading increases, but the VOC emission factor is reduced by a factor of two.

Differences in Arkansas were also observed between the GlobCover simulation and the DEFAULT simulation. In this case, a decrease in estimated emissions, particularly for VOCs, was evident. GlobCover land cover maps identify more forests than the default MODIS LCT data. The MODIS land cover had much more area identified as croplands, particularly in Arkansas where the fire activity was high during this time period. The VOC emission factor for croplands is considerably higher than emission factors for all other land cover classes; thus VOC emissions were higher for the default case in Arkansas. However, in most other areas, forests assigned by the GlobCover map produce higher emissions when they replace savanna/grasslands and shrublands.

Figure 19. (a) Total CO emissions (short tons) between September 1st – October 17th, 2008 from the FINN default configuration. (b) Difference in CO emissions between the NEWEMIS and FINN default scenarios. Differences in CO emissions between the (c) LOWEMIS (d) NEWEMIS_TEMPFOR and (e) HIGHEMIS and the NEWEMIS scenarios.

(a)

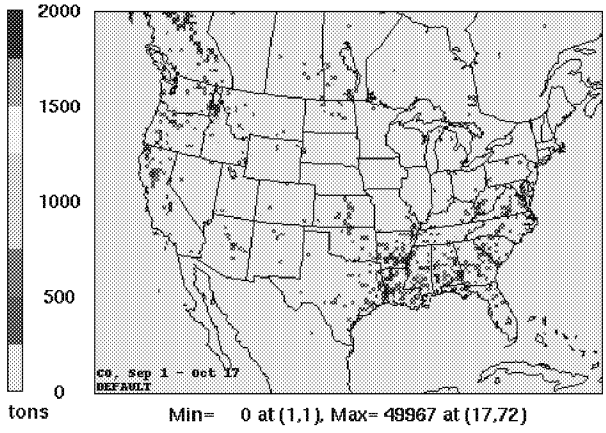

(b)

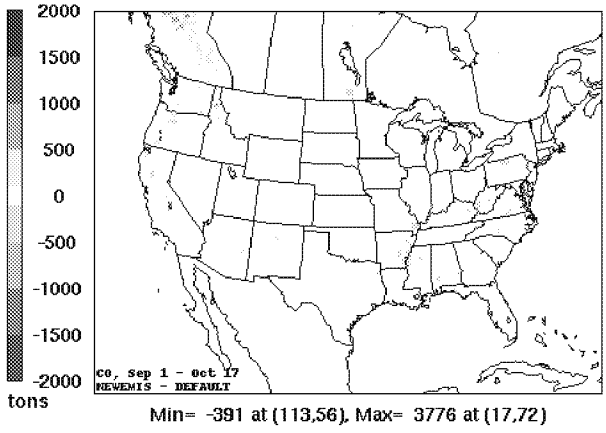

(c)

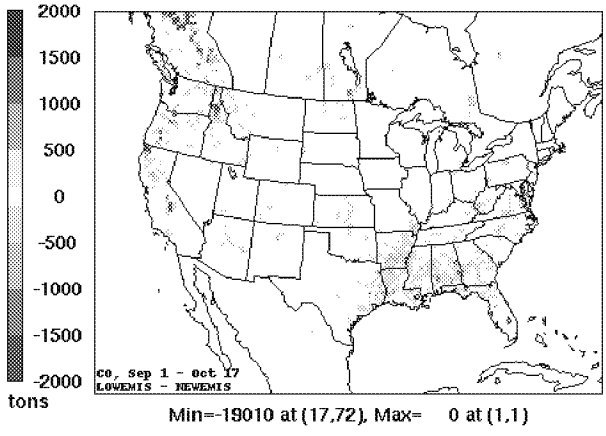

(d)

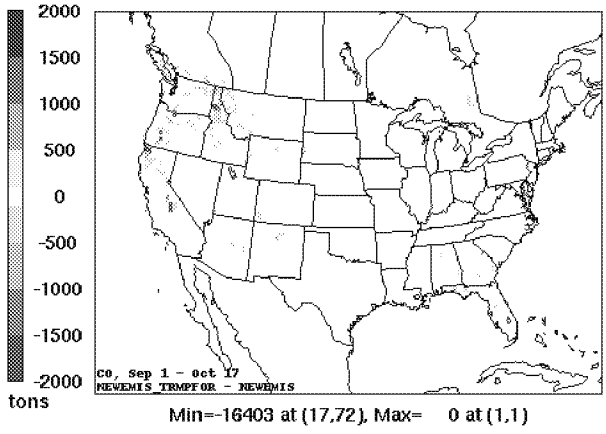

(e)

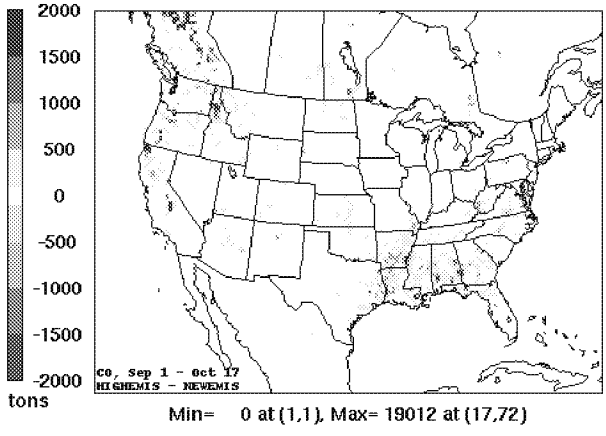

Figure 20. (a) Total NO_x emissions (short tons) between September 1st – October 17th, 2008 from the FINN default configuration. (b) Difference in NOx emissions between the NEWEMIS and FINN default scenario. Differences in NO_x emissions between the (c) LOWEMIS (d) NEWEMIS_TEMPFOR and (e) HIGHEMIS and the NEWEMIS scenarios.

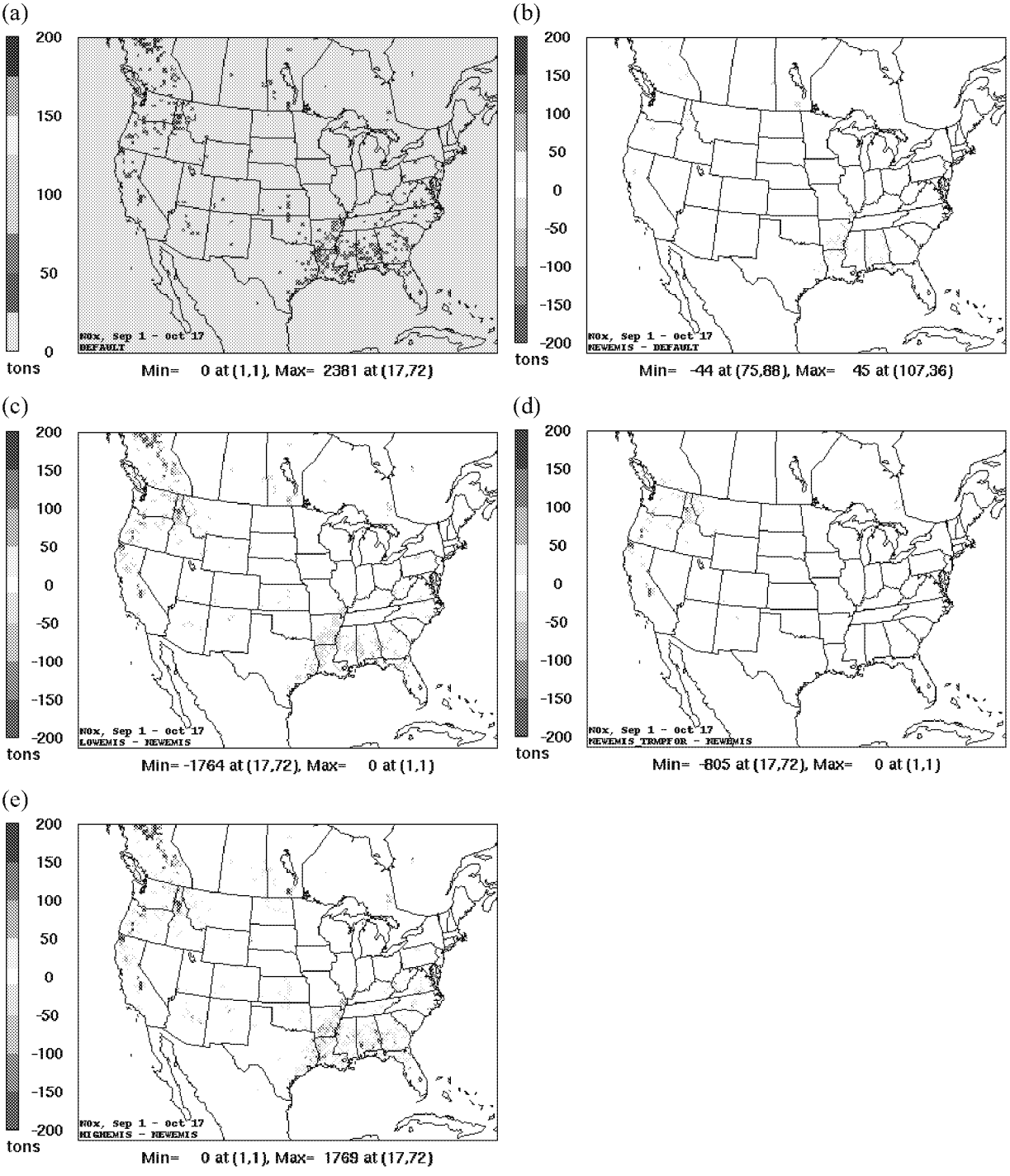

Figure 21. (a) Total VOC emissions (short tons) between September 1st – October 17th, 2008 from the FINN default configuration. (b) Difference in VOC emissions between the NEWEMIS and FINN default scenario. Differences in VOC emissions between the (c) LOWEMIS (d) NEWEMIS_TEMFOR and (e) HIGHEMIS and the NEWEMIS scenarios.

(a)

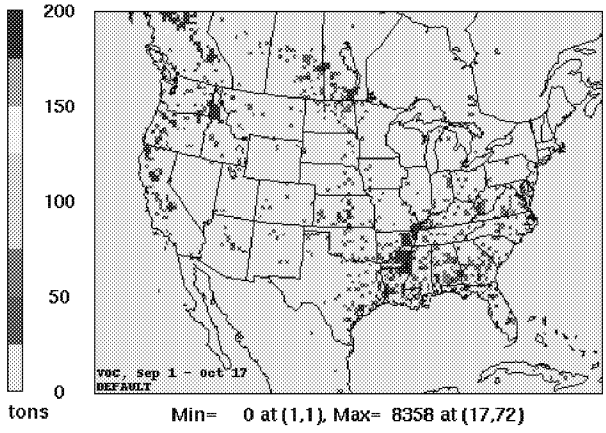

Min= 0 at (1,1), Max= 8358 at (17,72)

(b)

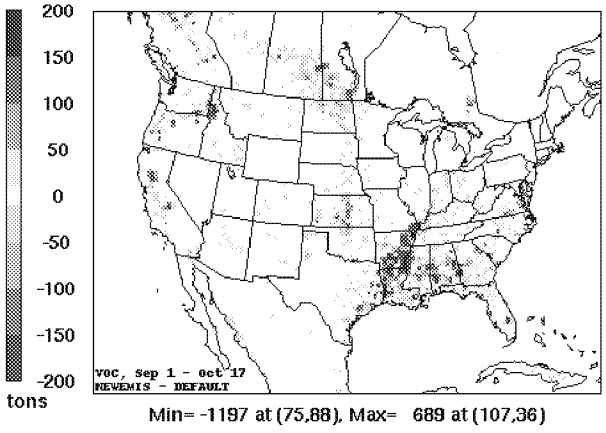

Min= -1197 at (75,88), Max= 689 at (107,36)

(c)

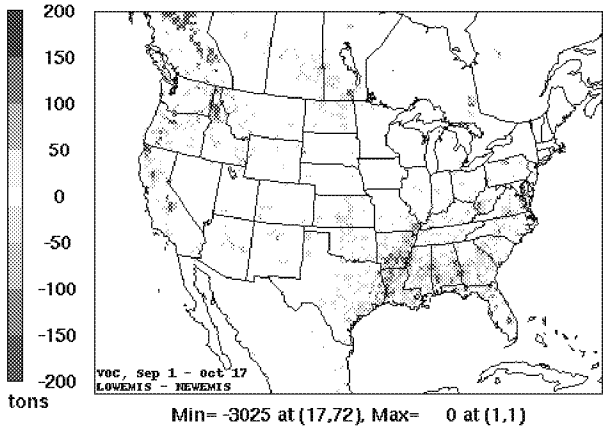

Min= -3025 at (17,72), Max= 0 at (1,1)

(d)

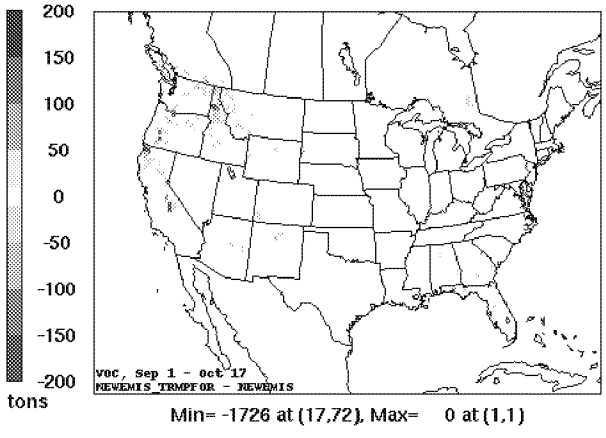

Min= -1726 at (17,72), Max= 0 at (1,1)

(e)

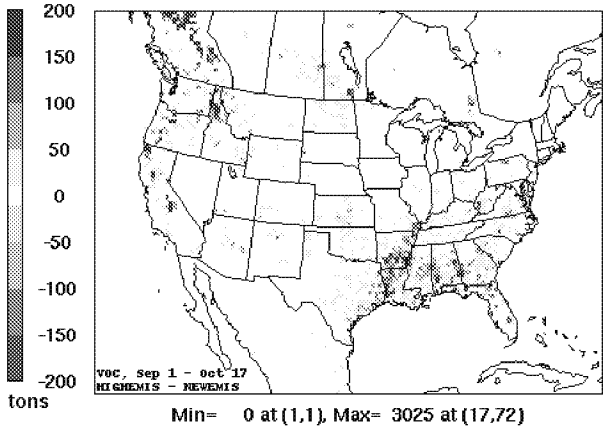

Min= 0 at (1,1), Max= 3025 at (17,72)

Figure 22. (a) Total $PM_{2.5}$ emissions (short tons) between September 1st – October 17th, 2008 from the FINN default configuration. (b) Difference in $PM_{2.5}$ emissions between the NEWEMIS and FINN default scenario. Differences in $PM_{2.5}$ emissions between the (c) LOWEMIS (d) NEWEMIS_TEMPFOR and (e) HIGHEMIS and the NEWEMIS scenarios.

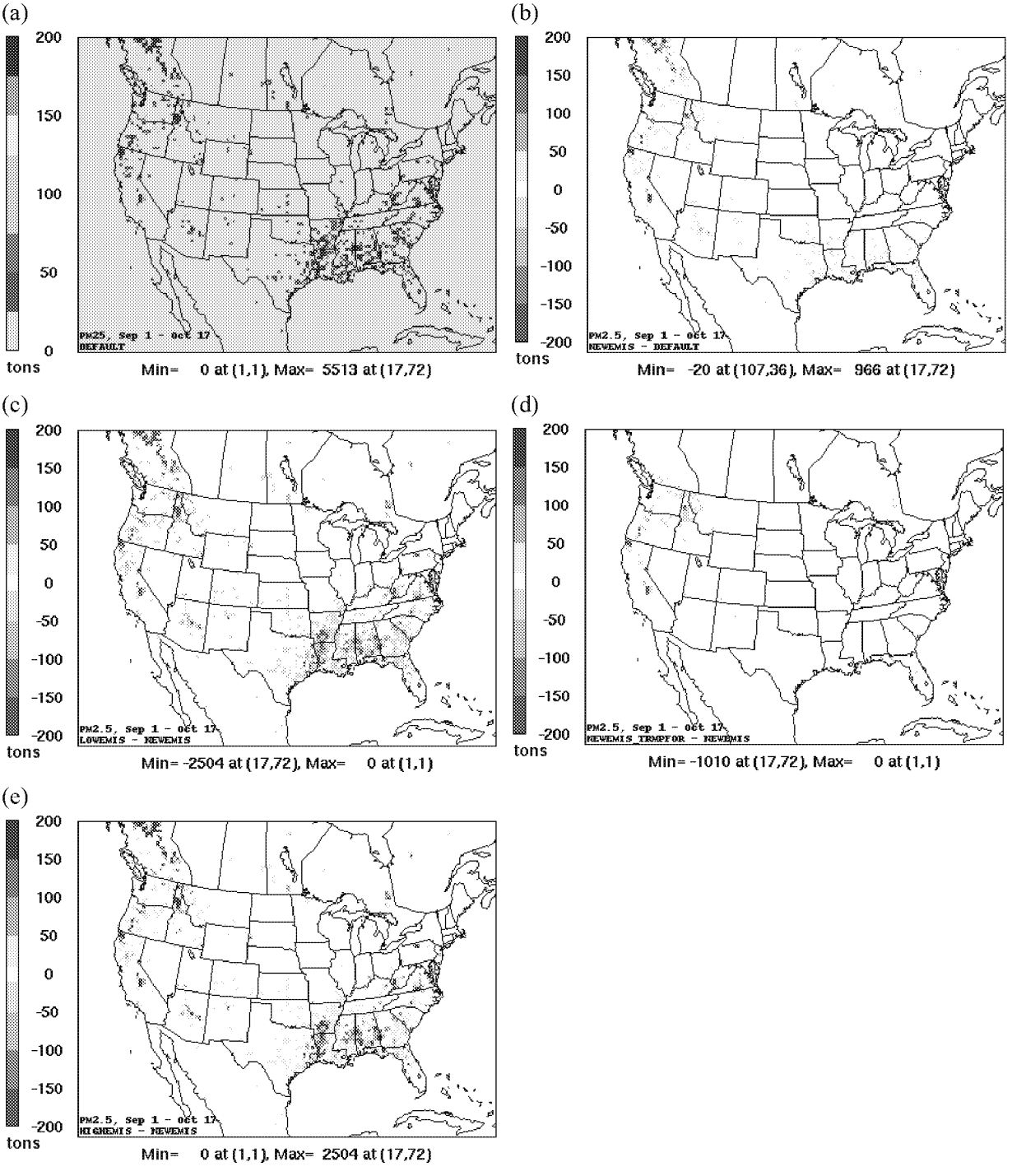

Figure 23. Difference in (a) CO, (b) NO_x, (c) VOC, and (d) $PM_{2.5}$ emissions between the FCCSFuel and FINN default scenarios during September 1st – October 17th, 2008.

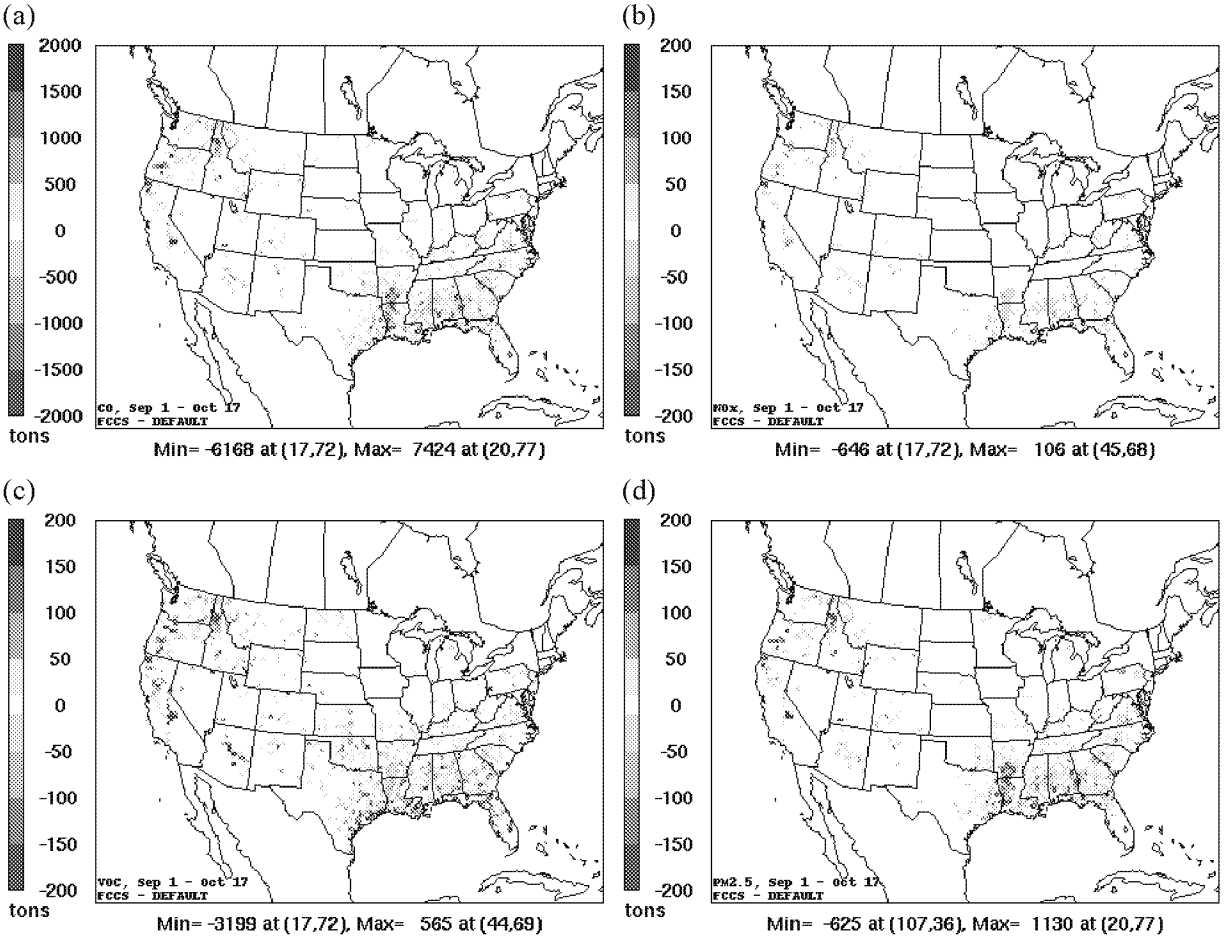

Figure 24. Difference in (a) CO, (b) NO_x, (c) VOC, and (d) $PM_{2.5}$ emissions between the SmartFireDetect and FINN default scenarios during September 1st – October 17th, 2008.

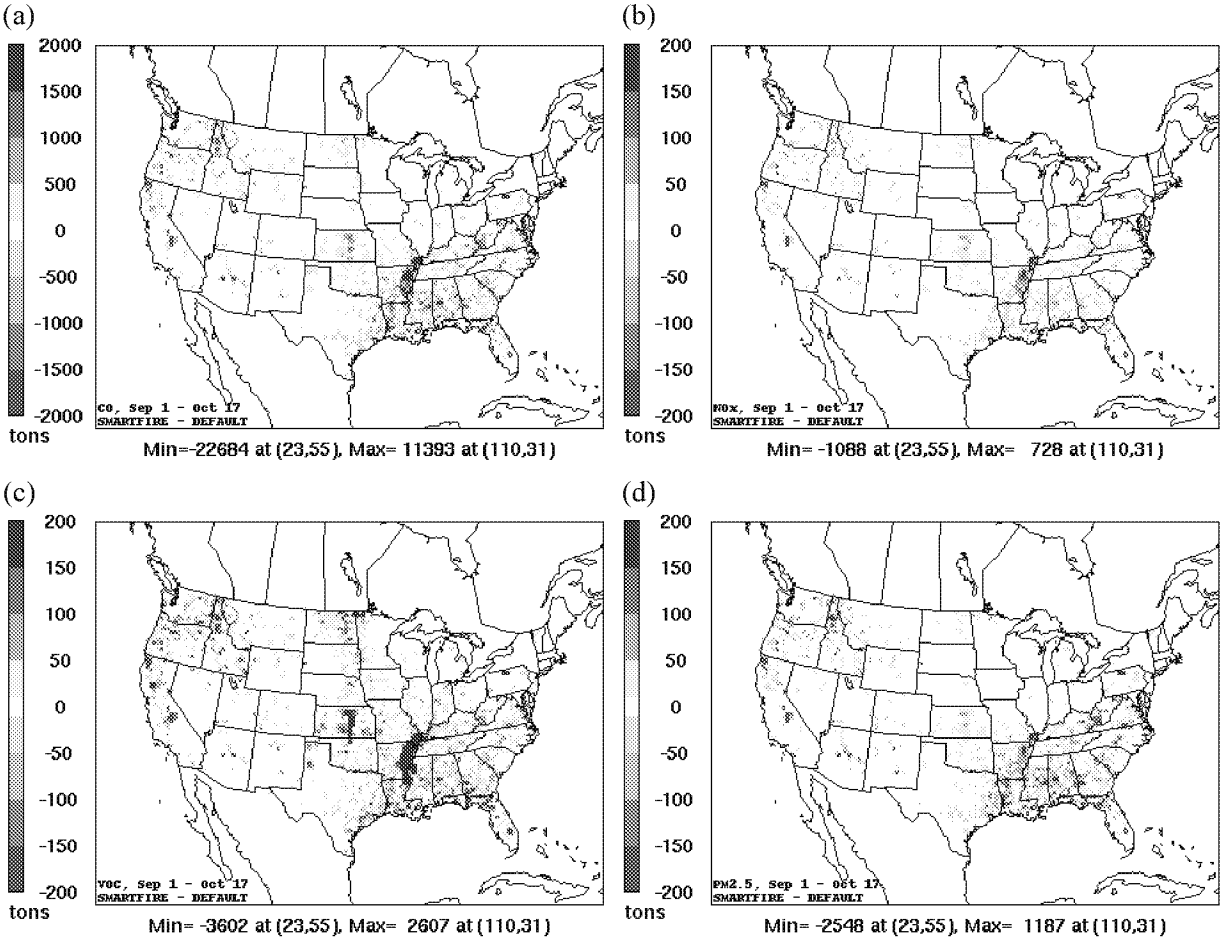

Figure 25. Fire detections by SmartFire and the FINN default configuration during September 16th through 30th, 2008.

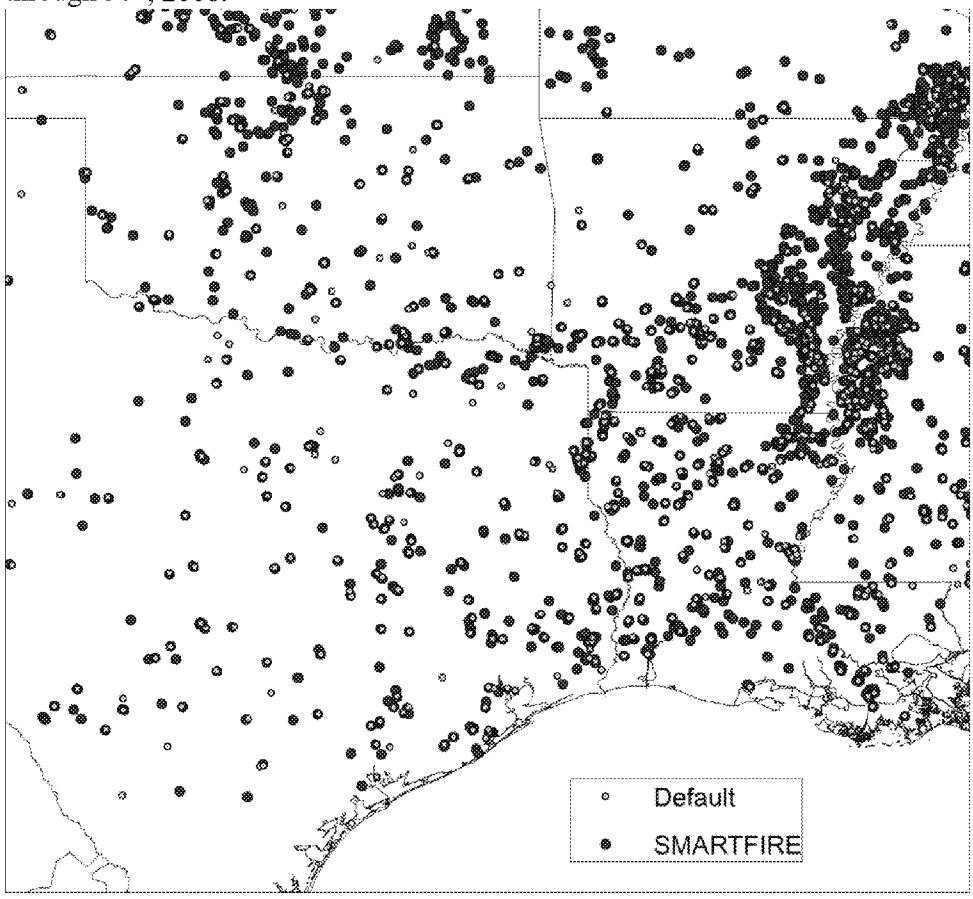

Figure 26. Difference in (a) CO, (b) NO_x, (c) VOC, and (d) $PM_{2.5}$ emissions between the GlobCover and FINN default scenarios during September 1st – October 17th, 2008.

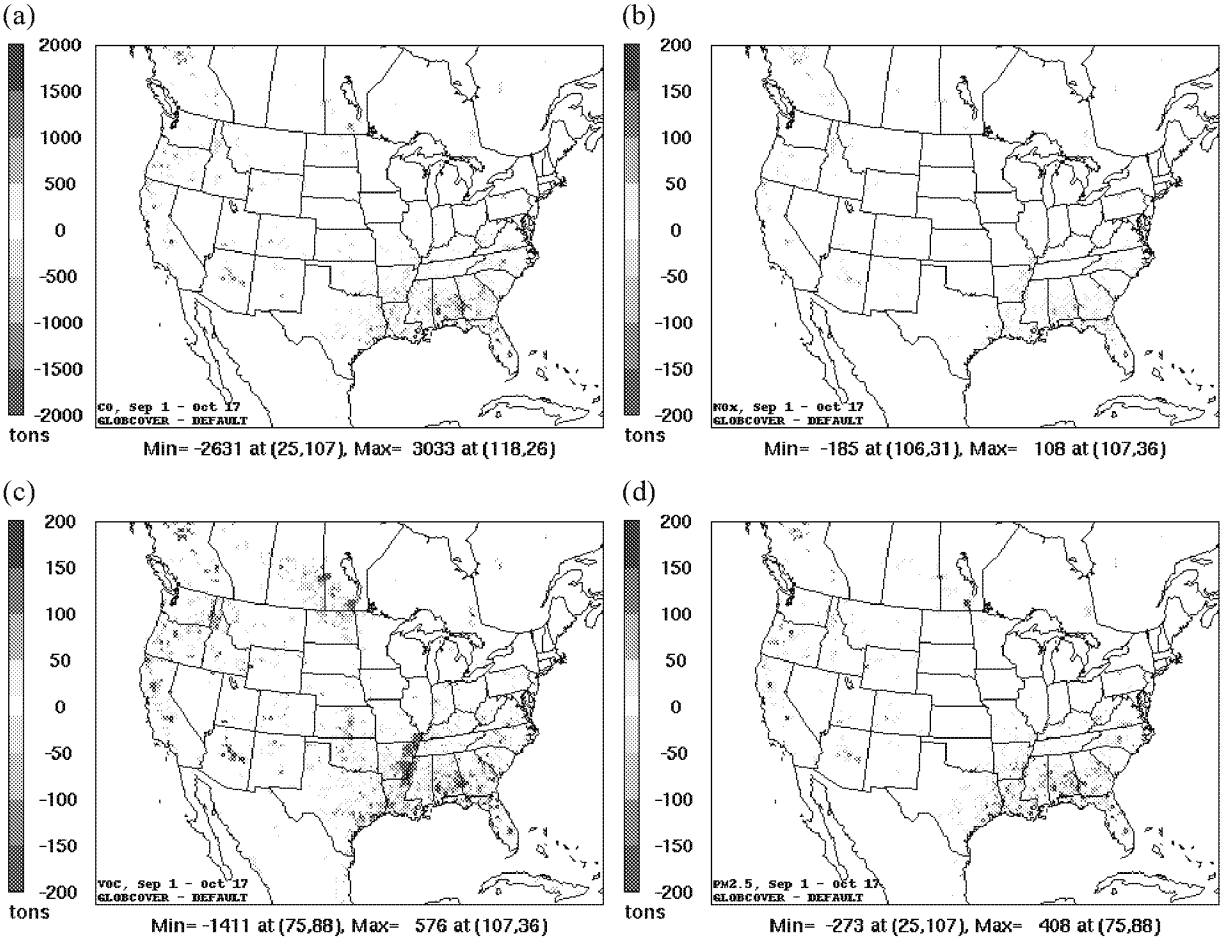

8. Effects of Modified FINN Inventories on Ozone and $PM_{2.5}$ Concentrations

Mean MDA8 ozone concentrations during April 15th – May 30th, 2008 and September 1st – October 17th, 2008 for the FINN default scenario are shown in Figure 27. Maximum differences in MDA8 ozone concentrations between the NEWEMIS, FCCSfuel, SmartFireDetect, and GlobCover scenarios and the FINN default scenarios during each time period are also shown in Figure 27; these provide an indication of the potential sensitivity in predicted air quality in Texas and other areas of the domain to changes in emission estimates. Maximum differences in MDA8 ozone concentrations between the LOWEMIS and NEWEMIS scenarios, NEWEMIS_TEMPFOR and NEWEMIS scenarios, and HIGHEMIS and NEWEMIS scenarios during April 15th – May 30th, 2008 and September 1st – October 17th, 2008 are shown in Figure 28. The range of differences in MDA8 ozone concentrations and 24-hour averaged $PM_{2.5}$ concentrations between each sensitivity scenario and the FINN default scenario by region during April 15th – May 30th, 2008 and September 1st – October 17th, 2008 are shown in Figure 29.

During 2008, a year with fire activity close to the decadal average, maximum predicted differences in MDA8 ozone concentrations associated with modifications in FINN input data sources ranged from 4 to more than 60 ppb over the 36-km domain. Differences were particularly evident for the SmartFire scenario in Texas, Louisiana, and the central and western U.S. in both seasons, and the Globcover scenario in Mexico during the spring. Improving the understanding of the detection and characteristics of specific fire events in Texas, its neighboring states, and those due to transport over longer-scales warrants further investigation. Beneficial to this effort would be analyses of the interannual variability in events, in particular during drought years, and tracking of the contribution of these events to Texas air quality using embedded CAMx tools (e.g., APCA).

Mean 24-hour averaged $PM_{2.5}$ concentrations during April 15th - May 30th, 2008 and September 1st - October 17th, 2008 for the FINN default scenario are shown in Figure 30. Maximum differences in 24-hour averaged $PM_{2.5}$ concentrations between the NEWEMIS, FCCS, SmartFire, and GlobCover scenarios and the FINN default scenarios during each time period are also shown in Figure 30. Maximum differences in 24-hour averaged $PM_{2.5}$ concentrations between the LOWEMIS and NEWEMIS scenarios, NEWEMIS_TEMPFOR, and NEWEMIS scenarios, and HIGHEMIS and NEWEMIS scenarios during April 15th – May 30th, 2008 and September 1st – October 17th, 2008 are shown in Figure 31.

Differences in $PM_{2.5}$ concentrations associated with modifications in FINN input data sources ranged from 0.5 to 85 $\mu g/m^3$ over the 36-km domain. Effects were less widespread than those for ozone, a finding consistent with the nature of ozone formation as a secondary pollutant. Geographic locations of differences in $PM_{2.5}$ concentrations between the sensitivity scenarios and the FINN default scenario were consistent with those of $PM_{2.5}$ emissions with relatively stronger effects in Mexico for the GlobCover scenario and in the central U.S. for the SmartFire scenario in the spring and in the western and southern/southeastern U.S. for the SmartFire, GlobCover, and FCCS scenarios in the late summer/early fall.

Summaries of metrics for 8-hour averaged ozone concentrations and 24-hour averaged $PM_{2.5}$ concentrations in Texas are shown by season and grid resolution in Tables S1 through S4 of the Supplemental Information. As illustrated for both ozone and $PM_{2.5}$, because of the intermittent frequency and variability in the spatial and temporal scales of fire events, impacts on percentile concentrations and mean concentrations over extended time periods may be minimal. On local and regional scales, air quality effects can be quite significant during specific fire events. Within the 12-km domain in Texas, predicted maximum absolute differences in MDA8 ozone concentrations were approximately 18 ppb (11 ppb) for the SmartFire scenario and 7 ppb (9 ppb) for the GlobCover and FCCS scenarios during the spring (late summer/early fall). Maximum absolute differences in 24-hour averaged $PM_{2.5}$ concentrations associated with changes in emissions factors, fuel loading (FCCS), or land cover characterization (GlobCover)

ranged from 10 to 40 $\mu g/m^3$ across both seasons; differences between the SmartFire and FINN default scenario were 78 $\mu g/m^3$ in the late summer/early fall and 168 $\mu g/m^3$ in the spring. Predicted changes in FINN fire emissions estimates on maximum (but to a much lesser extent mean and percentile) ozone and $PM_{2.5}$ concentrations were affected by the CAMx horizontal grid resolution and the spatial averaging of fire emissions.

Figure 27. (a) Mean of MDA8 ozone concentrations during April 15th – May 30th, 2008 (left) and September 1st – October 17th, 2008 (right) for the FINN default scenario. Maximum differences in MDA8 ozone concentrations (ppb) exceeding 0.5 ppb during April 15th – May 30th (left) and September 1st – October 17th (right) between the (b) NEWEMIS and FINN default scenarios, (c) FCCS and FINN default scenarios, (d) SmartFire and FINN default scenarios, and (e) GlobCover and FINN default scenarios.

(a)

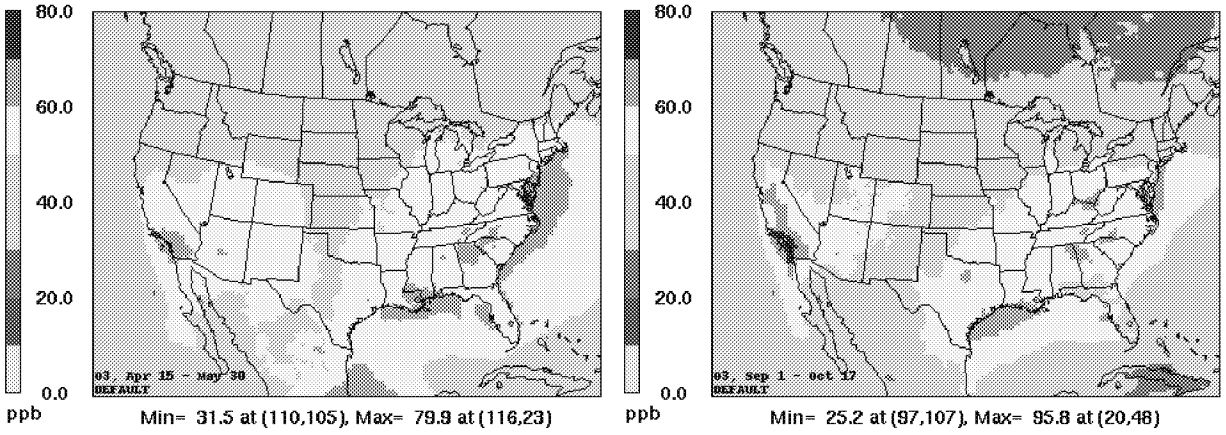

(b)

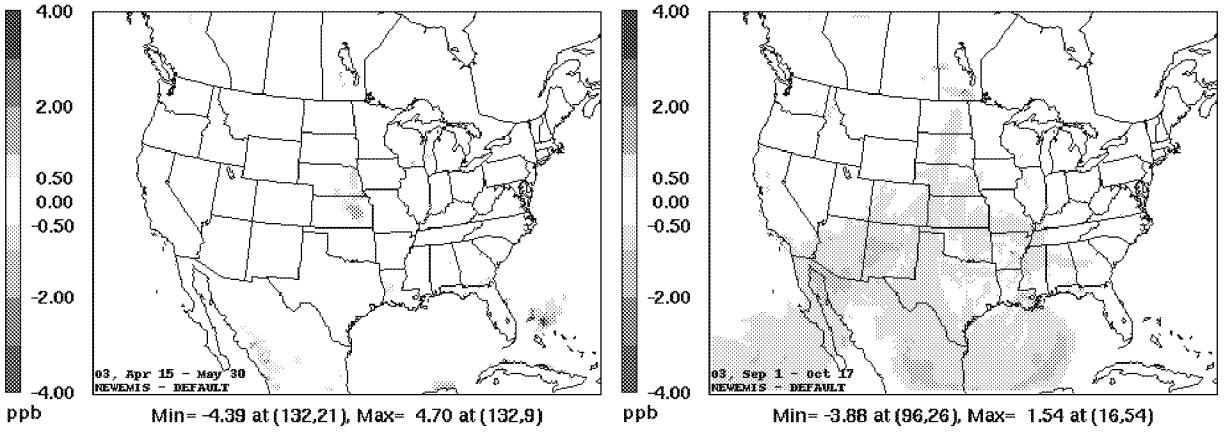

(c)

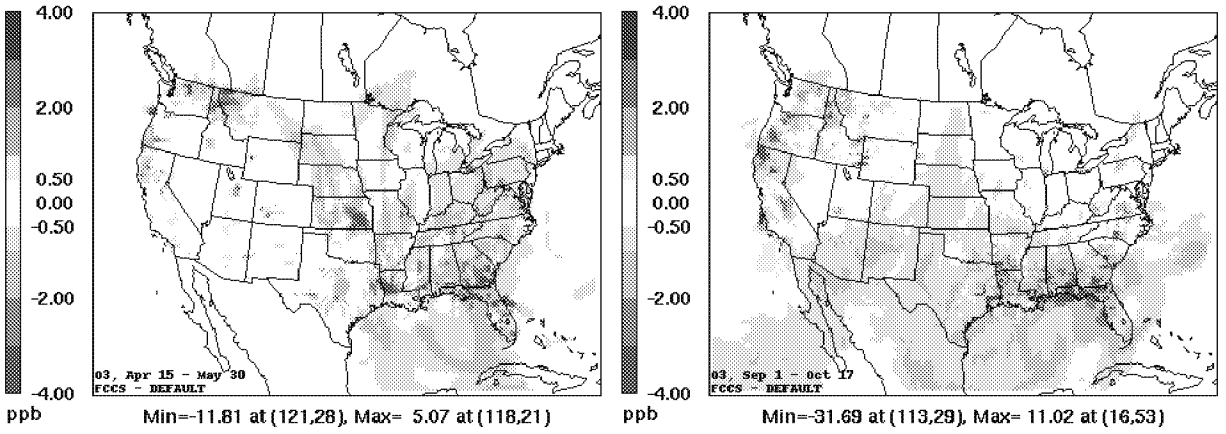

(d)

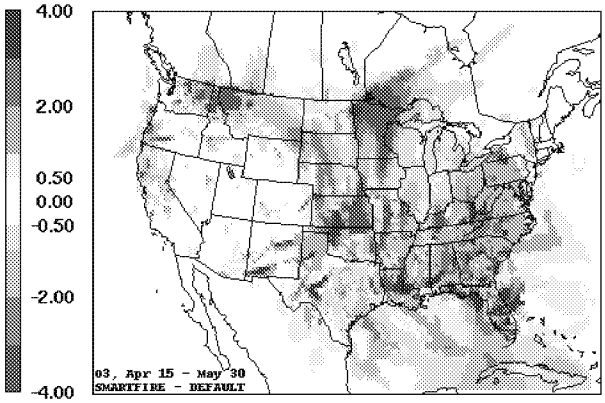

Min=-22.84 at (79,51), Max= 31.26 at (118,36)

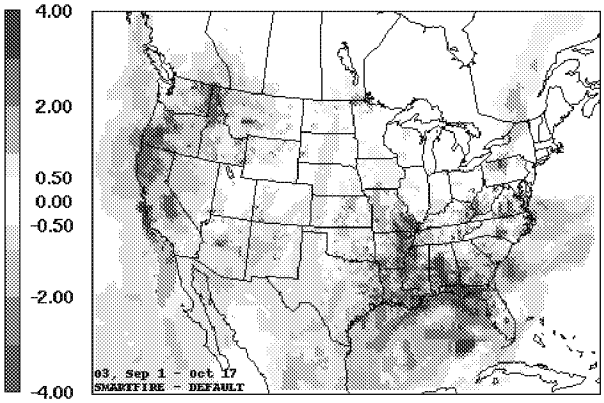

Min=-42.37 at (113,29), Max= 35.15 at (109,31)

(e)

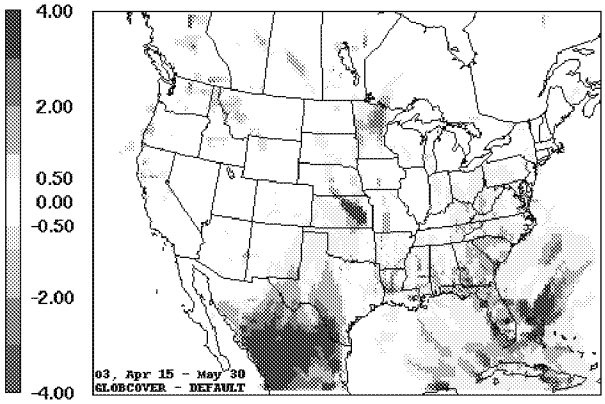

Min=-24.16 at (129,24), Max= 61.85 at (130,24)

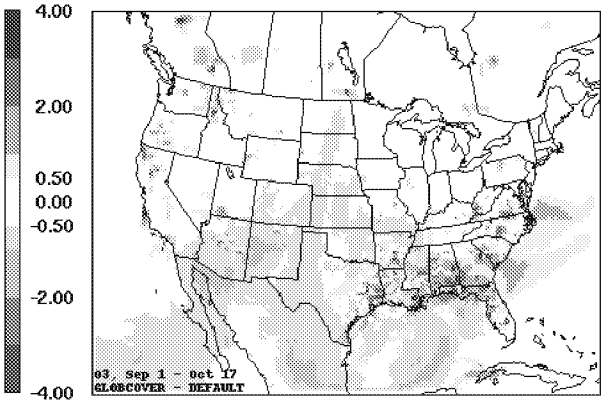

Min= -6.70 at (85,29), Max= 13.06 at (118,7)

Figure 28. Maximum differences in MDA8 ozone concentrations (ppb) exceeding 0.5 ppb between the (a) LOWEMIS and NEWEMIS scenarios (b) HIGHEMIS and NEWEMIS scenarios and (c) NEWEMIS_TEMPFOR and NEWEMIS scenarios during April 15th – May 30th, 2008 (left) and September 1st – October 17th, 2008 (right).

(a)

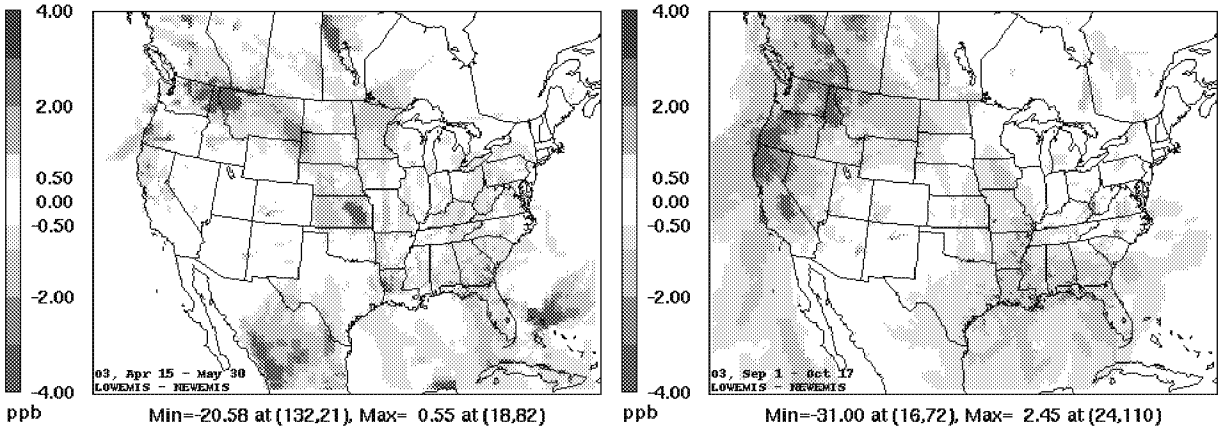

(b)

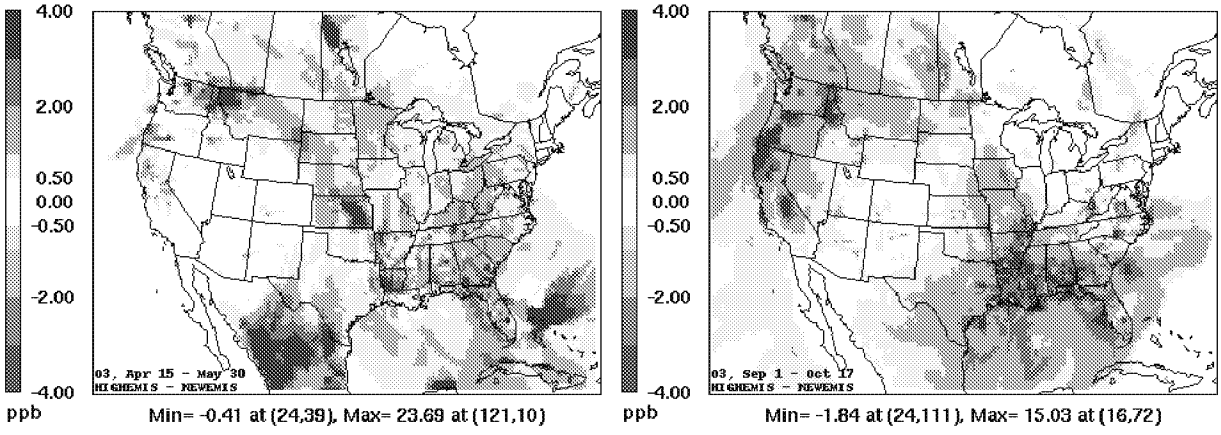

(c)

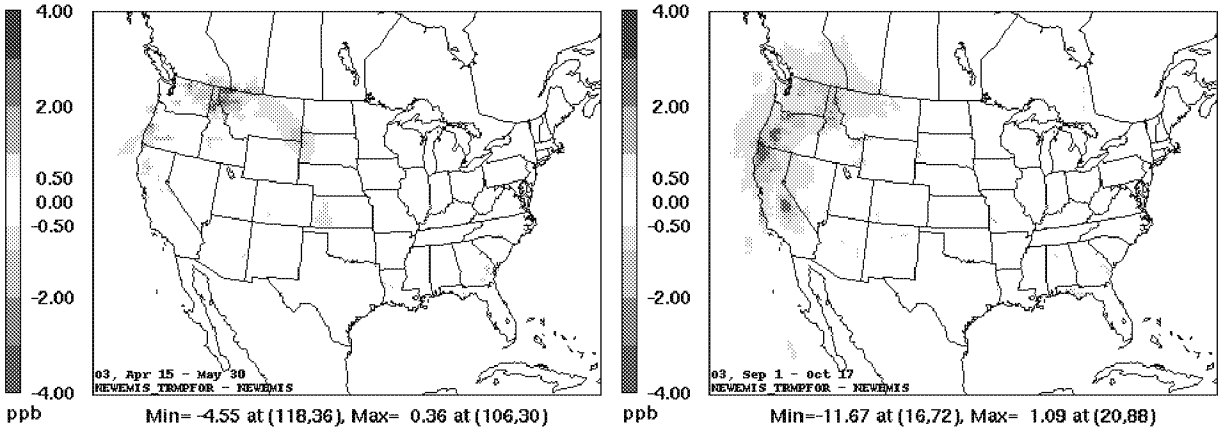

Figure 29. Range of differences in (a) MDA8 ozone concentrations (ppb) and (b) 24-hour averaged $PM_{2.5}$ concentrations (μg/m3) by region between each FINN sensitivity scenario and the FINN default configuration during April 15th – May 30th, 2008 (left) and September 1st – October 17th, 2008 (right).

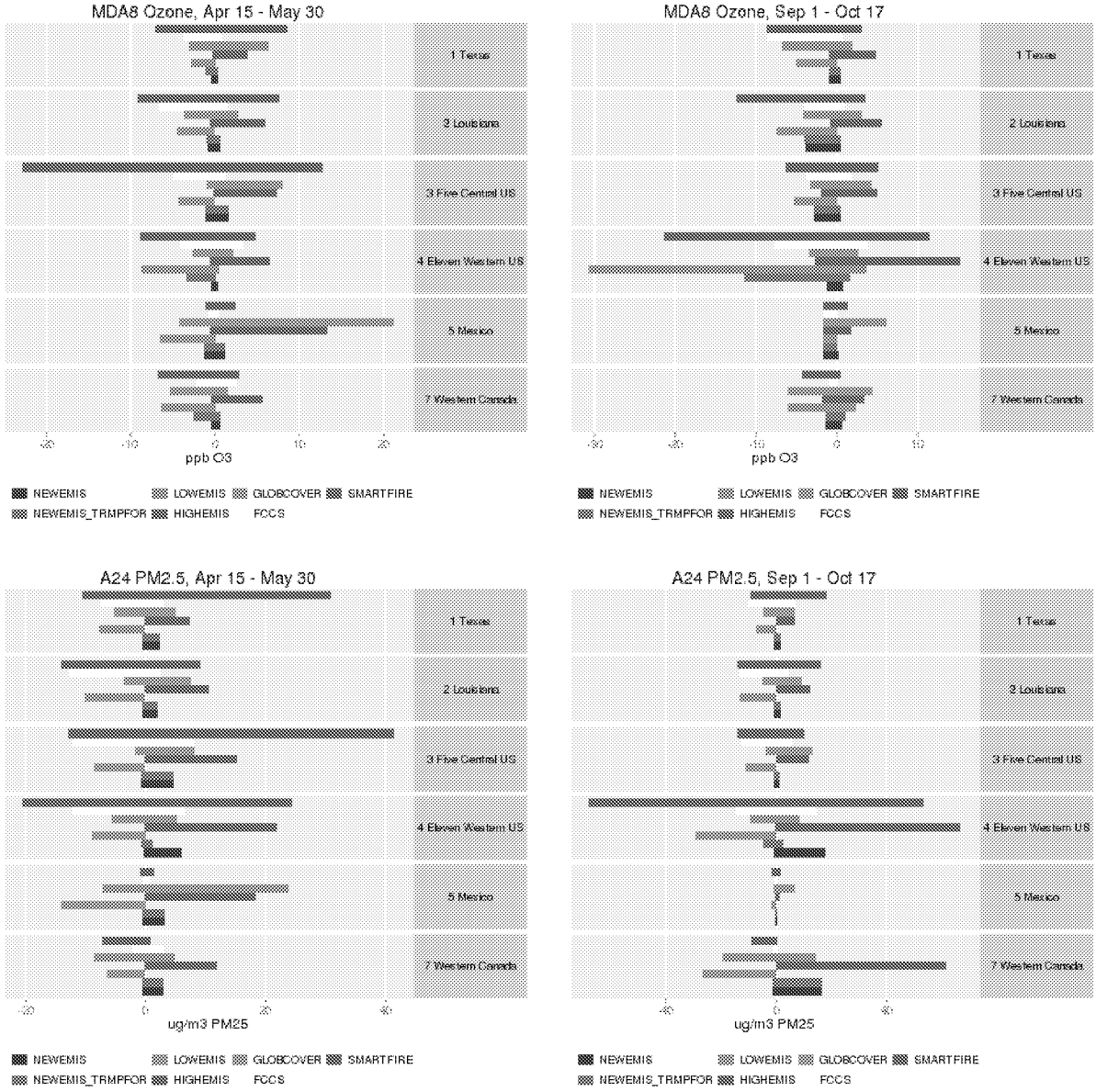

Figure 30. (a) Mean of 24-hour averaged $PM_{2.5}$ concentrations ($\mu g/m^3$) during April 15th – May 30th, 2008 (left) and September 1st – October 17th, 2008 (right) for the FINN default scenario. Maximum differences in 24-hour averaged $PM_{2.5}$ concentrations exceeding 1.25 $\mu g/m^3$ during April 15th – May 30th, 2008 (left) and September 1st – October 17th, 2008 (right) between the (b) NEWEMIS and FINN default scenarios, (c) FCCS and FINN default scenarios, (d) SmartFire and FINN default scenarios, and (e) GlobCover and FINN default scenarios.

(a)

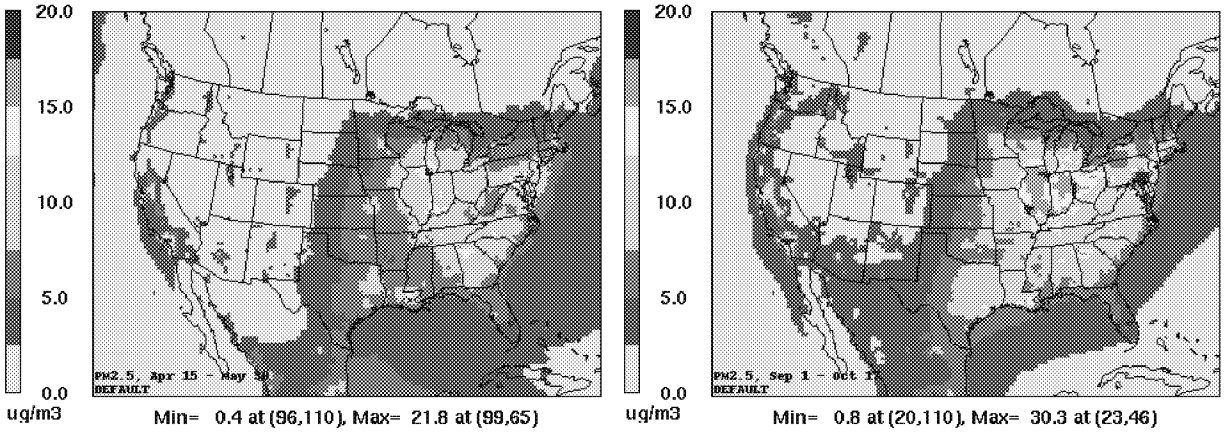

(b)

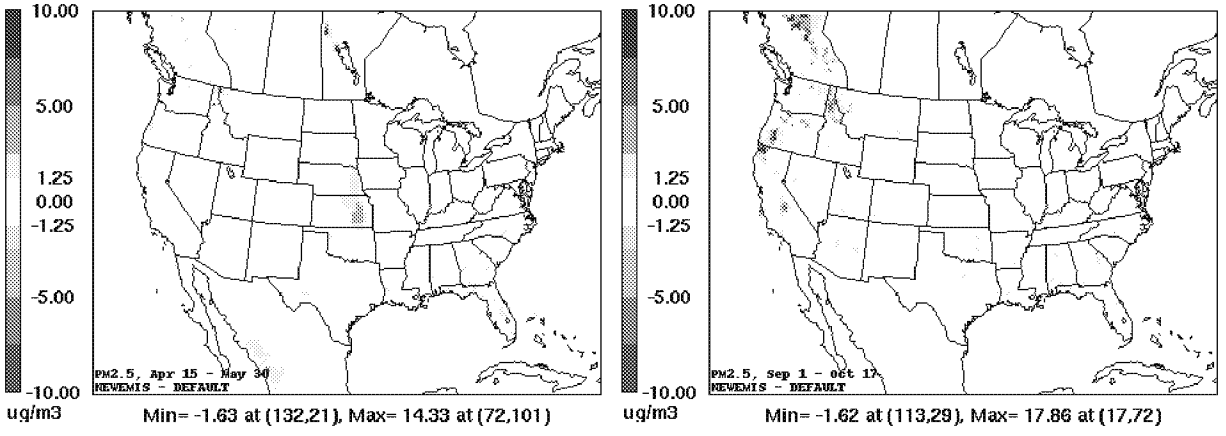

(c)

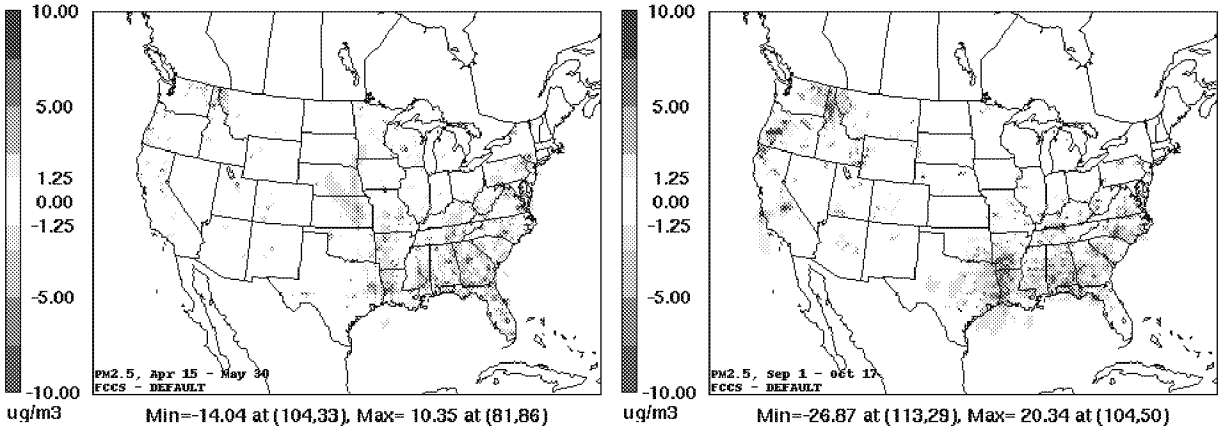

(d)

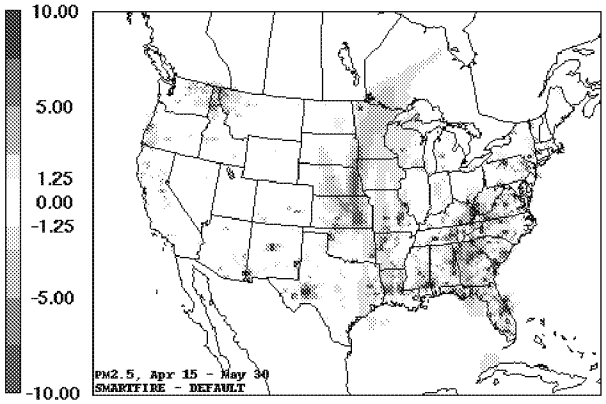

Min=-20.55 at (36,85), Max= 42.27 at (118,36)

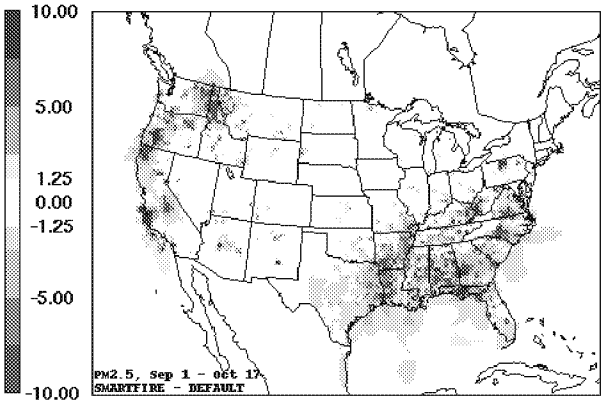

Min=-67.84 at (17,72), Max= 85.57 at (110,31)

(e)

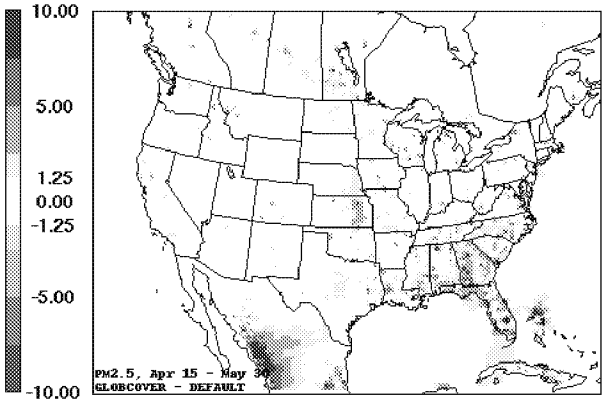

Min=-10.24 at (129,23), Max= 28.60 at (130,24)

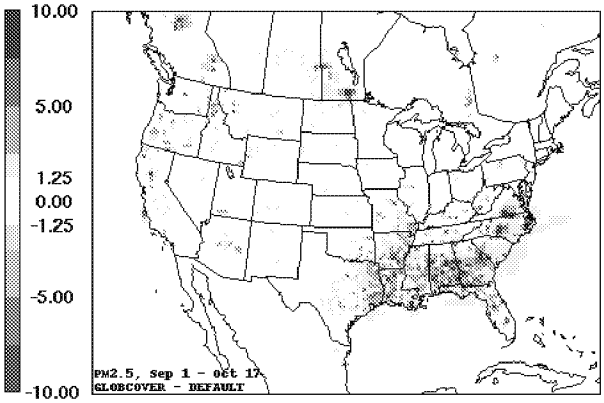

Min=-19.02 at (27,108), Max= 26.61 at (75,89)

Figure 31. Maximum differences in 24-hour averaged $PM_{2.5}$ concentrations ($\mu g/m^3$) exceeding 1.25 $\mu g/m^3$ between the (a) LOWEMIS and NEWEMIS scenarios (b) HIGHEMIS and NEWEMIS scenarios and (c) NEWEMIS_TEMPFOR and NEWEMIS scenarios during April 15th – May 30th, 2008 (left) and September 1st – October 17th, 2008 (right).

(a)

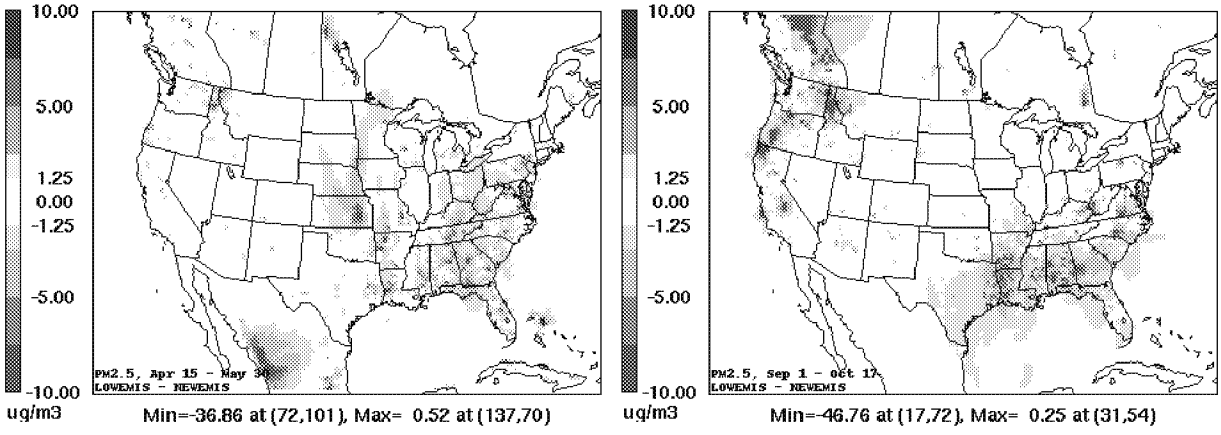

(b)

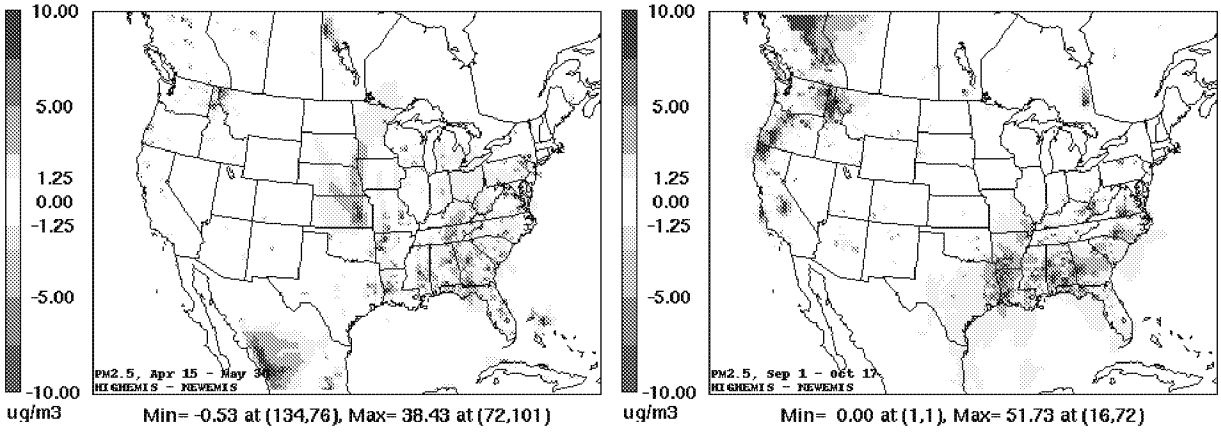

(c)

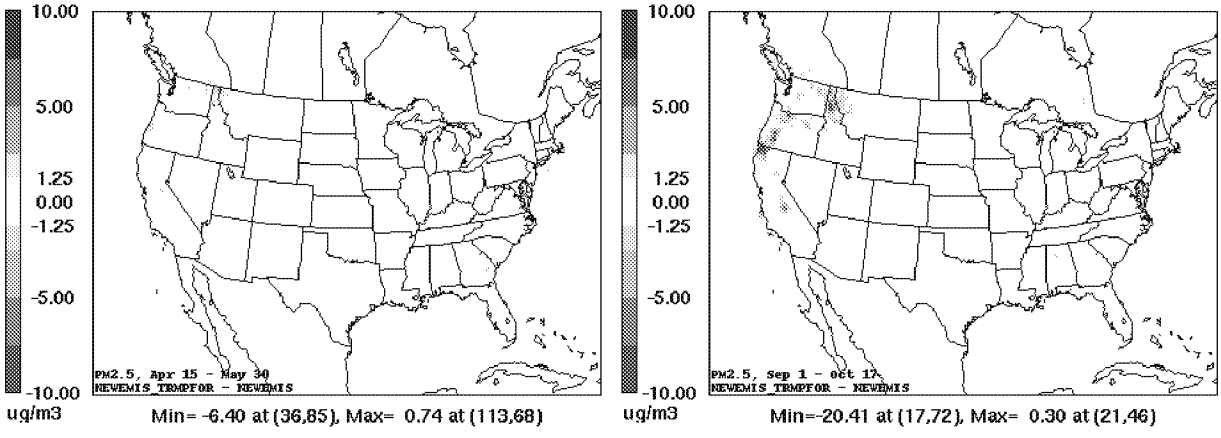

9. Conclusions

Wildland fires and open burning can be substantial sources of ozone precursors and particulate matter. The influence of fire events on air quality in Texas and other states has been well documented by observational studies. Fire emissions are often transported over multiple spatial scales and can contribute to exceedances of air quality standards. Accurate characterization of these events is necessary for understanding their influence on measured ambient concentrations, providing a weight of evidence for exceptional event exclusions, conducting air quality modeling for planning and attainment demonstrations, and estimating North American Background ozone concentrations used to inform policy decisions regarding the National Ambient Air Quality Standards. More than 80% of Texas was under exceptional drought in 2011, the worst year for wildfires in the state's history. An increase in future drought frequency in the southwestern United States may have complex and profound effects on the occurrence of fires.

This project evaluated the sensitivity of emissions estimates from FINN v.1 (referred to as the FINN default configuration for the purposes of this work) to variability in input parameters and the effects on modeled ozone and particulate matter concentrations using CAMx. The project included four major tasks:

1. Analysis of the climatology of fires in Texas and central and western states, Mexico and Central America, and western Canada between 2002-2012 using the FINN default configuration.

2. Comparison of fire emission estimates between the FINN default and BlueSky/SmartFire modeling frameworks

3. Evaluation of the sensitivity of FINN emissions estimates to emission factors, land cover classification, fuel loading data, and fire detection and area burned estimation

4. Assessment of the effects of FINN sensitivities on air quality using CAMx.

The time period of the CAMx episode spanned from April 1 through October 18, 2008. The analysis focused on the late spring, April and May, and the late summer/early fall, September and October. Fire climatology based on CO emissions estimates indicated that 2008 was close to the 2002-2012 average and varied strongly by region and season reflecting differences in the types of fire events, including prescribed burning, agricultural and crop residue burning, and wildfires.

Comparison of emissions estimates from the FINN default configuration with the Bluesky/SmartFire modeling framework that was used to provide emissions for the CAMx episode indicated that estimates of CO, VOC, and $PM_{2.5}$ emissions from BlueSky/SmartFire were higher than estimates from FINN; NO_x emissions, however, were higher from FINN than BlueSky/SmartFire. SmartFire uses reported area burned and detections from multiple satellite sensors. In contrast, FINN relies only on the MRR product. Overall, this difference generally results in a greater number of fire detections for BlueSky/SmartFire than FINN. A hypothesis is that higher NO_x emission factors in FINN may compensate for lower estimates of acreage burned, in particular in the central United States.

Sensitivity studies using FINN were constructed to examine the effects of uncertainty in emissions factors, fuel loading, land cover classification, and fire detection and estimation of area burned. The sensitivity studies highlighted the potential variability in predicted fire emissions, which were season and region dependent. Variability in emissions estimates among the sensitivity studies and between the sensitivity studies and the FINN default configuration exceeded a factor of two. Responses were particularly notable for the SmartFire scenarios in the central and southeastern U.S. during the spring and western and southern U.S. during late summer/early fall seasons and the Globcover scenario in Mexico during the spring. Interactions between input parameters were complex and not generalizable across geographic regions.

It was evident that fire emissions estimates using FINN, and likely similar models, would benefit from targeted improvements. In most regions of the U.S., fire detections and associated area burned estimates were substantially greater with the use of the SmartFire product than in the current default configuration of FINN that relies only on the MRR product. This suggested that potential benefits of reliance on a combination of ground reports and observations from multiple satellite sensors. However, careful scrutiny and validation of the algorithms used to identify the onset, persistence, and spatial extent of fires and to address repeat counting is necessary. A shortcoming of the current version SmartFire is that it does not include data for Canada and Mexico. An emerging data resource is the Visible Infrared Imaging Radiometer Suite (VIIRS) sensor onboard NASA's National Polar-orbiting Operational Environmental Satellite System Preparatory Project (NPP) satellite that launched on October 28, 2011. VIIRS is a scanning radiometer that collects visible and infrared imagery and radiometric measurements of the land, atmosphere, cryosphere, and oceans. VIIRS Land Cover and Fire Products are used to quantify vegetation disturbance and to support estimates of emissions from biomass burning, expanding on the legacies of the Advanced Very High Resolution Radiometer (AVHRR) and MODIS sensors (http://npp.gsfc.nasa.gov/viirs.html).

Improvements in measurement techniques and coordinated field validation efforts would reduce uncertainties in emission factors. This study suggested that uncertainties in emissions factors are particularly high for VOCs. The next version of FINN will include the most recent estimates, and emissions factors should continue to be updated as new information becomes available.

Fuel loadings in the current version of FINN are assigned for each generic vegetation classification within global regions. Future improvements should include the addition of new regions where data may become are available, incorporation of recent fuel loadings from the literature, and fuel loading values specified per vegetation types. More effort is needed to constrain fuel loadings estimates for fires in areas classified as croplands. The FCCS is expected to be the most specific data available for the United States and will be considered in the next version of FINN.

Land cover mapping in FINN is important, influencing, for example, fuel loadings and emission factors. Although the MODIS LCT map is readily available and widely used, classifications vary significantly from other land cover/land use maps. At the global scale, these maps have been validated in only a few regions and at small spatial scales. It is clear from the sensitivity simulations that agricultural areas with high fire activity (e.g., Arkansas in the fall) are highly sensitive to model input parameters. It is recommended that much more effort be applied to better constrain estimates of area burned, emission factors, and fuel loading for these cropland regions. The inclusion of maps and emissions from specific crop types is expected in the next version of FINN. A promising, potential data source is the publicly available EarthStat (http://www.earthstat.org/) initiative that focuses on global agricultural landscapes. Inclusion of a map with geographic locations where peat burning occurs is expected as well in the next version of FINN. Better representation of forest types within the United States is also necessary, including assignments of additional land cover classifications, specific fuel loadings, and emission factors.

The extensive resources that have been used to characterize land cover in Texas should be leveraged to compare to and substitute for classifications derived from global databases that may not have undergone validation in the state. In addition, because the influence of fires extends over regional or longer spatial scales, inclusion of specific land cover databases for neighboring states, such as Louisiana, would be beneficial for improving predictions of air quality in Texas.

In subsequent research, CAMx sensitivity studies could be conducted with 2006 and 2012 emissions inventories developed by the TCQE for air quality planning in eastern Texas. In addition, future CAMx modeling applications should consider the use of nested grids with 4-km horizontal resolution over eastern Texas and analysis of model predictions at daily time scales. Discussions will be held with project sponsors regarding these and other possible directions for follow-on work.

References

1) Akagi, S. K., R. J. Yokelson, C. Wiedinmyer, M. J. Alvarado, J. S. Reid, T. Karl, J. D. Crounse, and P. O. Wennberg (2011), Emission factors for open and domestic biomass burning for use in atmospheric models, *Atmospheric Chemistry and Physics*, *11*(9), 4039-4072.

2) Akagi, S. K., Yokelson, R. J., Burling, I. R., Meinardi, S., Simpson, I., Blake, D. R., McMeeking, G. R., Sullivan, A., Lee, T., Kreidenweis, S., Urbanski, S., Reardon, J., Griffith, D. W. T., Johnson, T. J., and Weise, D. R.: Measurements of reactive trace gases and variable O_3 formation rates in some South Carolina biomass burning plumes, Atmos. Chem. Phys., 13, 1141-1165, doi:10.5194/acp-13-1141-2013, 2013.

3) Al-Saadi, J., et al. (2008), Intercomparison of near-real-time biomass burning emissions estimates constrained by satellite fire data, *Journal of Applied Remote Sensing*, *2*.

4) Andreae, M.O., (2008) personal communication with C. Wiedinmyer, October 2008.

5) Andreae, M.O., and Merlet, P. (2001), Emissions of trace gases and aerosols from bimass burning, *Global Biogeochemical Cycles*, *15*(4), 955-966.

6) de Foy, B., S. P. Burton, R. A. Ferrare, C. A. Hostetler, J. W. Hair, C. Wiedinmyer, and L. T. Molina (2011), Aerosol plume transport and transformation in high spectral resolution lidar measurements and WRF-Flexpart simulations during the MILAGRO Field Campaign, *Atmospheric Chemistry and Physics*, *11*(7), 3543-3563.

7) Emmons, L. K., et al. (2010), Impact of Mexico City emissions on regional air quality from MOZART-4 simulations, *Atmospheric Chemistry and Physics*, *10*(13), 6195-6212.

8) Fast, J., et al. (2009), Evaluating simulated primary anthropogenic and biomass burning organic aerosols during MILAGRO: Implications for assessing treatments of secondary organic aerosols, *Atmospheric Chemistry and Physics*, *9*(16), 6191-6215.

9) Hodzic, A., S. Madronich, B. Bohn, S. Massie, L. Menut, and C. Wiedinmyer (2007), Wildfire particulate matter in Europe during summer 2003: meso-scale modeling of smoke emissions, transport and radiative effects, *Atmospheric Chemistry and Physics*, *7*(15), 4043-4064.

10) Hoelzemann, J.J., M.G. Schultz, G.P. Brasseur, C. Granier, and M. Simon (2004), Global Wildland Fire Emission Model (GWEM): Evaluating the use of global area burnt satellite data, *Journal of Geophysical Research*, *109*, D14S04, doi:10.129/2003JD003666.

11) Junquera , V., M.M. Russell, W. Vizuete, Y. Kimura, and D. Allen, Wildfires in eastern Texas in August and September 2000: Emissions, aircraft measurements, and impact on photochemistry, *Atmospheric Environment*, *39*(27), 4983-4996.

12) McMeeking, G.R. (2008), The optical, chemical and physical properties of aerosols and gases emitted by the laboratory combustion of wildland fuels, Ph.D. Dissertation, Department of Atmospheric Sciences, Colorado State University, 109-113.

13) McMillan, W.W., R.B. Pierce, L.C. Sparling, G. Osterman, K. McCann, M.L. Fischer, B. Rappengluck, R. Newson, D. Turner, C. Kittaka, K. Evans, S. Biraud, B. lefer, A. Andrews, and S. Oltmans (2010), An observational and modeling strategy to invetigate the impact of remote

sources on local air quality: A Houston, Texas, case study from the Second Texas Air Quality Study (TexAQS II), *Journal of Geophysical Research, 115*, D01301, doi:10.1029/2009JD011973.

14) Morris, G.A., S. Hersey, A.M. Thompson, S. Pawson, J. E. Nielsen, P.R. Colarco, W.W. McMillan, A. Stohl, S. Turquety, J. Warner, B.J. Johnson, T. L. Kucsera, D. E. Larko, S.J. Oltmans, and J.C. Witte (2006), Alaskan and Canadian forest fires exacerbate ozone pollution over Houston, Texas, on 19 and 20 July 2004, *Journal of Geophysical Research, 111,* D24S03, doi:10.1029/2006JD007090.

15) Morris, R.E., C. Loomis, Z. Adelman (2012). Final Technial Memorandum No. 5: Fire Emissions, Wildfires, Prescribed Burns and Agricultural Burning Emissions. Prepared for the Western Regional Air Partnerhsip (April 27, 2012). http://www.wrapair2.org/pdf/ Memo_5_Fires_Apr27_2012_Final.pdf.

16) Pfister, G.G., J. Avise, C. Wiedinmyer, D.P. Edwards, L.K. Emmons, G.D. Diskin, J. Podolske, and A. Wisthaler (2011), CO source contribution analysis for California during ARCTAS-CARB, *Atmospheric Chemistry and Physics*, *11*(15), 7515-7532.

17) Pfister, G.G., C. Wiedinmyer, and L.K. Emmons (2008), *Geophysical Research Letters*, *35*(19), L19814.

18) UNC (2010), SMOKE v2.7 User's Manual, University of North Carolina, Institute for the Environment (2010/09/30 14:58:15). http://www.smoke-model.org/version2.7/ SMOKE_v27_manual.pdf.

19) Villanueva-Fierro, I., C.J. Popp, R.W. Dixon, R.S. Martin, J.S. Gafney, N.A. Marley, J.M. Harris (2009), Ground-level chemical analysis of air transported from the 1998 Mexican-Central American fires to the Southwestern USA, *Revista Internacional de Contaminacion Ambiental*, *25*(1), 23-32.

20) Westerling, A. L.; Bryant, B. P., Climate change and wildfire in California. *Climatic Change* 2008, *87*, S231-S249.

21) Westerling, A. L.; Turner, M. G.; Smithwick, E. A. H.; Romme, W. H.; Ryan, M. G., Continued warming could transform greater Yellowstone fire regimes by mid-21st century. Proceedings of the National Academy of Sciences 2011, 108, 13165-13170.

22) Westerling, A. L.; Hidalgo, H. G.; Cayan, D. R.; Swetnam, T. W., Warming and earlier spring increase western U.S. forest wildfire activity. Science 2006, 313, 940-943.

23) Wiedinmyer, C., B. Quayle, C. Geron, A. Belote, D. McKenzie, X. Zhang, S. O'Neill, and K.K. Wynne (2006), Estimating emissions from fires in North America for air quality modeling, *Atmopsheric Environment*, *40*, 3419-3432.

24) Wiedinmyer, C., S. K. Akagi, R. J. Yokelson, L. K. Emmons, J. A. Al-Saadi, J. J. Orlando, and A. J. Soja (2011), The Fire INventory from NCAR (FINN): a high resolution global model to estimate the emissions from open burning, *Geoscientific Model Development*, *4*(3), 625-641.

25) Wiedinmyer, C., S. K. Akagi, R. J. Yokelson, L. K. Emmons, J. A. Al-Saadi, J. J. Orlando, and A. J. Soja (2011), The Fire INventory from NCAR (FINN): a high resolution global model to estimate the emissions from open burning, Geoscientific Model Development, 4(3), 625-641.

26) Wiedinmyer, C. American Geophysical Union Fall Meeting, San Francisco, CA, December 2011b.

27) Yokelson, R. J., Burling, I. R., Gilman, J. B., Warneke, C., Stockwell, C. E., de Gouw, J., Akagi, S. K., Urbanski, S. P., Veres, P., Roberts, J. M., Kuster, W. C., Reardon, J., Griffith, D. W. T., Johnson, T. J., Hosseini, S., Miller, J. W., Cocker III, D. R., Jung, H., and Weise, D. R.: Coupling field and laboratory measurements to estimate the emission factors of identified and unidentified trace gases for prescribed fires, Atmos. Chem. Phys., 13, 89-116, doi:10.5194/acp-13-89-2013, 2013.

The Effects of Uncertainties in Fire Emissions Estimates on Predictions of Texas Air Quality

Supplemental Information

AQRP Project No. 12-018

Elena McDonald-Buller (PI) and Yosuke Kimura
Center for Energy and Environmental Resources
The University of Texas at Austin

Christine Wiedinmyer (Co-PI)
The National Center for Atmospheric Research

Chris Emery (Co-PI) and Ed Tai
ENVIRON International Corporation

Figure S1. (a) Total CO emissions (short tons) between April 15th – May 30th, 2008 from the FINN default configuration. (b) Difference in CO emissions between the NEWEMIS and FINN default scenarios. Differences in CO emissions between the (c) LOWEMIS, (d) NEWEMIS_TEMPFOR and (e) HIGHEMIS and the NEWEMIS scenarios.

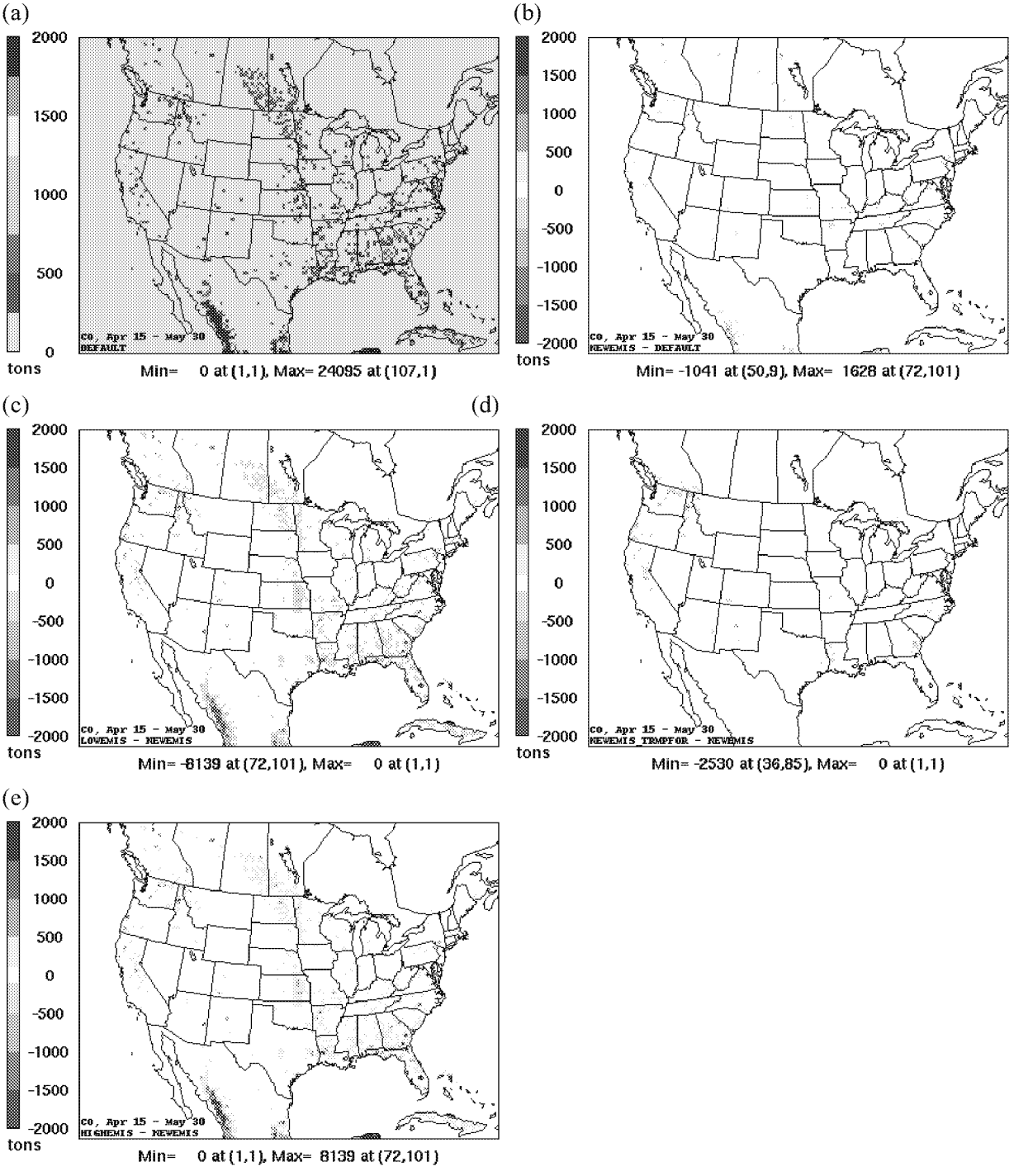

Figure S2. (a) Total NO_x emissions (short tons) between April 15th – May 30th, 2008 from the FINN default configuration. (b) Difference in NO_x emissions between the NEWEMIS and FINN default scenario. Differences in NO_x emissions between the (c) LOWEMIS, (d) NEWEMIS_TEMPFOR and (e) HIGHEMIS and the NEWEMIS scenarios.

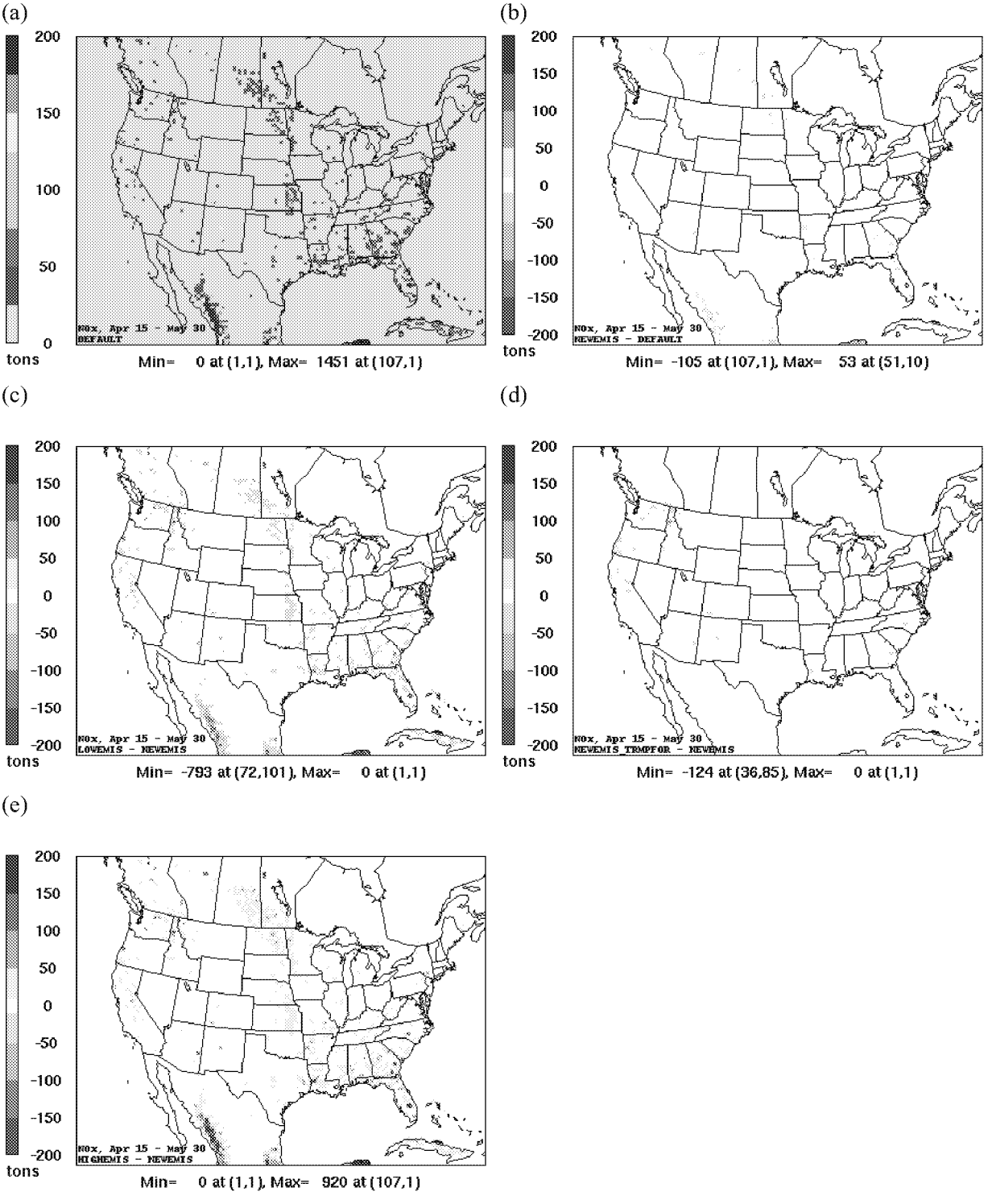

Figure S3. (a) Total VOC emissions (short tons) between April 15th – May 30th, 2008 from the FINN default configuration. (b) Difference in VOC emissions between the NEWEMIS and FINN default scenario. Differences in VOC emissions between the (c) LOWEMIS, (d) NEWEMIS_TEMPFOR and (e) HIGHEMIS and the NEWEMIS scenarios.

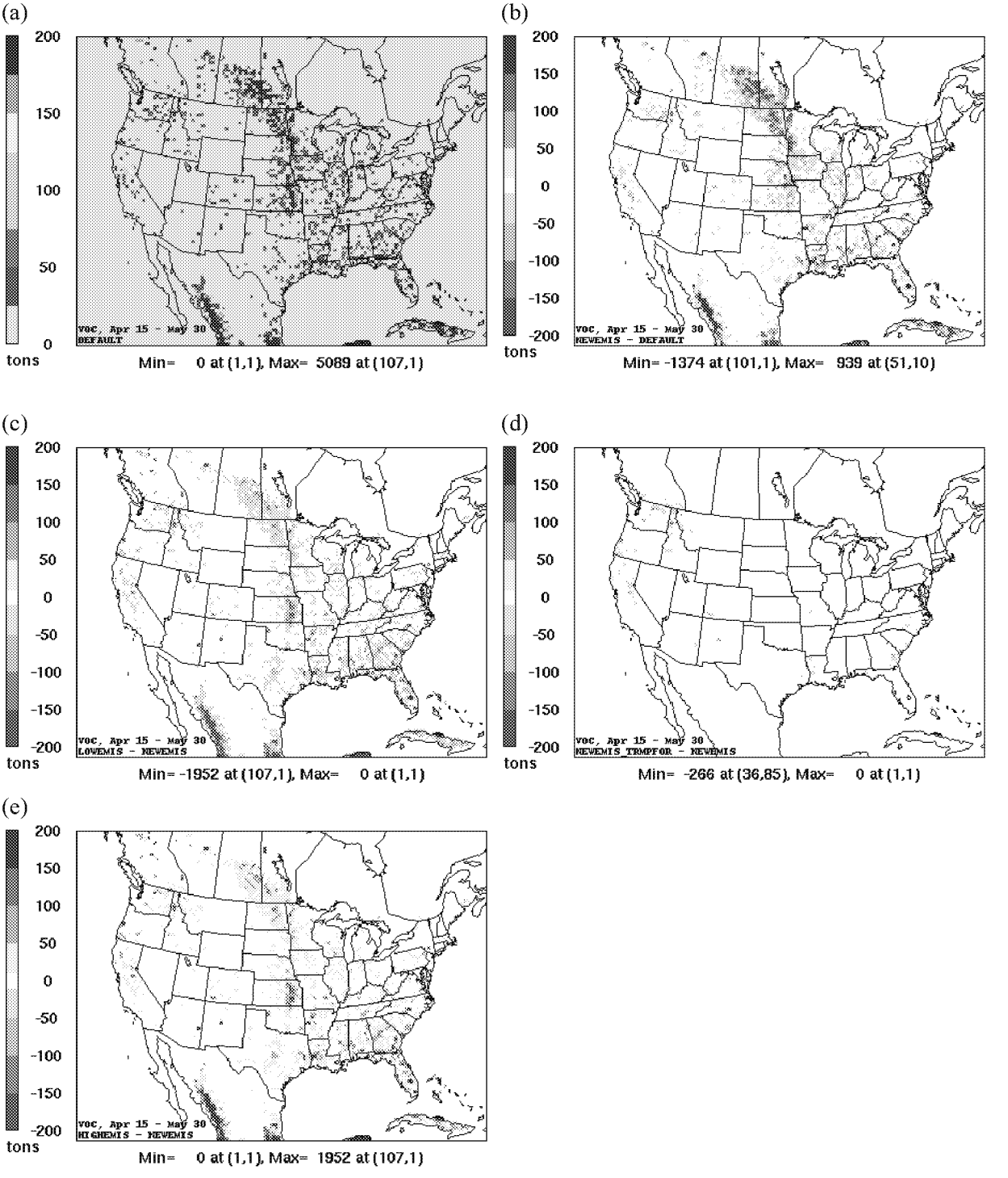

Figure S4. (a) Total $PM_{2.5}$ emissions (short tons) between April 15th – May 30th, 2008 from the FINN default configuration. (b) Difference in $PM_{2.5}$ emissions between the NEWEMIS and FINN default scenario. Differences in $PM_{2.5}$ emissions between the (c) LOWEMIS, (d) NEWEMIS_TEMPFOR and (e) HIGHEMIS and the NEWEMIS scenarios.

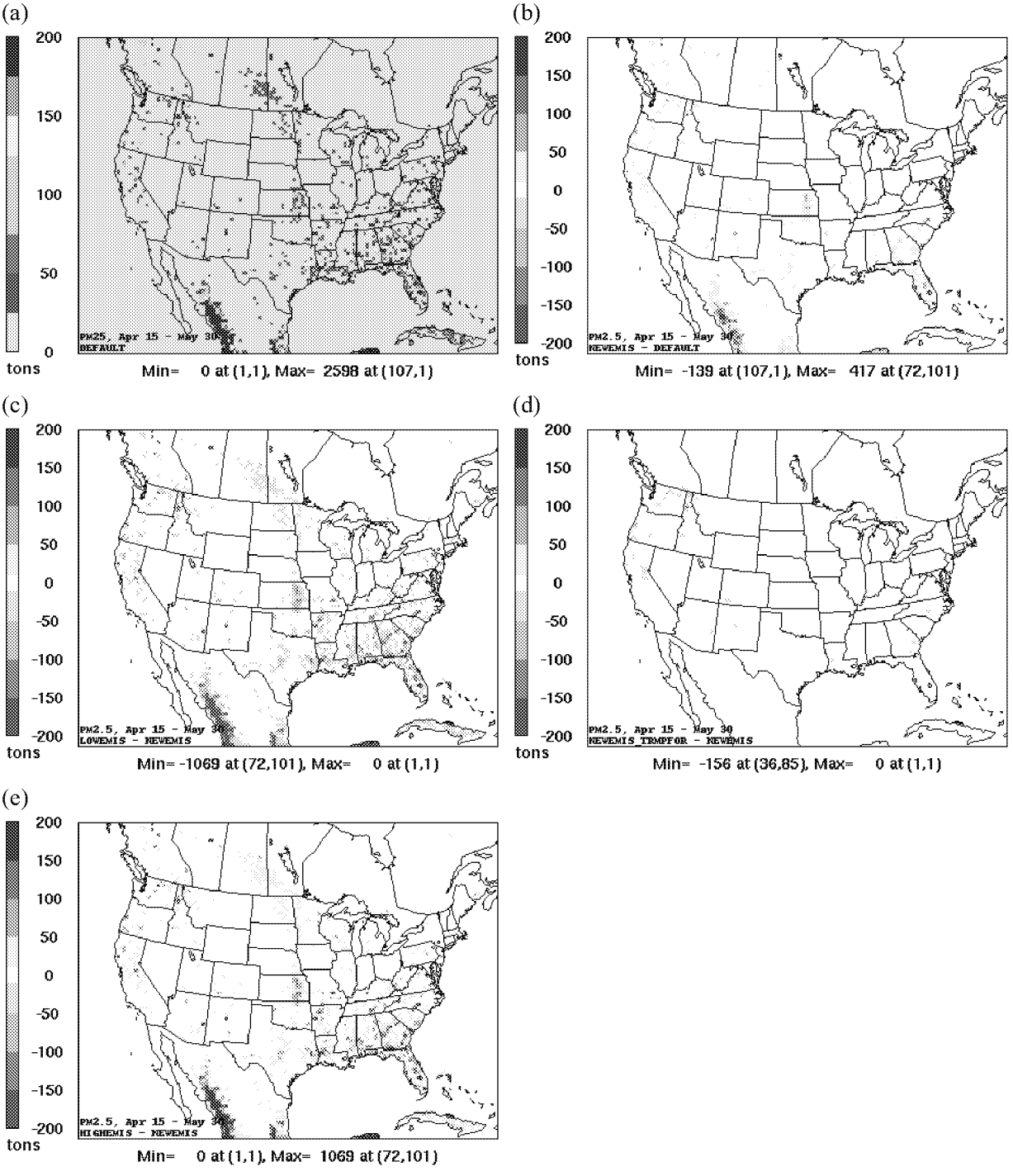

Figure S5. Difference in (a) CO, (b) NO_x, (c) VOC, and (d) $PM_{2.5}$ emissions between the FCCSFuel and FINN default scenarios during April 15th – May 30th, 2008.

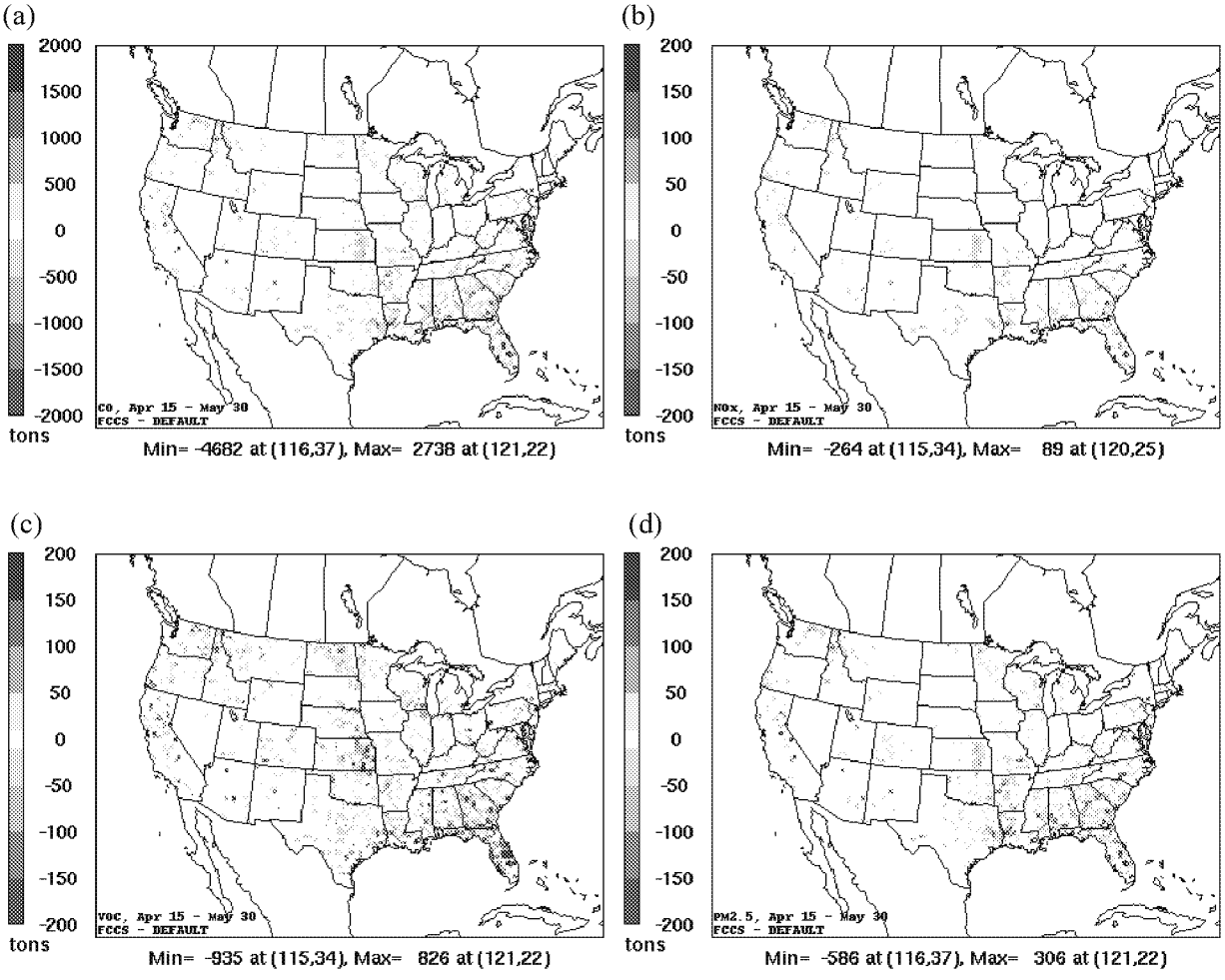

Figure S6. Difference in (a) CO, (b) NO_x, (c) VOC, and (d) $PM_{2.5}$ emissions between the SmartFireDetect and FINN default scenarios during April 15th – May 30th, 2008.

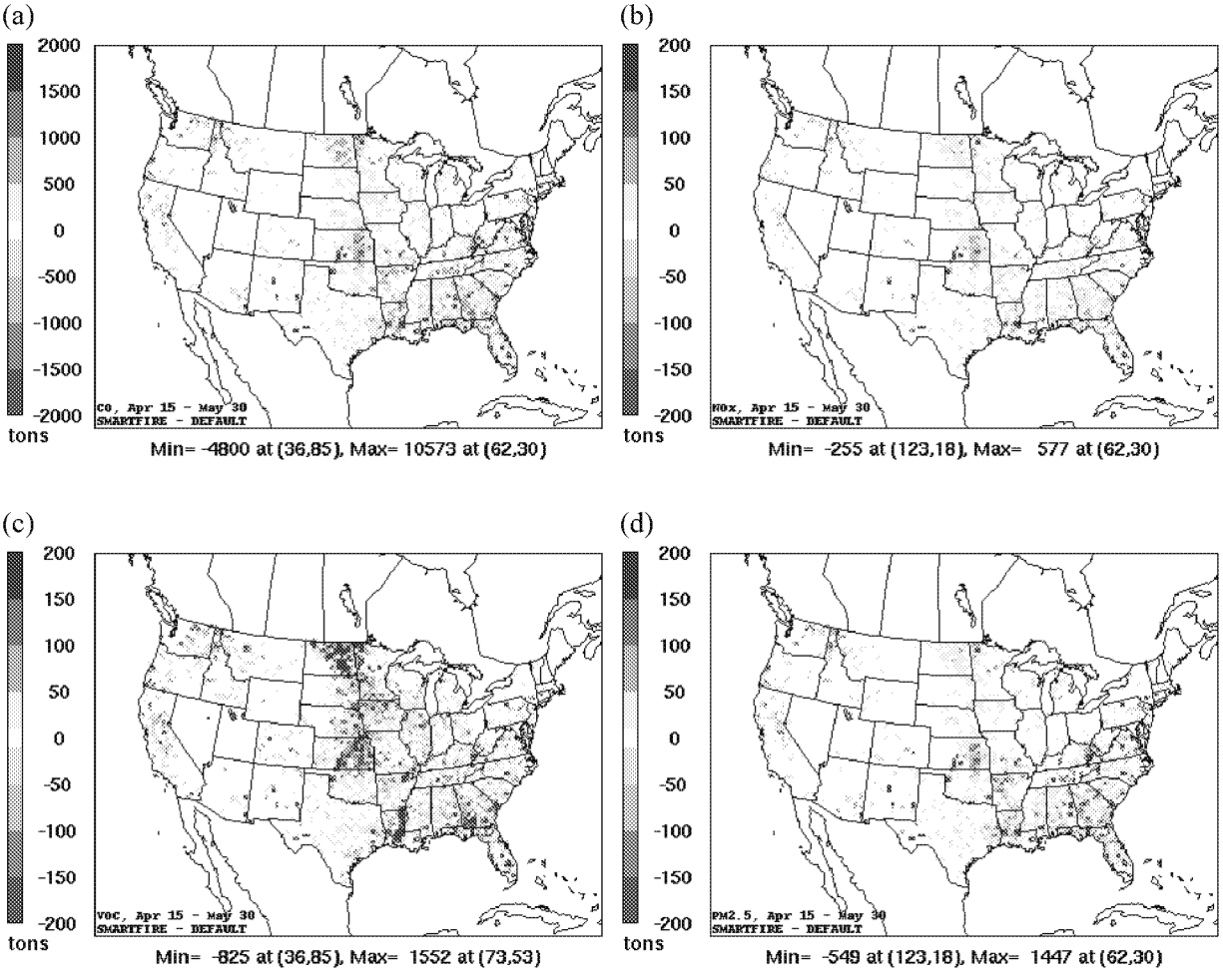

Figure S7. Difference in (a) CO, (b) NO_x, (c) VOC, and (d) $PM_{2.5}$ emissions between the Globcover and FINN default scenarios during April 15th –May 30th, 2008.

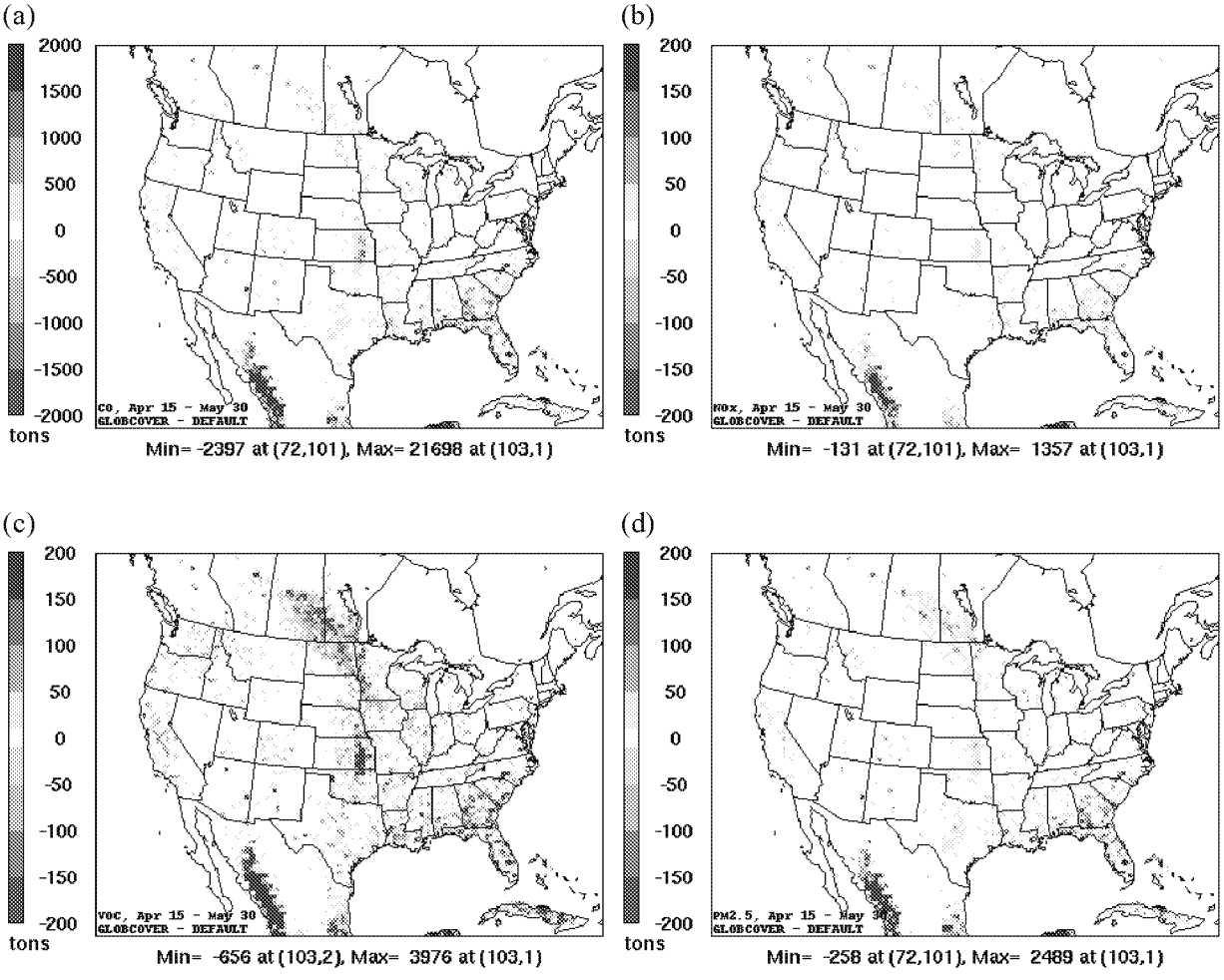

Table S1. Ozone metrics* (ppb) during April 15th through May 30th, 2008 within the 12-km grid in Texas. Metrics for the 36-km grid are shown in parentheses.

	Percentile 8-hour Ozone Concentrations			Mean Difference in 8-Hour Averaged Ozone Concentrations	Maximum Difference in 8-hour Averaged Ozone Concentrations	Mean Daily Maximum 8-hour Averaged Ozone Concentrations	Mean Difference in Daily Maximum 8-hour Averaged Ozone Concentrations	Maximum Difference in Daily Maximum 8-hour Averaged Ozone Concentrations
	25th	50th	75th					
DEFAULT	37.42 (37.23)	43.47 (43.33)	49.23 (49.11)	n.a.	n.a.	51.73 (51.66)	n.a.	n.a.
GlobCover	37.50 (37.31)	43.56 (43.41)	49.32 (49.20)	0.08 (0.08)	8.35 (8.00)	51.82 (51.76)	0.10 (0.10)	6.99 (6.53)
NEWEMIS	37.41 (37.23)	43.47 (43.32)	49.23 (49.10)	-0.01 (-0.01)	-3.00 (-0.61)	51.72 (51.65)	-0.01 (-0.01)	-1.73 (0.39)
HIGHEMIS	37.53 (37.35)	43.60 (43.45)	49.36 (49.24)	0.12 (0.12)	6.77 (4.78)	51.86 (51.80)	0.14 (0.14)	6.25 (3.88)
LOWEMIS	37.34 (37.15)	43.39 (43.25)	49.15 (49.02)	-0.08 (-0.08)	-4.55 (-2.94)	51.64 (51.57)	-0.09 (-0.09)	-4.55 (-2.74)
NEWEMIS_ TEMPFORE	37.41 (37.22)	43.46 (43.32)	49.22 (49.10)	-0.01 (-0.01)	-3.00 (-1.12)	51.72 (51.65)	-0.01 (-0.01)	-1.73 (-1.07)
SmartFire	37.46 (37.27)	43.50 (43.35)	49.27 (49.15)	0.03 (0.03)	-28.13 (8.69)	51.77 (51.70)	0.04 (0.04)	-17.75 (8.64)
FCCS	37.39 (37.21)	43.43 (43.29)	49.18 (49.06)	-0.04 (-0.04)	8.09 (-4.00)	51.69 (51.62)	-0.04 (-0.04)	-6.98 (-3.58)

*8-Hour Ozone Concentration Percentile:

$$\underset{i\in R,h\in P}{\mathrm{P}(percentile)}\left(A8_{i,h}\right)$$

Mean Difference in 8-Hour Ozone Concentration

$$\underset{i\in R,h\in P}{\mathrm{mean}}\left(A8_{i,h,sensitivity}-A8_{i,h,default}\right)$$

Maximum Difference in 8-Hour Ozone Concentration- From either below that has a greater absolute value:

$$\begin{cases}\underset{i\in R,h\in P}{\max}\left(A8_{i,h,sensitivity}-A8_{i,h,default}\right)\\ \underset{i\in R,h\in P}{\min}\left(A8_{i,h,sensitivity}-A8_{i,h,default}\right)\end{cases}$$

Mean MDA8 Ozone Concentration

$$\underset{i\in R,d\in P}{\mathrm{mean}}\left(MDA8_{i,d}\right)$$

Mean Difference in MDA8 Ozone Concentration

$$\underset{i\in R,d\in P}{\mathrm{mean}}\left(MDA8_{i,d,sensitivity}-MDA8_{i,d,default}\right)$$

where R: Spatial region of interest; P: Temporal period of interest; i: A model grid cell index within region of interest, R; h: An hour within analysis period, P; d: A day within analysis period, P; *sensitivity* refers to sensitivity study; *default*: refers to FINN model configuration; $C_{i,h}$: Hourly concentration at cell i, hour h; $A8_{i,h}$: Eight hour moving average concentration at cell i, hour h; $MDA8_{i,d}$: Daily maximum eight hour concentration at cell i, day d.

Table S2. Ozone metrics (ppb) during September 1st through October 17th, 2008 within the 12-km grid in Texas. Metrics for the 36-km grid are shown in parentheses.

	Percentile 8-hour Ozone Concentrations			Mean Difference in 8-Hour Averaged Ozone Concentrations	Maximum Difference in 8-hour Averaged Ozone Concentrations	Mean Daily Maximum 8-hour Averaged Ozone Concentrations	Mean Difference in Daily Maximum 8-hour Averaged Ozone Concentrations	Maximum Difference in Daily Maximum 8-hour Averaged Ozone Concentrations
	25th	50th	75th					
DEFAULT	35.92 (35.68)	43.78 (43.55)	52.58 (52.29)	n.a.	n.a.	52.96 (52.83)	n.a.	0.00 (0.00)
GlobCover	35.90 (35.66)	43.77 (43.54)	52.59 (52.30)	0.00 (0.00)	-9.05 (-6.97)	52.95 (52.82)	-0.01 (-0.01)	-9.02 (-6.70)
NEWEMIS	35.88 (35.64)	43.74 (43.51)	52.54 (52.25)	-0.04 (-0.03)	-4.79 (-0.98)	52.92 (52.79)	-0.04 (-0.04)	-2.89 (-0.95)
HIGHEMIS	35.99 (35.75)	43.89 (43.67)	52.80 (52.51)	0.16 (0.16)	7.90 (4.99)	53.14 (53.00)	0.18 (0.18)	7.71 (4.94)
LOWEMIS	35.81 (35.57)	43.65 (43.42)	52.40 (52.11)	-0.15 (-0.15)	-5.99 (-5.13)	52.80 (52.66)	-0.16 (-0.17)	-5.89 (-5.00)
NEWEMIS_ TEMPFORE	35.87 (35.63)	43.73 (43.51)	52.53 (52.24)	-0.04 (-0.04)	-4.80 (-0.98)	52.91 (52.78)	-0.05 (-0.05)	-2.89 (-0.95)
SmartFire	35.91 (35.66)	43.78 (43.55)	52.56 (52.27)	-0.02 (-0.02)	-11.74 (-9.20)	52.94 (52.81)	-0.02 (-0.02)	-11.19 (-8.61)
FCCS	35.84 (35.60)	43.68 (43.46)	52.45 (52.17)	-0.11 (-0.10)	-10.40 (-9.06)	52.85 (52.71)	-0.12 (-0.12)	-9.84 (-8.46)

*8-Hour Ozone Concentration Percentile:

$$\underset{i\in R,h\in P}{\mathrm{P}(percentile)}\left(A8_{i,h}\right)$$

Mean Difference in 8-Hour Ozone Concentration

$$\underset{i\in R,h\in P}{\mathrm{mean}}\left(A8_{i,h,sensitivity}-A8_{i,h,default}\right)$$

Maximum Difference in 8-Hour Ozone Concentration- From either below that has a greater absolute value:

$$\begin{cases}\underset{i\in R,h\in P}{\max}\left(A8_{i,h,sensitivity}-A8_{i,h,default}\right)\\ \underset{i\in R,h\in P}{\min}\left(A8_{i,h,sensitivity}-A8_{i,h,default}\right)\end{cases}$$

Mean MDA8 Ozone Concentration

$$\underset{i\in R,d\in P}{\mathrm{mean}}\left(MDA8_{i,d}\right)$$

Mean Difference in MDA8 Ozone Concentration

$$\underset{i\in R,d\in P}{\mathrm{mean}}\left(MDA8_{i,d,sensitivity}-MDA8_{i,d,default}\right)$$

where R: Spatial region of interest; P: Temporal period of interest; i: A model grid cell index within region of interest, R; h: An hour within analysis period, P; d: A day within analysis period, P; *sensitivity* refers to sensitivity study; *default*: refers to FINN model configuration; $C_{i,h}$: Hourly concentration at cell i, hour h; $A8_{i,h}$: Eight hour moving average concentration at cell i, hour h; $MDA8_{i,d}$: Daily maximum eight hour concentration at cell i, day d.

Table S3. $PM_{2.5}$ metrics* ($\mu g/m^3$) during April 15th through May 30th, 2008 within the 12-km grid in Texas. Metrics for the 36-km grid are shown in parentheses.

	Percentile 24-Hour Averaged $PM_{2.5}$ Concentrations			Mean Difference in 24-Hour Averaged $PM_{2.5}$ Concentrations	Maximum Difference in 24-Hour Averaged $PM_{2.5}$ Concentrations
	25th	50th	75th		
DEFAULT	2.40 (2.42)	3.92 (3.95)	5.96 (5.99)	n.a.	n.a.
GlobCover	2.44 (2.46)	4.00 (4.03)	6.06 (6.08)	0.08 (0.08)	22.55 (-5.10)
NEWEMIS	2.41 (2.43)	3.94 (3.97)	5.98 (6.01)	0.02 (0.02)	10.54 (2.48)
HIGHEMIS	2.46 (2.48)	4.05 (4.08)	6.11 (6.13)	0.12 (0.12)	31.37 (7.42)
LOWEMIS	2.36 (2.38)	3.84 (3.86)	5.86 (5.89)	-0.08 (-0.08)	-31.18 (-7.69)
NEWEMIS_ TEMPFORE	2.41 (2.43)	3.94 (3.97)	5.98 (6.00)	0.02 (0.02)	10.54 (2.48)
SmartFire	2.43 (2.44)	3.90 (3.93)	5.95 (5.98)	0.01 (0.01)	168.15 (31.09)
FCCS	2.38 (2.40)	3.89 (3.92)	5.93 (5.95)	-0.03 (-0.03)	-38.22 (-7.36)

*$A24_{i,d}$: 24 hour average concentration at cell i, day d.

24-Hour PM2.5 Concentration Percentile"

$$\underset{i\in R, h\in P}{P percentile}\left(A24_{i,d}\right)$$

Mean Difference in 24-Hour $PM_{2.5}$ Concentration

$$\underset{i\in R, d\in P}{\text{mean}}\left(A24_{i,d,sensitivity} - A24_{i,d,default}\right)$$

Maximum Difference in 24-Hour $PM_{2.5}$ Concentrations- From either below that has a greater absolute value:

$$\begin{cases} \max\limits_{i\in R, h\in P}\left(A24_{i,d,sensitivity} - A24_{i,d,default}\right) \\ \min\limits_{i\in R, h\in P}\left(A24_{i,d,sensitivity} - A24_{i,d,default}\right) \end{cases}$$

Table S4. $PM_{2.5}$ metrics ($\mu g/m^3$) during September 1st through October 17th, 2008 within the 12-km grid in Texas. Metrics for the 36-km grid are shown in parentheses.

	Percentile 24-Hour Averaged $PM_{2.5}$ Concentrations			Mean Difference in 24-Hour Averaged $PM_{2.5}$ Concentrations	Maximum Difference in 24-Hour Averaged $PM_{2.5}$ Concentrations
	25th	50th	75th		
DEFAULT	3.38 (3.40)	5.41 (5.43)	9.00 (9.02)	n.a.	n.a.
GlobCover	3.41 (3.43)	5.50 (5.52)	9.19 (9.22)	0.15 (0.15)	37.92 (7.08)
NEWEMIS	3.38 (3.41)	5.42 (5.44)	8.99 (9.03)	0.01 (0.01)	10.05 (1.98)
HIGHEMIS	3.44 (3.47)	5.55 (5.58)	9.32 (9.34)	0.26 (0.26)	34.40 (6.74)
LOWEMIS	3.33 (3.34)	5.27 (5.28)	8.68 (8.69)	-0.23 (-0.23)	-40.20 (-7.19)
NEWEMIS_ TEMPFORE	3.38 (3.40)	5.41 (5.43)	8.99 (9.02)	0.01 (0.01)	10.02 (1.96)
SmartFire	3.38 (3.40)	5.34 (5.36)	8.81 (8.82)	-0.12 (-0.13)	75.67 (18.28)
FCCS	3.36 (3.38)	5.35 (5.37)	8.85 (8.87)	-0.10 (-0.10)	-39.62 (-10.10)

*$A24_{i,d}$: 24 hour average concentration at cell i, day d.

24-Hour PM2.5 Concentration Percentile"

$$\underset{i\in R,h\in P}{P percentile}\left(A24_{i,d}\right)$$

Mean Difference in 24-Hour $PM_{2.5}$ Concentration

$$\underset{i\in R,d\in P}{\text{mean}}\left(A24_{i,d,sensitivity}-A24_{i,d,default}\right)$$

Maximum Difference in 24-Hour $PM_{2.5}$ Concentrations- From either below that has a greater absolute value:

$$\begin{cases}\underset{i\in R,h\in P}{\max}\left(A24_{i,d,sensitivity}-A24_{i,d,default}\right)\\ \underset{i\in R,h\in P}{\min}\left(A24_{i,d,sensitivity}-A24_{i,d,default}\right)\end{cases}$$